Enhanced Ethylene Production Using Proton-conducting Electrochemical Cells

A Techno-economic Analysis

By

Tijmen C. Steneker

Student number:	4612140	
Project duration:	November 21st, 2022 – August 4th, 2023	
Supervisors:	Prof. dr. ir. Earl Goetheer,	TU Delft
	Prof. dr. Michael Golombok,	Shell GS
	Dr. ir. Ben Rowley,	Shell GS
University:	Delft University of Technology	
Faculty:	Faculty of Electrical Engineering, Mathematics and Computer Science (EEMCS)	
Master program:	Sustainable Energy Technology (SET)	
Company:	Shell Global Solutions International B.V. (Shell GS)	

TU Delft

Preface

The master thesis presented here explores the potential of proton-conducting electrochemical cells (PCECs) for enhanced ethylene production. It does so by investigating the mechanism, economic viability, and environmental impacts of this novel approach, aiming to bring forth a shift in the petrochemical industry. I hope this thesis can catalyze a more sustainable, efficient, and profitable transition in ethylene manufacturing.

Through this thesis, I have discovered the vital role of critical thinking when referencing online information and scientific publications. Authors creatively define concepts to make their work stand out, especially in less documented fields. As an aspiring engineer, it is crucial to extract reliable data and substantiate assumptions. This learning has been the most important takeaway from this project.

Writing this thesis has been a tough but enlightening endeavor, surpassing any academic exam in its challenges. It truly has had its ups and downs, but I take pride in the final product. Realizing that I could contribute to the science behind the topic, despite not being an initial expert, was particularly rewarding. By applying the engineering principles and a critical mindset, I was able to explore a topic beyond my master's program scope. This experience enhanced my comprehension of chemical engineering and electrochemical systems, offering insights into future industrial sustainability challenges. I aim to carry these learnings into my future work and inspire others to tackle technical challenges while contributing to industrial decarbonization efforts.

The intended audience for this thesis includes researchers, academics, and industry professionals interested in sustainable alternatives in petrochemical production, specifically ethylene. Background in chemical engineering or electrochemistry could be beneficial for understanding. However, the report is written in a way that makes it accessible for readers from various disciplines with an interest in sustainable technologies and industrial decarbonization.

This thesis would not have been possible without the support of my supervisors both at TU Delft and Shell Global Solutions International. Therefore, I would like to thank Earl for the interesting and enlightening discussions we had. Also, I would like to thank Michael for your continuous feedback and thoughtful contribution. Our weekly meetings brought me a lot of confidence, insights, and above all, a good laugh. Finally, I want to thank Ben for sharing his expertise on electrochemistry and upscaling of lab-scale technologies.

This final piece of work marks the end of my time at TU Delft, a journey filled with knowledge, good experiences, and the forging of lifelong friendships. Writing this thesis has been a rewarding experience and I hope you find the content as interesting as I do.

Tijmen C. Steneker

Delft, August 2023

Abstract

The petrochemical industry accounts for approximately 20% of global industrial CO_2 emissions. Ethylene manufacturing is one of the major components and has a high carbon footprint. This study explores the use of proton-conducting electrochemical cells (PCECs) for ethylene production - the WINNER process. This non-oxidative dehydrogenation (NODH) reaction is still thermochemical, but the hydrogen is electrochemically removed, enhancing the conversion of ethane.

The electrochemically enhanced production of ethylene demonstrates substantial improvements over conventional steam cracking. It decreases Specific Energy Consumption (SEC) by approximately 20%, curtails thermal energy demand by 80% and enables operations at a lower temperature of 550°C. Some parameters are less favourable, but nonetheless, the reduction in SEC indicates a promising potential to decrease carbon emissions attributed to utility consumption.

Economically, the WINNER process outperforms the steam cracking benchmark, with a nearly doubled margin, almost tripled Net Present Value (NPV), and a seven-times higher Internal Rate of Return (IRR). The Minimum Selling Price (MSP) of ethylene reduces by roughly 30% in the WINNER process. Additionally, the WINNER process produces pure, pressurized hydrogen as a high-value byproduct, adding to the economic viability of the process. A sensitivity analysis indicates that the most influential parameters are the prices of ethylene, ethane, and fuel gas.

Under current U.S. grid conditions, the Product Carbon Footprints (PCFs) of the WINNER process and the steam cracking benchmark are approximately equal. An increased contribution from renewable energy sources would enable the WINNER process to lower the utility-based PCF of ethylene production.

In conclusion, the WINNER process exhibits superior techno-economic performance and potential environmental advantages over the steam cracking benchmark, making it a promising alternative for sustainable ethylene production. Therefore, this work lays the groundwork for a sustainable and profitable transition in ethylene production, leveraging advances in electrochemistry.

Table of Contents

List of Figures

List of Tables

Nomenclature

Symbol	Definition
R_{H2}	Hydrogen removal rate [%]
J_{H+}	Proton flux [mol/cm^2*s]
D_H	Proton diffusion coefficient [m^2/s]
C_H	Proton concentration [1/m^3]
R	Gas constant = 8.314 [J/(K·mol)]
z	Charge number [-]
F	Faraday constant = 96485 [C/mol]
μ_H	Chemical potential [J/mol]
φ	Electrical potential [V]
Ω	Ohm – unit for electrical resistance
barg	Gauge pressure [bar]
C_2=	Ethylene
ΔH	Enthalpy change [J/mol]
ΔG	Gibbs free energy change [J/mol]
ΔS	Entropy change [J/mol]
E^0	Standard cell potential

Abbreviation	Definition
AEA	Aspen Energy Analyzer
ASR	Area Specific Resistance
CAPEX	Capital Expenditure
DE	De-ethanizer
DM	Demethanizer
ECU	Ethylene Cracker Unit
EOS	Equation of State
HER	Hydrogen Evolution Reaction
HK	Heavy Key

HTE	High-temperature Electrolysis
IRA	Inflation Reduction Act
IRR	Internal Rate of Return
ISPT	Institute for Sustainable Process Technology
LCA	Life Cycle Assessment
LHV	Lower Heating Value
LK	Light Key
MIEC	Mixed Ionic-Electronic Conductor
MPEC	Mixed Proton and Electron Conducting
MSP	Minimum Selling Price
NODH	Non-oxidative Dehydrogenation of Ethane
NPV	Net Present Value
OCV	Open Circuit Voltage
ODH	Oxidative Dehydrogenation of Ethane
OPEX	Operational Expenditure
PCEC	Proton-conducting Electrochemical Cell
PCF	Product Carbon Footprint
PENG-ROB	Peng Robinson (Equation of State model)
R&D	Research and Development
RE	Renewable Energy
SCC	Social Cost of Carbon
SEC	Specific Energy Consumption
SET	Sustainable Energy Technology
SOEC	Solid Oxide Electrolyzer Cell
SOEMR	Solid Oxide Electrochemical Membrane Reactor
SRF	Standard Refinery Fuel
TCI	Total Capital Investment
TRL	Technology Readiness Level
TVC	Total Variable Costs
UOM	Unit of Measurement

1. Introduction

1.1. Ethylene

Ethylene, C_2H_4, is a fundamental building block within the petrochemical industry. It is used to manufacture a diverse range of chemical products, from plastics and polymers to valuable chemicals like ethylbenzene, synthetic lubricants, and detergents [1]. Its global consumption exceeded 175 million tons in 2022 [2]. With rising living standards and a growing global population, production rates are expected to continue increasing [3]. Currently, ethylene is mainly produced through steam cracking of naphtha or ethane, converting hydrocarbon feedstocks into ethylene, other light olefins, and hydrogen co-products [4]. Over recent decades, this process has been optimised, and capacities have increased, making ethylene production through steam cracking a commercially established technology with favourable economics driven by economies of scale [5].

1.2. Need for Alternative Methods

Conventional thermal steam cracking reactions are energy- and carbon-intensive, releasing 1-2 tons of CO_2 per ton of ethylene produced, depending on the feedstock utilised [4]. This high energy consumption and emission level is due to the endothermic nature of cracking reactions, such as the cracking of ethane ($\Delta H_{298K} = 136\ kJ\ mol^{-1}$ [6]). These reactions operate at high temperatures, leading to significant thermal energy requirements, currently fulfilled by burning (fossil) refinery fuels. Given the environmental concerns associated with the conventional ethylene production process, there is a need for a well-established, sustainable alternative to steam cracking. Process optimisation alone may not yield significant reductions in processing energy and carbon footprints. Hence, more disruptive methods are required to explore alternative, low-thermal-budget (LTB) and low-carbon-footprint (LCF) methods [7].

1.3. Research Focus and Motivation

The research presented investigates an electrochemically enhanced alternative for producing ethylene and hydrogen from ethane. It aims to reduce CO_2 emissions and heating requirements associated with steam cracking. The process employs proton-conducting electrochemical cells (PCECs) for the non-oxidative dehydrogenation of ethane (NODH). The "World class Innovative Novel Nanoscale optimised electrodes and electrolytes for Electrochemical Reactions" ("WINNER") project, funded by Hydrogen Europe [8], is exploring this technology. However, this novel technology's anticipated economic performance and environmental impacts are not yet known, making it crucial to assess before committing resources for further research.

From a scientific perspective, this research provides novel insights into the electrochemically enhanced NODH process, offering a detailed understanding of its

operating mechanism and potential implications on an industrial scale. It gives a critical review of the few papers published on this topic. The social relevance of this thesis lies in its potential to contribute to a more sustainable petrochemical industry. By investigating an alternative ethylene production process that is less energy- and carbon-intensive, it aligns with global and Shell's efforts towards reducing industrial carbon footprints and by doing so, combating climate change.

1.4. Research Questions

This research aims to assess the potential of this novel technology in terms of economic performance and environmental impacts. To do so, it answers the following research question:

"What is the techno-economic performance and environmental impact of electrochemically enhanced ethylene production in proton-conducting electrochemical cells (PCECs), and how does this process compare to commercial ethane steam cracking in these aspects?"

1.5. Methodology

Figure 1-1 visualizes the systematic methodology used to answer the research questions. The procedure starts with the construction of a conceptual process design (CPD), based on process data drawn from literature. This data is integrated into a process plant design capable of simulating a mass-energy balance. The output of this balance includes product yields, process duties, and corresponding specific energy consumption.

Next, a Techno-Economic Analysis (TEA) is performed. By combining CPD outcomes with economic indicators, the TEA provides an in-depth evaluation of the system's economic performance.

To assess the environmental performance of the system, the mass-energy balance is combined with emission factors and a list of critical raw materials. This results in a comprehensive evaluation of the environmental impacts associated with the process.

To enhance the robustness of the assessment, several scenarios are modelled and simulated to account for variations in inputs. The results are then compared with Shell's state-of-the-art Monaca ethylene cracking unit in a benchmark comparison.

The approach outlined here relies on the assumption that lab-scale parameters can scale to industrial operations without significant discrepancies in process parameters. The research thus employs a systematic approach to explore the economic viability and environmental impact of the electrochemically enhanced NODH process compared to an ethane steam cracker benchmark. Although this approach offers a comprehensive evaluation, it is subject to the limitation of the availability and accuracy of the underlying experimental data.

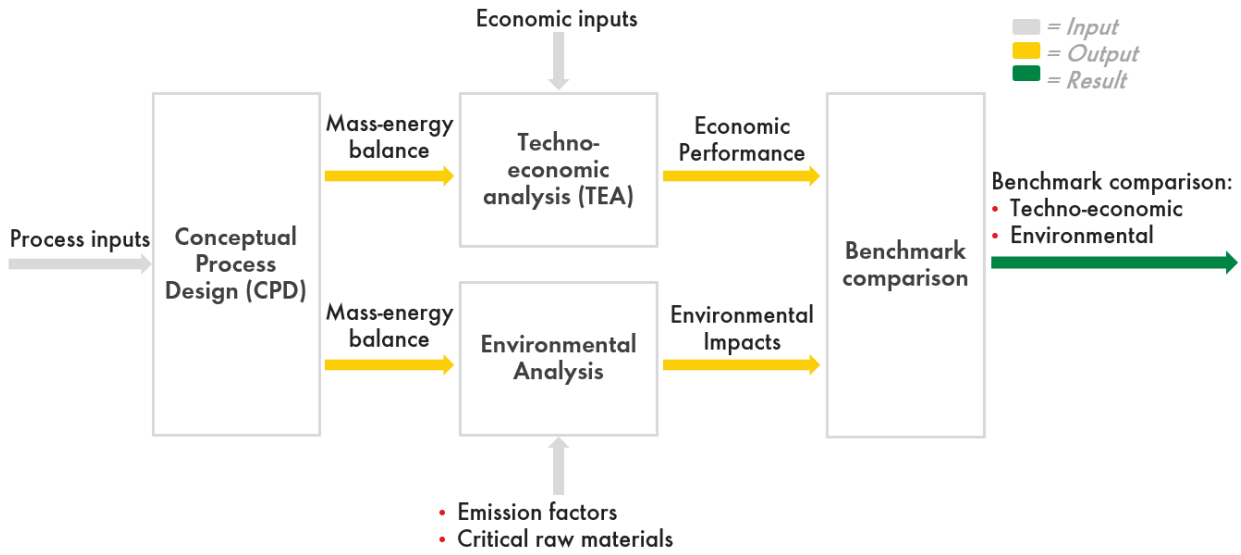

Figure 1-1: Flow diagram of the research methodology used to assess the potential of the WINNER process.

1.6. Relevance to the SET master's Program

This thesis will be the final work to complete the Sustainable Energy Technology (SET) master's program at TU Delft. The SET master's program focuses on the development and deployment of sustainable technologies for energy generation, storage, and utilization. The work in this thesis specifically adheres to the storage profile, since the technology used in the PCEC reactor shows similarities with electrolytic devices for hydrogen production, such as, Solid Oxide Electrolyzers (SOEs). The separate production of hydrogen in the electrochemically enhanced NODH process presents an unexplored opportunity for low-carbon hydrogen production. In a broader context, it aligns with the SET program's emphasis on technological innovation to solve complex environmental problems and potentially decarbonize industry by electrifying ethylene production. Furthermore, the skills and methodologies applied in this research, - ranging from a literature review to process simulation, techno-economic analysis, and environmental impact assessment – all are integral aspects of the SET curriculum.

1.7. Thesis Structure

This thesis is structured as follows: Chapter 2 provides the necessary theoretical background, focusing on ethylene production pathways and the working principles of PCECs. Building on the theoretical background, Chapter 3 designs a simulation of the process under thermodynamically realistic conditions in AspenPlus software. Using the results of this simulation, Chapter 4 compares the product outputs and energy consumption of the WINNER process with the Monaca benchmark. Next, Chapter 5 applies a techno-economic approach to these simulation results, offering a comparative analysis of the process economics and Product Carbon Footprints (PCFs). Finally, Chapter 6 summarizes the main findings of this thesis work and offers recommendations for further research.

2. Theory

This chapter provides the background for this thesis. It provides insights into existing technologies for ethylene production, the challenges, and the emerging search for alternatives. It addresses these various technologies and selects a promising alternative for ethylene production: electrochemically enhanced non-oxidative dehydrogenation of ethane. The working principles of this process and the chosen configuration are explained. Section 2.1 provides an overview of commercially common techniques, setting a first benchmark in terms of economic figures and environmental impact. Section 2.2 presents a qualitative analysis and evaluation of emerging technologies for ethylene production. It ultimately selects a technology with considerable potential for decarbonizing ethylene production. Finally, Section 2.3 discusses the working principle, selected operational mode, and cell configuration of the PCEC (Proton-conducting Electrochemical Cell) reactor.

2.1. Commercial Ethylene Production

Ethylene is currently primarily produced through steam cracking of ethane or naphtha. In these processes, hydrocarbon feedstocks are combined with steam and cracked at high temperatures (>750 °C) into ethylene, other light olefins, and hydrogen coproducts [4]. This thermal conversion generally takes place in a tubular reactor and the choice of feedstock mainly depends on its profitability and availability at the plant location [9]. Over the last few decades, this process has been highly optimised, and capacities have been increased. As a result, ethylene production through steam cracking is a well-established commercial technology with favourable economics [5]. Cracking reactions are energy and carbon-intensive due to high endothermicity and complex cryogenic separation schemes. They generate 1-2 tons of CO_2 for every ton of ethylene produced, depending on the feedstock utilised [4]. Since new technologies still have a relatively low Technology Readiness Level (TRL), the production of ethylene will continue to be primarily driven by the steam cracking of hydrocarbons in the coming decades.

Figure 2-1 shows the basic operation of a hydrocarbon steam cracker. A hydrocarbon feedstock, either liquid naphtha or gaseous ethane, is sequentially mixed with steam, pre-heated, and thermally cracked. The heat required is provided by the combustion of fuel outside the reactor tubes containing hydrocarbons and steam. Next, the product stream is quenched to prevent further cracking of the products, compressed, and the desired products are recovered through separation units [10].

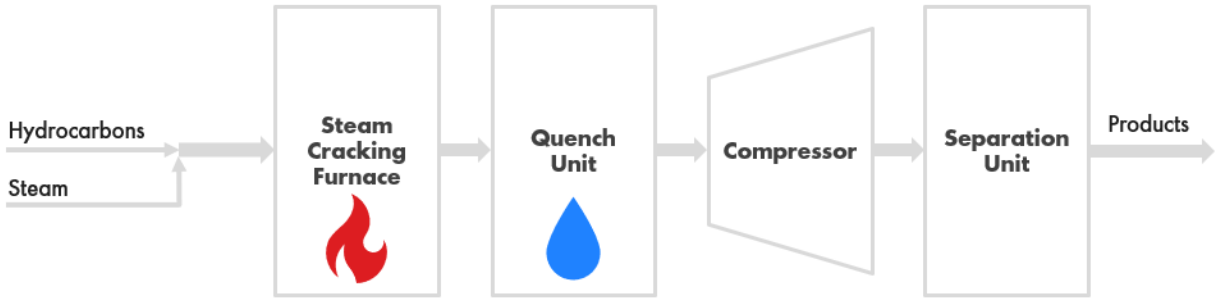

Figure 2-1: Simplified hydrocarbon steam cracker process scheme.

The yield of steam cracking products is contingent on the type of feedstock employed, and the prices of such products are subject to frequent fluctuations, thereby significantly affecting the income generated from sales of these outputs. Hence, price forecasting plays a crucial role in determining the profitability of a proposed future plant. Ethylene (C_2H_4), propylene (C_3H_6), and butene (C_4H_8) are valuable light olefins derived from steam cracking. Their US market prices between 2015 - 2020 are listed in Table 2-1.

Table 2-1: U.S. prices of ethylene, propylene, and butene between 2015 - 2020.

Product name	U.S. 2015 – 2020 average price [$/ton]
Ethylene	1200 [11] [12]
Propylene	1200 [13, 14]
Butene	1050 [15, 16]

2.1.1. Naphtha Steam Cracking

About 45% of the ethylene produced globally is created by steam cracking of naphtha. Naphtha is a lightweight petrochemical feedstock, that is separated from crude oil during fractional distillation within a boiling range between 30 - 200°C [10, 17]. It is a complex mixture of hydrocarbons, ranging from straight-chain alkanes to aromatics [10]. Equation (2-1) describes a typical naphtha cracking reaction of hexane to ethylene. The strongly positive reaction enthalpy stresses the high endothermicity of this thermal cracking process. The reaction enthalpy is expressed in kJ/mol of the reactant, in this case, hexane. This convention will be used consistently throughout this report. Furthermore, it deals with challenges such as equilibrium limitations, high energy intensity, significant CO_2 emissions, and the problem of coke formation [18]. Typical operating temperatures lie in the range of 750 – 900°C [10].

$$C_6H_{14}(g) \rightarrow 3C_2H_4 + H_2 \qquad \Delta H_{1048K} = +319.6 kJ/mol \qquad (2\text{-}1)$$

Figure 2-2 illustrates the weight percentage (wt%) distribution of products of a typical naphtha cracker. The product spectrum of this reaction is diverse, with ethylene being the

major contributor to the final product yield. The ethylene selectivity for naphtha steam cracking is 32%. Additionally, propylene, methane, aromatics, and C_{4+} molecules also significantly contribute to the product spectrum. The category "other" partly refers to unreacted ethane, recycled to the refinery.

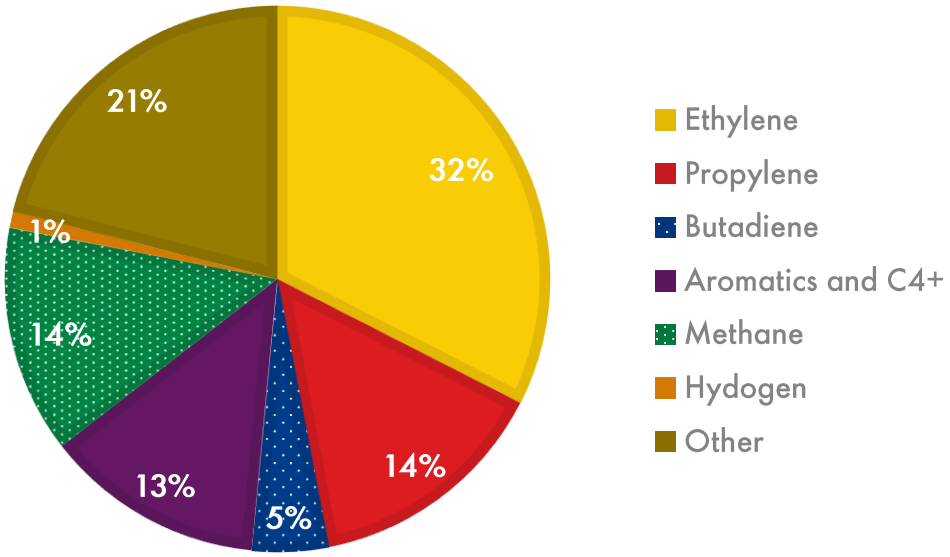

Figure 2-2: Typical product yield (in wt%) in a naphtha steam cracker (the figure was drawn based on Table 0-1 in APPENDIX B [4]).[1]

For a detailed process scheme of naphtha steam cracking with an explanation of the unit operations, please refer to APPENDIX A.

2.1.2. Ethane Steam Cracking

Aside from naphtha, ethane in gaseous form is also a viable hydrocarbon feedstock for steam cracking processes. Recent advances in extracting natural gas from previously untapped shale gas reserves have resulted in a 25% increase in the supply of ethane in the US. This increase in ethane availability increases the interest in using ethane as a feedstock for steam crackers [19].

The process of ethane steam cracking roughly follows the same process steps as naphtha cracking. Figure 2-3 illustrates a process scheme of ethane steam cracking. First, gaseous ethane is heated to temperatures in the range of 880°C - 900°C [20] at low pressures to produce ethylene and other by-products, which are then quenched to avoid further reactions (A). The cracking temperature of ethane is higher compared to naphtha. This is

[1] The percentages shown in Figure 2-2 represent the mean of the values per category as presented in Table 0-1 in APPENDIX B. The category "other" refers to the remaining part in terms of wt%.

due to larger hydrocarbons having more carbon-carbon bonds, some of which are weaker due to the complexity of the molecular structure. As a result, these bonds break more easily under the influence of thermal energy [21].

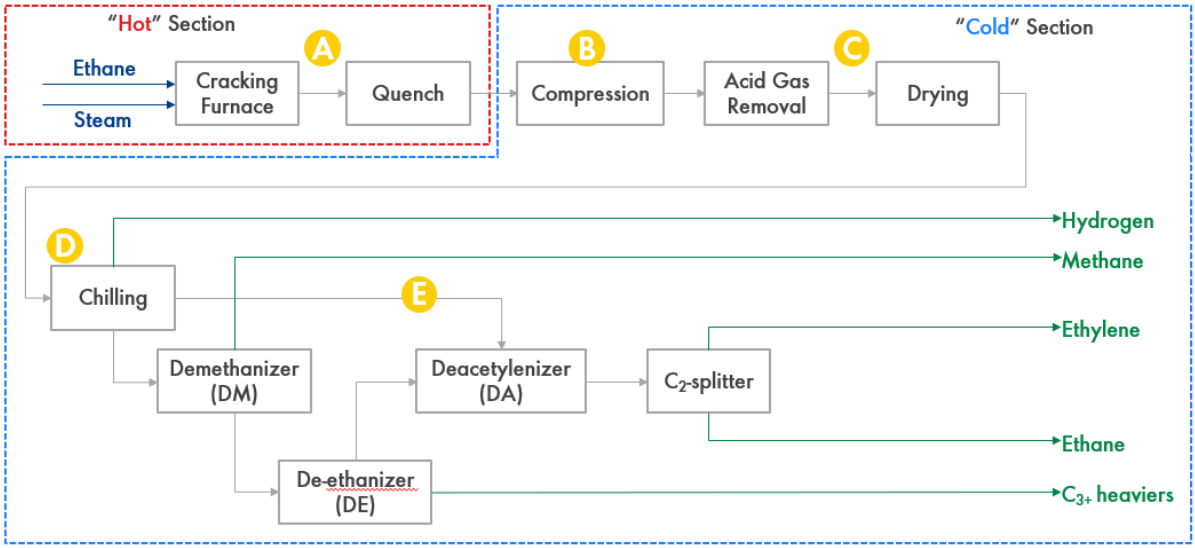

Figure 2-3: Process scheme of ethane steam cracking process (the figure was drawn based on [22]).

2.1.3. Product Stream Treatment

The quenched products are then compressed to high pressure (~40 bar) in four stages to effectively separate ethylene from other compounds (B). In the compression section, acid gases are removed by using caustic scrubbing, and any remaining moisture is also removed (C). The product stream coming out of the compression section is further cooled in the "chilling" unit using refrigerants. This is done to effectively separate hydrogen gas from the rest of the product stream, which is then sent to the separation section (D). The hydrogen gas obtained from the separation section is used to react with produced acetylene to form ethylene (E). The product stream from the separation section is passed through a series of distillation columns to remove methane, propane, and ethane from the ethylene product stream. The ethylene product obtained has a purity of 99.99%. The unreacted ethane is recycled back to the cracker feed [22].

2.1.4. Product Components

The chemistry of the ethane steam cracking reaction is dictated by the main reactions described by Equations (2-2) - (2-9) [23]:

$$C_2H_6 \leftrightarrow C_2H_4 + H_2 \quad (2\text{-}2)$$

$$2C_2H_6 \rightarrow C_3H_8 + CH_4 \quad (2\text{-}3)$$

$$C_3H_8 \leftrightarrow C_3H_6 + H_2 \quad (2\text{-}4)$$

$$C_3H_8 \rightarrow C_2H_4 + CH_4 \quad (2\text{-}5)$$

$$C_3H_6 \leftrightarrow C_2H_2 + CH_4 \quad (2\text{-}6)$$

$$C_2H_2 + C_2H_4 \rightarrow C_4H_6 \quad (2\text{-}7)$$

$$2C_2H_6 \rightarrow C_2H_4 + 2CH_4 \quad (2\text{-}8)$$

$$C_2H_6 + C_2H_4 \rightarrow C_3H_6 + CH_4 \quad (2\text{-}9)$$

These main reactions lead to the typical product slate of an ethane steam cracker, as presented in Figure 2-4. The primary product produced is ethylene, as can be observed by its dominance in terms of weight percentage and the relatively low contribution of other products. Therefore, it can be concluded that the process of ethane steam cracking is highly selective to ethylene production compared to naphtha steam cracking. The ethylene selectivity for ethane steam cracking is 82%. This stems from the molecular similarities of ethane (C_2H_6) and ethylene (C_2H_4) [24].

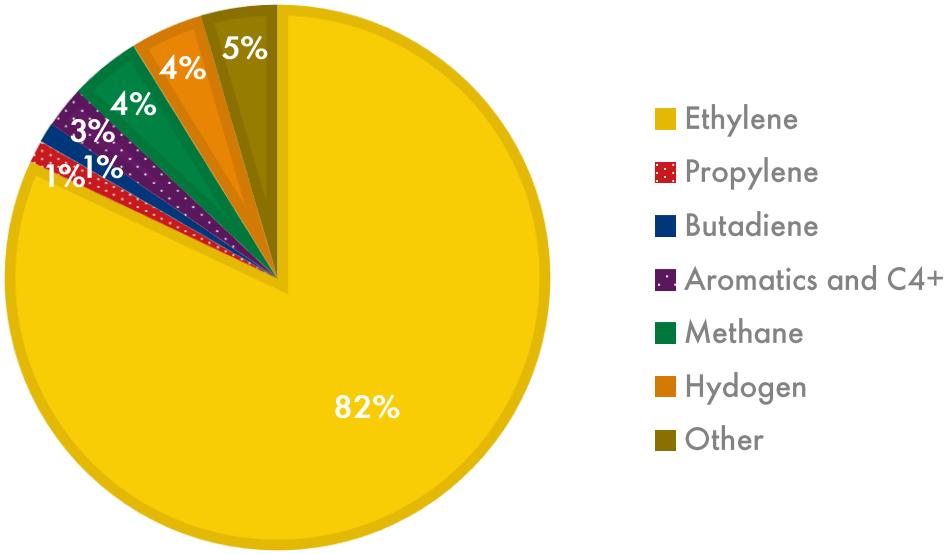

Figure 2-4: Typical product yield (in wt%) in an ethane steam cracker (the figure was drawn based on Table 0-1 in APPENDIX B [4]).[2]

The benchmark technology for the evaluation of the economic and environmental performance of WINNER's technology for ethylene production is the commercial method of ethane steam cracking. The reason for ethane steam cracking to be chosen over naphtha steam cracking is twofold. Firstly, ethane steam cracking has a higher ethylene selectivity (82% vs. 32%), which simplifies the identification and quantification of the

[2] The percentages shown in Figure 2-4 represent the mean of the values per category as presented in Table 0-1 in APPENDIX B. The category "other" refers to the remaining part in terms of wt%.

emissions and energy consumption associated with the production of ethylene. Secondly, the utilization of ethane as the feedstock in the WINNER project facilitates the comparison by maintaining consistency in the feedstock used.

2.1.5. Comparison

The energy consumption in olefin processes is the combination of fuel, steam, and electricity in primary forms utilised for reactions and related processes. This concept is referred to as "process energy use" and is a standard metric for quantifying energy consumption in industrial processes. The Specific Energy Consumption (SEC) metric is employed to express process energy use and it is calculated as the sum of the theoretical thermodynamic energy requirement and the energy loss incurred in steam cracking processes. The energy loss refers to the portion of energy input that is not included in the total energy output, such as heat dissipation and is calculated as the difference between the total energy input and total energy output [4].

The efficiency of energy utilization is quantified by the SEC, expressed in units of Gigajoules per metric ton of products produced (GJ/t products). In the case of steam crackers, the SEC is expressed in either GJ/t ethylene or GJ/t High-Value Chemicals (HVCs). HVCs refer to the valuable chemicals produced during steam cracking and, besides ethylene, encompass chemicals such as propylene, butadiene, aromatics, and other C_4+ chemicals [4]. When using the GJ/t ethylene unit, total energy consumption is allocated to ethylene production and other co-products are considered as having negligible energy impact. However, this metric results in an inaccurate comparison between naphtha and ethane steam cracking processes, as the latter has a higher selectivity towards ethylene production, while the former yields significant amounts of other valuable chemicals.

Table 2-2 compares the operating conditions, SEC, and carbon intensity of the naphtha and ethane steam cracking processes. The cracking temperature of ethane is higher than that of naphtha steam cracking, which is explained in Section 2.1.2. As previously discussed, the metric of SEC in GJ/t ethylene results in a less favourable comparison for naphtha steam cracking, with values of 26-31 GJ/t ethylene, compared to 17-21 GJ/t ethylene for ethane steam cracking. However, when expressed in terms of GJ/t HVCs, naphtha cracking displays a higher energy efficiency, with values of 14-17 GJ/t HVCs, compared to 16-19 GJ/t HVCs for ethane. With regards to CO_2 emissions, the ethane steam crackers demonstrate a lower carbon footprint compared to naphtha steam crackers, both when expressed in terms of ethylene production and HVC production.

Table 2-2: Process conditions, specific energy consumption, and CO_2 emissions of naphtha and ethane steam cracking (the table was made based on [4, 22, 25]).

Process parameters	Naphtha	Ethane
Cracking temperature [°C]	750 - 900	880 - 900
Cracking pressure [bar]	1.7 – 2.5	1.3 – 3.5
SEC (GJ/t ethylene)	26 – 31	17 – 21
SEC (GJ/t HVCs)	14 – 17	16 – 19
CO_2 emissions (tCO_2/t ethylene)	1.8 – 2.0	1.0 – 1.2
CO_2 emissions (tCO_2/t HVCs)	1.6 – 1.8	1.0 – 1.2

2.2. Emerging Ethane Dehydrogenation Technologies

As crude oil and natural gas reserves continue to decline and public awareness of the environmental impacts of human activity increases, research into cleaner alternative methods for producing ethylene is becoming increasingly important. Mere process optimization may not be sufficient to decrease energy consumption and reduce the carbon footprint associated with the production of ethylene. This is particularly true in an industry where materials and energy efficiencies have already been extensively optimised and reliable operation is of importance [5]. A lot of research on alternative pathways for ethylene production has been documented in the literature. However, despite significant research efforts, no novel technologies for intensifying ethylene production have yet been implemented at an industrial scale.

In general, ethylene can be produced from methane, ethane, and naphtha through both non-oxidative and oxidative methods [18]. Ethane is the most appropriate feedstock for ethylene production among the alkanes due to their compositional, structural, and chemical similarities. This section provides an overview of non-commercial ethane-based ethylene production technologies. Figure 2-5 shows the different methods to produce ethylene using ethane as a feedstock. The main categories for ethane-based ethylene production are:

- Oxidative Dehydrogenation of Ethane (ODH)
- Non-oxidative Dehydrogenation of Ethane (NODH)
- Electrochemically Enhanced Dehydrogenation of Ethane

The selectivities and conversion rates of the reaction mechanisms are not presented in this chapter, since these figures vary too much for different configurations documented in the literature.

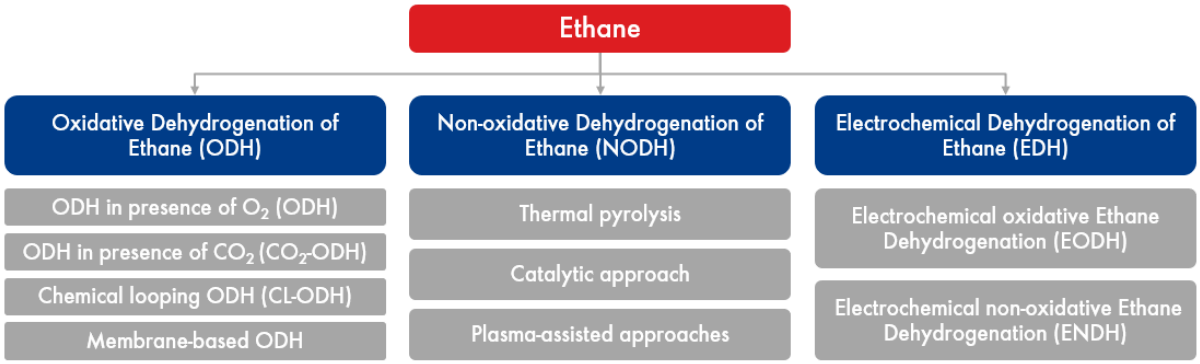

Figure 2-5: Schematic overview of the different ethane-based ethylene production routes (the figure is drawn based on [18]).

2.2.1. Oxidative

The oxidative dehydrogenation of ethane (ODH) involves partially oxidizing ethane to produce ethylene and water. The desired reactions are shown in Equations (2-10) and (2-11). Byproducts include C_3+, CO, CO_2, and coke [18], [26], [27].

$$C_2H_6 + \frac{1}{2}O_2 \rightarrow C_2H_4 + H_2O \qquad \Delta H_{298K} = -105.5\ kJ\ mol^{-1} \qquad (2\text{-}10)$$

$$C_2H_6 + CO_2 \rightarrow C_2H_4 + H_2O + CO \qquad \Delta H_{298K} = 134\ kJ\ mol^{-1} \qquad (2\text{-}11)$$

Equation (2-10) takes place under atmospheric conditions with the use of appropriate catalysts in the temperature range of 400 - 600°C, in the presence of oxygen [26]. The exothermic nature of the oxidative dehydrogenation reaction, combined with lower operating temperature requirements compared to those of steam cracking processes, can result in energy savings of over 30% [28]. In addition, the ODH reaction is less dependent on catalysts since the reaction often proceeds at a reasonable rate without the use of one. However, the ODH reaction has three main drawbacks. Firstly, the exothermic nature of the process presents challenges in terms of heat management and safety controls. Secondly, overoxidation can negatively impact the balance between conversion and selectivity, imposing challenges for commercial applications [29]. And thirdly, the presence of oxygen can lead to the formation of unwanted CO_x byproducts, contributing to the carbon emissions of ethylene production.

Equation (2-11) represents the CO_2-oxidative ethane dehydrogenation reaction. This reaction is endothermic and typically occurs in a temperature range of 600 - 700°C [27]. Recently there also has been interest in integrated technologies for ODH (e.g., chemical-looping and membrane-based). All the different types of ODH reactions are listed below [18]:

- ODH with O_2 co-feed (O_2-ODH) - Equation (2-10)
- ODH with CO_2 co-feed (CO_2-ODH) - Equation (2-11)
- Chemical-looping ODH
- Membrane-based ODH

2.2.2. Non-oxidative

The desired NODH (non-oxidative dehydrogenation of ethane) reaction is shown in Equation (2-12). Byproducts include CH_4, C_3H_6, C_3H_8, C_4H_8 and coke [6].

$$C_2H_6 \rightarrow C_2H_4 + H_2 \qquad \Delta H_{298K} = 136\ kJ\ mol^{-1} \qquad (2\text{-}12)$$

NODH has the potential to overcome the safety and heat management challenges associated with ODH. However, it faces other limitations such as high energy requirements, low single-pass conversion due to thermodynamic limitations, and catalyst deactivation caused by rapid coking. Solutions to these issues could include using membrane reactors to separate H_2 from the product mixture and shift the reaction equilibrium towards ethylene formation, as well as developing highly selective and coke-resistant catalysts [29]. The temperature dependence of the equilibrium conversion of the NODH process is shown in Figure 2-6 for different pressures. At T = 550 °C (823K) and p = 1 bar, the NODH equilibrium conversion is equal to 9% [30, 31].

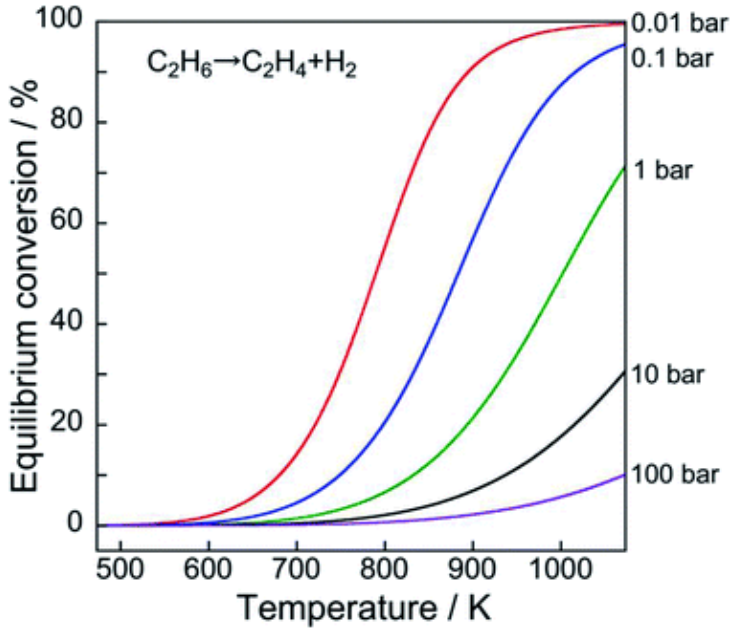

Figure 2-6: Temperature dependence of equilibrium conversion of NODH (non-oxidative ethane dehydrogenation) at different C_2H_6 pressures [30].

The equilibrium conversion increases with increasing temperature. Moreover, equilibrium conversion increases with decreasing pressure. Therefore, from a purely thermodynamic point of view, the ideal operating conditions for the NODH reaction are at a high temperature and a low pressure.

2.2.3. Electrochemically Enhanced Methods

Electrochemically enhanced methods for ethylene production from ethane have the potential to be more energy efficient and can bypass thermodynamic limitations by removing product species. These methods can be divided into oxidative and non-oxidative

approaches, and further divided into membrane-based and solid oxide fuel cell-based methods [18]. For electrochemically enhanced ODH, the same reactions as for ODH (Equations (2-10) and (2-11)) apply, while for electrochemically enhanced NODH, the same reaction as for NODH (Equation (2-12)) apply.

The classification of solid oxide electrochemical membrane reactors (SOEMRs) is based on the type of charge carrier used in the electrolyte. The oxygen ion-conducting membrane reactor is typically deployed in ODH processes due to the transport of O^{2-}-ions, while the proton-conducting membrane reactor is utilised in NODH processes as it involves the transport of H^{+}-ions [18]. The electrochemically enhanced NODH process has the potential to achieve high selectivity and conversion at reduced temperatures, resulting in decreased energy consumption and reduced carbon emissions.

According to Le Chatelier's principle, the thermodynamic equilibrium of the electrochemically enhanced NODH process can be shifted towards ethylene production by using an H_2-permeable membrane to extract H_2. Figure 2-7 illustrates this principle of hydrogen extraction in a packed-bed membrane reactor. Ethane is fed into the reactor on the left and the NODH process takes place in the packed bed depicted in light blue. The packed bed refers to the specific region where the catalyst is located and thus, where the chemical reactions take place. Next, hydrogen permeates through the membrane and is swept by a sweep gas.

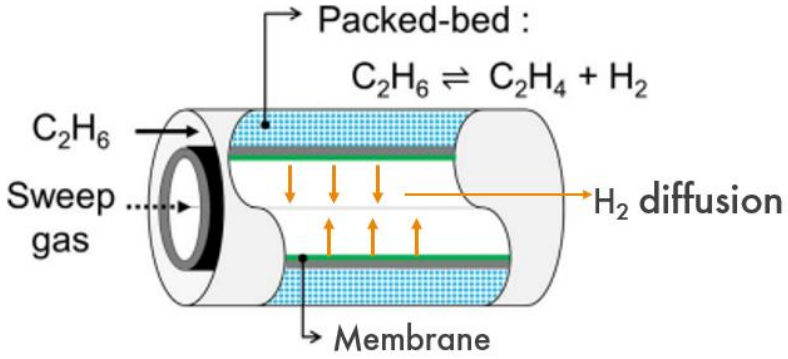

Figure 2-7: Schematic visualization of a packed-bed membrane reactor for the NODH process [32].

Pd-based membranes are widely studied membranes for H_2 permeation in reactors, although they are not yet used commercially. These membranes are unstable at temperatures above 600 °C. Since typical operating temperatures of NODH reactions lie in the range of 650 – 750 °C, this poses a challenge. As a result, most membrane-based NODH reactors that have been demonstrated to date utilize ceramic proton-conducting membranes with an electrical field as the driving force [33]. BCYN ($Ba(Ce_{0.9}Y_{0.1})_{0.8}Ni_{0.2}O_{3-\delta}$) and BZCY-based ($BaZr_{0.1}Ce_{0.7}Y_{0.2}O_{3-\delta}$) membranes are commonly reported in the literature [18].

In the literature, both passive and active membranes have been proposed for enhancing the NODH reaction. The key difference between them lies in the use of an electrical circuit

in an active membrane, which provides greater control over the proton flux and, consequently, the overall reaction rate. Three examples of passive membrane applications are discussed in APPENDIX C.

Different membrane configurations each possess unique benefits and limitations. The focus within the scope of the WINNER project is on employing an active membrane to promote the electrochemical enhancement of ethane dehydrogenation. The preference for a configuration involving an active membrane and an electrical circuit inducing a proton flux highlights the potential advantage of controlling the reaction rate. The specifications of the electrochemical cell (e.g., cell potential, overpotential) are defined in Section 2.3.2. The overarching objective is to achieve considerable energy savings and reduce carbon emissions. In Section 2.3, the operational principles and particular process conditions of the WINNER configuration will be examined further.

2.3. Proton-conducting Electrochemical Cells (PCECs)

2.3.1. Working Principle

The deployment of PCECs in the production of ethylene has gained increasing attention as a promising alternative to standard NODH (non-oxidative dehydrogenation of ethane) and ODH (oxidative dehydrogenation of ethane) processes. This is due to the potential to overcome limitations in conversion rates and selectivity encountered in these processes through the utilization of proton-conducting membranes [34]. Figure 2-8 shows a schematic representation of a PCEC. At the hydrocarbon electrode (anode), hydrogen-containing feed is oxidized to produce H^+-ions, among others. These H^+-ions then permeate from the feed side (anode) to the permeate side (cathode), driven by an electrical potential. At the cathode, the H^+-ions recombine with electrons to form hydrogen [35].

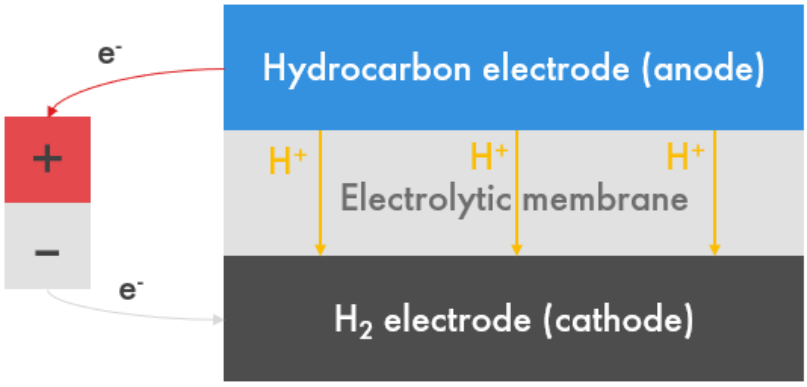

Figure 2-8: Schematic graph of a PCEC showing the working principle of a proton-conducting membrane (the figure was drawn based on [35]).

PCECs utilize proton-conducting oxide electrolyte materials, possessing high proton conductivity at intermediate temperatures. The typical operating temperature range of PCECs is 550 – 750°C. However, research aims to lower operating temperatures to the

range of 450 - 550 °C, because higher operating temperatures lead to faster degradation of the system [36]. Besides the application for ethylene production, PCECs can be deployed for several other electrochemical processes. These electrochemical cells for different applications all have diverse electrodes. PCECs are mainly known for their application in electrolysis systems but can also serve as the reactor in ammonia cracking [37]. Two main operating modes for PCECs in ethylene production have been identified, namely the fuel cell mode and the hydrogen pump mode [38]. For an explanation of the fuel cell mode, please refer to APPENDIX D.

2.3.2. Ethylene Production

The hydrogen pump mode refers to the process of simultaneous ethylene and hydrogen production from ethane and is shown in Figure 2-9. The overall reaction is similar to the NODH reaction and is shown in Equation (2-13):

$$C_2H_6 \rightarrow C_2H_4 + H_2 \tag{2-13}$$

At the anode, ethane is thermochemically dehydrogenated into ethylene and hydrogen following Equation (2-13). Subsequently, hydrogen is electrochemically oxidized into H^+ ions and electrons (Equation (2-14)).

$$H_2 \rightarrow 2H^+ + 2e^- \tag{2-14}$$

The H^+-ions permeate through the electrolyte under the influence of an applied electrical potential and combine with electrons in the absence of oxygen at the hydrogen electrode (cathode) to produce hydrogen, following Equation (2-15):

$$2H^+ + 2e^- \rightarrow H_2 \tag{2-15}$$

Figure 2-9 illustrates the distinct half-reactions, components of the cell, and the movement of protons and electrons.

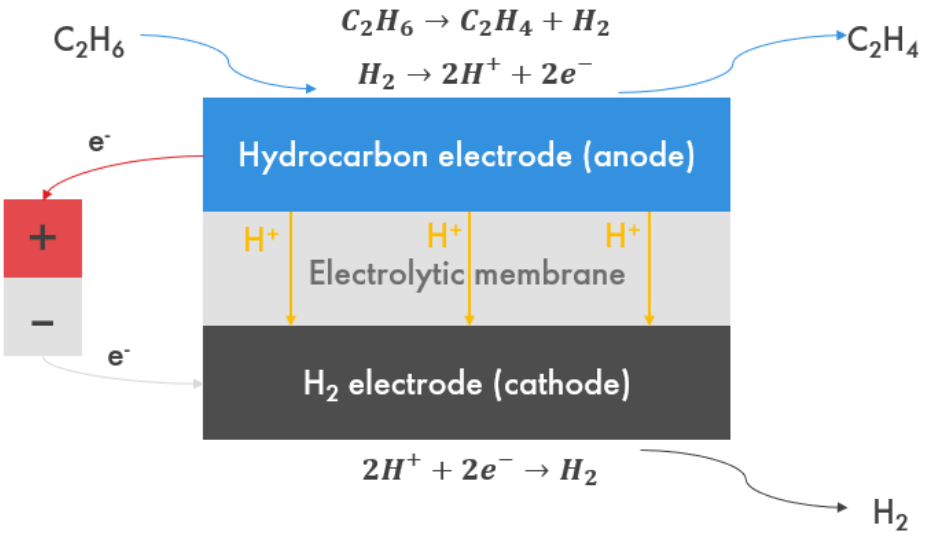

Figure 2-9: Schematic of PCECs for the co-production of ethylene and hydrogen in hydrogen pumping mode via the electrochemically enhanced NODH process (figure was drawn based on [38]).

As a result of applying a potential over the electrodes, a current is induced over the electrolytic membrane. This results in a proton flux from the hydrocarbon electrode to the H_2 electrode to ensure charge equilibrium. Thus, the applied potential over the electrodes (E_{cell}) is related to the current density and subsequently to the diffusion of hydrogen through the membrane. The electric field serves as the driving force for the transport of protons through the membrane, which is a characteristic of an electrical-driven reactor [38]. This transport mechanism offers an additional degree of freedom, as the permeation of the removed component can be adjusted by the electrical potential across the cell [7]. The reaction rate in this system is determined by the flow of protons through the electrolyte, the kinetics of the ethane oxidation reaction, and the hydrogen evolution reaction (HER). The proton flux, J_{H+}, is regulated by the voltage applied across the membrane, as outlined in Equation (2-16) [7]:

$$J_{H^+} = -\frac{D_H C_H}{RT} z_H F \cdot \nabla(\mu_H + z_H F \varphi) \tag{2-16}$$

Where:

D_H	is the proton diffusion coefficient [m^2/s],
C_H	is the proton concentration [$1/m^3$],
R	is the gas constant [J/(K·mol)],
T	is the temperature [K],
z_H	is the charge number [-],
F	is Faraday's constant [C/mol],
μ_H	is the chemical potential [J/mol],
φ	is the electrical potential [V]. The electrical potential φ is equal to the applied potential across the cell (E_{cell}).

Equation (2-17) illustrates the NODH equilibrium reaction and its corresponding Gibbs free energy at a temperature of 550°C. The Gibbs free energy, as defined in Equation (2-18), is a thermodynamic potential that measures the maximum reversible work a closed thermodynamic system can perform at constant pressure and temperature [39].

$$C_2H_6 \rightarrow C_2H_4 + H_2 \qquad \Delta G_{823K} = 51.7 \frac{kJ}{mol} \tag{2-17}$$

$$\Delta G = \Delta H - T\Delta S \tag{2-18}$$

Equation (2-19) relates the Gibbs free energy to the thermodynamic potential [39]:

$$E_{cell} = \frac{\Delta G}{-zF} \tag{2-19}$$

In this equation, E_{cell} represents the thermodynamic potential of the PCEC [V], ΔG stands for the Gibbs free energy change of the NODH reaction [J/mol], z is the charge number [-] (which is 2 in this case), and F is the Faraday constant [C/mol].

The thermochemical potential of the NODH reaction is calculated to be –0.268 V. However, this does not represent the actual cell potential for the PCEC, as the NODH

reaction purely runs thermochemically. The applied voltage provides the potential difference to split hydrogen, giving up two electrons and two protons in the process (Equation (2-20)). These then diffuse through the membrane and recombine at the cathode to form hydrogen (Equation (2-21)). It is crucial to understand that the electrons in this process are exclusively used for the splitting of hydrogen and not for the NODH of ethane. Therefore, the electrochemical cell potential is dictated by the potential required for hydrogen splitting [40].

$$H_2 \rightarrow 2H^+ + 2e^- \qquad \Delta G^0 = 0 \frac{kJ}{mol} \qquad (2\text{-}20)$$

$$2H^+ + 2e^- \rightarrow H_2 \qquad \Delta G^0 = 0 \frac{kJ}{mol} \qquad (2\text{-}21)$$

The standard Gibbs free energy change ΔG^0 in the hydrogen splitting reaction is zero at all temperatures since it is a defined reference case [40]. Consequently, the standard electrode potential (E^0) equals 0 V. This implies that the applied potential solely arises from the open circuit voltage and overpotentials due to ohmic resistances and side reactions. An overview of the cell voltages, overpotentials, and FE are given in Table 3-4 (Section 3.2.2) and stem from the calculations in APPENDIX E. Overpotentials can cause heat production through resistive heating, which is explained in Section 3.3.

2.3.3. Cell Configuration

In general, PCECs for ethylene production consist of a proton-conducting electrolyte thin film, a porous hydrocarbon electrode (anode), and a porous hydrogen electrode (cathode). A desirable hydrocarbon electrode should possess a high electronic conductivity in combination with low area-specific resistance (ASR) and the ability to efficiently dehydrogenate ethane and oxidize hydrogen. For electrochemically enhanced NODH reactions, it is of crucial importance that the electrodes have a low tendency towards coking [36].

Two types of membrane reactors suited for this process include planar membrane reactors and tubular membrane reactors. Planar membrane reactors, due to their higher surface area to volume ratio in comparison with tubular membrane reactors, can potentially yield higher conversion rates [41]. Furthermore, the scalability of planar membrane reactors is more straightforward than their tubular counterparts [42]. Conversely, tubular membrane reactors exhibit superior robustness, tolerating higher pressures and temperatures. However, with an operating temperature of 550 °C and a pressure of 1 bar, (Section 3.1), this resilience is not deemed necessary, as a result, a planar membrane configuration was selected for the process design.

In a study by Wu et al., a configuration to produce ethylene and hydrogen from ethane in a planar membrane reactor is presented [6]. The key part of the membrane reactor is a PCEC of which the electrode and electrolyte materials are listed in Table 2-3. The fully assembled cell comprises a dense 15 µm-thick BZCYYb electrolyte thin film on a porous

BZCYYb-Ni hydrogen electrode support (450 µm) and a catalyst-integrated 3D ultra-porous perovskite PBFM (80 µm) as the hydrocarbon electrode.

Table 2-3: Cell configuration of the PCEC for hydrogen pumping mode as presented by Wu et al. [6].

Cell component	Material	Thickness [µm]
Hydrocarbon electrode	Catalyst-integrated 3D ultra-porous perovskite $(PrBa)_{0.95}(Fe_{0.9}Mo_{0.1})_2O_{5+\delta}$ (PBFM)	80
Electrolyte	Acceptor-doped barium zirconate cerate $BaZr_{0.1}Ce_{0.7}Y_{0.1}Yb_{0.1}O_{3-\delta}$ (BZCYYb)	15
Hydrogen electrode	Porous Ni-BZCYYb support $Ni\text{-}BaZr_{0.1}Ce_{0.7}Y_{0.1}Yb_{0.1}O_{3-\delta}$	450

The PBFM material is an appropriate choice for hydrocarbon electrodes due to its catalytic activity for fuel oxidation and anti-coking ability [43]. Nickel-free materials are intentionally chosen for hydrocarbon electrodes to avoid coking issues associated with nickel-based materials in contact with hydrocarbon feeds. In contrast, Ding et al. used a nickel-based hydrocarbon electrode, finding no carbonaceous buildup on the surface after a 45-minute test at 400°C, which resulted in negligible ethane conversion. However, at 500°C, coke formation was detected visually and via Raman spectroscopy. This indicates that raising the temperature from 400°C to 500°C significantly increases ethane thermodynamic cracking into carbon on nickel-based hydrocarbon electrodes [7]. This observation from the literature led to the decision to select a nickel-free material as the hydrocarbon electrode. The hydrogen electrode is a nickel containing BZCYYb support that gives strength to the PCEC, due to its relatively large thickness.

Both electrodes need current collectors and wires to create an electrical circuit for electron transfer. Wu et al. opted for silver mesh and wire, and to maintain consistency, the same materials will be used. Silver offers high conductivity and corrosion resistance but is expensive and has limited availability, which could hinder scalability. In the future, copper and aluminium could be considered viable alternatives.

2.3.4. Membranes

In membrane reactor systems, the established operating conditions determine the selection of an appropriate membrane. Membranes roughly fall into two distinct categories: organic and inorganic. Organic membranes, characterized by their carbon-based structure, are typically derived from polymers such as polyethene and polystyrene. On the other hand, inorganic membranes are fabricated from inorganic materials such as ceramics, silica, zeolite, palladium, or carbon and are commonly used in gas processing applications. A

comparison of organic and inorganic membranes following different performance criteria is given in Table 2-4 [44] [45]:

Table 2-4: Comparison of different performance criteria for organic and inorganic membranes.

Performance criteria	Organic membranes	Inorganic membranes
Temperature Range	Lower	Higher
Fabrication complexity	Easy	Complex
Cost	Lower	Higher (due to fabrication complexity)
Flexibility	Higher (due to polymeric nature)	Lower (brittle)
Chemical stability	Lower (more prone to degradation)	Higher (chemically and thermally more stable)
Permeability	Usually higher	Usually lower

Regarding the choice of an electrolytic membrane, BZCYYb exhibits high ionic conductivity at temperatures around 550 °C. This enables efficient and accurate control of the proton flux during the process [46]. As a result, the reaction rate can be controlled by regulating the voltage applied across the membrane.

2.3.5. Catalyst

The selection of an appropriate catalyst is crucial to the potential of electrochemically enhanced ethane dehydrogenation. Several potential catalyst materials have been identified, including platinum (Pt), chromium (Cr), gallium (Ga), and zeolite-based materials. Zeolites, being microporous aluminosilicate minerals, possess the capability to adsorb and release species, making them suitable catalysts [47]. The primary advantages of Pt and Ga-based catalysts include their high activity (conversion), selectivity towards ethylene, and prolonged lifespan. However, Pt and Ga come with the drawback of being expensive and less abundant [30]. An alternative involves the incorporation of iron oxides on zeolites. When supported on ZSM-5 zeolite, Fe oxides can serve as highly active, selective, and stable catalysts for the NODH reaction [29]. This catalyst choice would circumvent the cost and scarcity issue potentially arising from the industrial scaling of a PtGa/ZSM-5 catalyst-based system. Yet, given that Wu et al. chose a PtGa/ZSM-5 catalyst and published open-source data on the fractional conversions of the reaction, this catalyst was selected for use.

2.3.6. WINNER Project

Figure 2-10 shows the process conditions and Key Performance Indicators (KPIs) of ethane dehydrogenation in the WINNER project. Unfortunately, the material compositions of the PCECs as developed in the WINNER project are still confidential and are therefore intentionally left out of this report. Regarding the projected times to commercialization, a rough estimation is ten years. The WINNER consortium has not been able to produce a lab-scale pilot cell for the hydrogen pumping mode to date. General definitions of performance factors can be found in APPENDIX F.

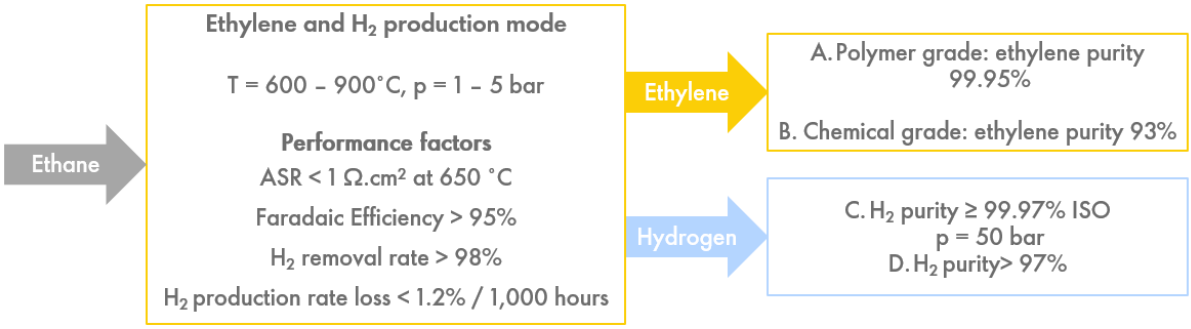

Figure 2-10: Process conditions and performance factors for ethane dehydrogenation to ethylene and pressurized H_2 in WINNER's PCCs (the figure was drawn based on [8]).

The KPIs in the co-production of ethylene and hydrogen are as follows [8]:

- ASR (Area Specific Resistance) of cells/stacks: < 1 Ω.cm² at 650°C, Faradaic Efficiency (FE) > 95%
- Validation of the durability of cells for at least 3,000 hours and validation of short stacks/mini reactors for at least 1,000 hours of operation
- Processing of hydrogen with a production loss rate of less than 1.2% / 1,000 hours

In electrochemistry, FE (Faradaic Efficiency) describes the efficiency of charge transfer in a system facilitating an electrochemical reaction [48]. In the context of the hydrogen pumping mode in the PCEC, as described in Section 2.3.2, the FE provides insight into the fraction of electrons effectively utilised for proton migration through the electrolyte compared to the total amount of electrons consumed by the system. The FE ($\eta_{Faradaic}$) can be calculated by using Equation (2-22) [6].

$$\eta_{Faradaic} = \frac{n_{H_2,actual}}{n_{H_2,theoretical}} = \frac{n_{H_2,actual}}{I * (z * F)^{-1}} * 100\% \qquad (2\text{-}22)$$

Where:

$\eta_{Fararadaic}$ is the FE of the process [%],
$n_{H2,actual}$ is the actual hydrogen production rate measured by experiments [mol/s],
$n_{H2,theoretical}$ is the theoretical hydrogen production rate [mol/s],
z is the number of transferred electrons per H_2 molecule [=2],
F is Faraday's constant [=96485 C/mol],

3. Conceptual Process Design

Chapter 3 outlines the conceptual process design for ethylene production in PCECs. It aims to answer the sub-question of how the process can be modelled in terms of unit operations. Section 3.1 explores the thermodynamic aspects of the process, focusing on reactor temperature and pressure. Section 3.2 discusses product removal, with an emphasis on hydrogen extraction through the membrane and its impact on (electro)chemical process parameters such as conversion, selectivity, yield, and FE (Faradaic Efficiency). Section 3.3 determines the feed source and gives a critical analysis of the choice of feedstock in referenced experiments. Section 3.4 presents the relevant separation conditions for the product stream leaving the PCEC reactor. Finally, Section 0 introduces the process flow diagram, followed by Section 3.6, which details each process unit and the associated assumptions. By breaking down the process into different process areas and dealing with thermodynamics, this chapter lays the groundwork for further analysis and assessments.

3.1. Thermodynamics

Table 3-1 provides an overview of the established process parameters:

Table 3-1: Process parameters used to conceptually model the WINNER process [6, 8].

Process parameters	Value
Reactor temperature	550 °C
Reactor pressure	1 bar
Hydrogen removal rate	95%
Hydrocarbon electrode	Catalyst-integrated 3D ultra-porous perovskite $(PrBa)_{0.95}(Fe_{0.9}Mo_{0.1})_2O_{5+\delta}$ (PBFM) – t = 80 µm
Membrane (thin film electrolyte)	Acceptor-doped barium zirconate cerate $BaZr_{0.1}Ce_{0.7}Y_{0.1}Yb_{0.1}O_{3-\delta}$ (BZCYYb) – t = 15 µm
Hydrogen electrode	Porous Ni-BZCYYb support Ni-$BaZr_{0.1}Ce_{0.7}Y_{0.1}Yb_{0.1}O_{3-\delta}$ – t = 450 µm
Catalyst	PtGa/ZSM-5

3.1.1. Reactor Temperature

High temperatures are required for the endothermic non-oxidative dehydrogenation of ethane as displayed in Equation (3-1) [30].

$$C_2H_6 \rightarrow C_2H_4 + H_2 \qquad \Delta H_{T=298K} = 137 \frac{kJ}{mol} \tag{3-1}$$

According to Le Chatelier's principle, increasing the temperature favours endothermic reactions, whereas decreasing the temperature favours exothermic reactions. Therefore, in this case, increasing the temperature increases conversion rates, which is desired. However, operating at high temperatures also has several downsides:

- Heating duties increase when operating at higher temperatures.
- High temperatures lead to increased thermodynamic cracking of ethane into carbon and favour coke formation. It promotes side reactions over ethane dehydrogenation and leads to lower ethylene selectivity [7].
- Elevated operating temperatures can lead to catalyst particle sintering. This sintering of catalysts leads to a decrease in active surface area, subsequently decreasing catalyst performance over time [6].

On the other hand, operating the system below 450 °C significantly reduces electrolyte conductivity and electrode catalytic performance, causing degradation of ohmic and polarization losses [6]. Therefore, optimizing the reactor temperature is crucial in maximizing ethylene production while minimizing side reactions and catalyst degradation.

Typical operating temperatures for the NODH process range from 600 °C to 800 °C, and the initial estimate regarding operating temperature from the WINNER project consortium lies between 600 °C and 900 °C. Yet, stable electrode and catalyst performance in PCEC configurations have only been observed in the 400-550 °C range. Consequently, an operating temperature of 550 °C is selected, as it provides sufficient data for conversion, selectivity, and yield to create a model. Figure 3-1 visualizes the pros and cons of different operating temperatures and the eventual choice to select an operating temperature of 550 °C.

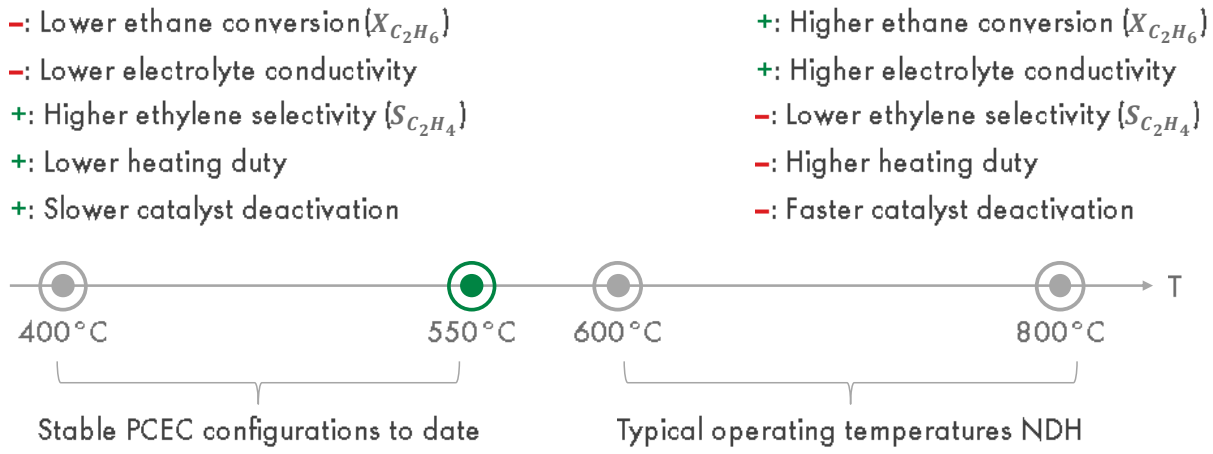

Figure 3-1: Graphic representation of the considerations for selecting operating temperature, showing the advantages and disadvantages of operating at relatively low and high temperatures. The chosen operating temperature of 550 °C is highlighted in green.

3.1.2. Reactor Pressure

Table 3-2 summarizes the effects of increasing reactor pressure on several process parameters. It should be read as: e.g., "Effect of pressure increase on equilibrium conversion." The pressure dependence on these process parameters is explained below.

Table 3-2: Influences of an increase or decrease in reactor pressure on several process parameters.

Effect of... on	**Pressure increase ↑**	**Pressure decrease ↓**
Equilibrium conversion	Decrease	Increase
Reactor size	Decrease	Increase
Materials strength requirements	Increase	Increase

The choice of operating pressure in the PCEC reactor involves balancing thermodynamic reasoning with economic considerations. The NOHD reaction (Equation (3-2))) concerns a reaction in which 1 mole of gas reactant (C_2H_6) converts into 2 moles of gas products (C_2H_4 and H_2). The ideal gas law (Equation (3-3)) states that pressure is proportional to the number of moles present. Therefore, the pressure will increase when ethane is dehydrogenated. According to Le Chatelier's principle, the system will try to reduce the increased pressure by shifting the equilibrium towards the side of the reaction with fewer gas molecules. In this case, the reactant (C_2H_6) side. So, operating at lower pressures is advantageous from a strictly equilibrium-based perspective.

$$C_2H_6 \rightarrow C_2H_4 + H_2 \quad (3\text{-}2)$$

$$pV = nRT \rightarrow p \propto n \quad (3\text{-}3)$$

Where:

p	is the reactor pressure [Pa],
V	is the reactor volume [m^3],
n	is the amount of substance [mol],
R	is the ideal gas constant [=8.314 J/(mol*K),
T	is the reactor temperature [K].

This thermodynamic favorability of lower operating pressures can be observed when looking at the NODH equilibrium conversion in Figure 2-6 (Section 2.2.2). At a temperature of 823K (550°C), the equilibrium conversion increases with decreasing pressure.

The main disadvantage of operating at low pressure is the increased reactor size, which increases capital expenditure (CAPEX). However, operating at higher pressure can also

increase CAPEX, because of the necessity for thicker-walled materials or components and compression costs. Besides, OPEX will also increase because of compression duties for both the feed and the recycle stream. By assuming the operating pressure to be atmospheric (1 bar), these additional capital and operational costs can be bypassed. This strategy balances the thermodynamic preference for low-pressure operations with the economic benefits of operating at ambient pressure. Besides, experimental data found on the fractional conversion of the main and side reactions occurring inside the PCEC are specified at a pressure of 1 bar [6].

3.2. Product Removal

3.2.1. Hydrogen

The goal of the WINNER project is to develop an integrated process of the ethane dehydrogenation reaction and the separation of hydrogen in a single-unit operation. The benefits of removing hydrogen in the reactor by creating a proton flux through the electrolytic membrane with an electrical circuit as the driving force are threefold:

- Higher conversions can be achieved by shifting the equilibrium.
- Pure, pressurized hydrogen is obtained as a valuable byproduct.
- Lower separation requirements reduce downstream process energy consumption.

As explained in Section 2.2.3, the electrolytic membrane qualifies as an active membrane. This means that an electrical circuit, connected to the cathode and anode of the PCEC, drives the proton flux across the membrane and subsequently determines the hydrogen removal. The hydrogen removal rate (R_{H2}) is expressed in Equation (3-4) [49]:

$$R_{H2} = \frac{V_{H2\ H2side}}{V_{H2\ total}} * 100\% \qquad (3\text{-}4)$$

Where:

R_{H2} is the hydrogen removal rate [%],

$V_{H2\ H2\ side}$ is the measured volume of hydrogen recovered at the high-pressure side of the reactor (H_2-side) [L/min],

$V_{H2\ cell}$ is the total measured volume of hydrogen evolved from the cell [L/min] ($=V_{H2\ H2\ side} + V_{H2\ hydrocarbon\ electrode}$).

Figure 3-2 shows a schematic illustration of PCECs operating in hydrogen pumping mode. The flow of hydrogen at the hydrocarbon electrode side and the hydrogen electrode side of the cell can be distinguished. These two flows determine the hydrogen removal rate (R_{H2}), which is defined as the flow of hydrogen measured at the hydrogen electrode (cathode) divided by the total measured flow of hydrogen evolved from the cell. It should be noted that the representation in Figure 3-2 is oversimplified since it does not display any by-product formation. In addition, the hydrogen flow at the hydrocarbon electrode

($V_{H2\ hydrocarbon\ electrode}$) forms part of the heterogeneous product stream that emerges from the PCEC reactor.

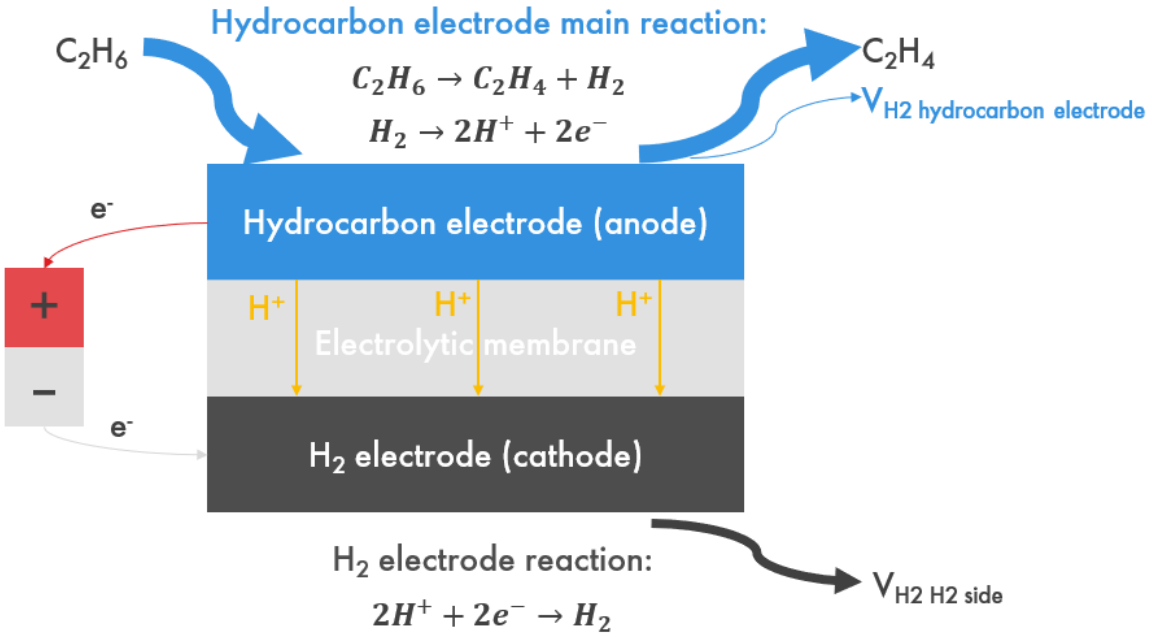

Figure 3-2: Schematic of PCECs for the co-production of ethylene and hydrogen in hydrogen pumping mode via the electrochemically enhanced NODH process (figure was drawn based on [38]).

The hydrogen removal rate affects various process parameters, which are shown in Table 3-3. It has the same structure as Table 3-2 and should be read as: e.g., "Effect of a high H_2-removal rate on C_2H_6 conversion."

Table 3-3: Effects of hydrogen removal on several process parameters [49].

Effect of a ... on...	**High H_2- removal rate**	**Low H2- removal rate**
Ethane conversion ($X_{C_2H_6}$)	High	Low
Byproduct formation	High	Low
Ethylene selectivity ($S_{C_2H_4}$)	Low	High
Ethylene yield ($Y_{C_2H_4}$)	High	Low
Coke formation	High	Low
Time between regeneration cycles	Short	Long
Downstream H_2 separation requirements	Low	High

Conversion is a measure that defines how much of a reactant has reacted in the process. In the NODH process, the definition of ethane conversion is shown in Equation (3-5):

$$X_{C_2H_6} = \frac{n_{C_2H_6,inlet} - n_{C_2H_6,outlet}}{n_{C_2H_6,inlet}} * 100\% \quad (3\text{-}5)$$

Where:

$X_{C_2H_6}$ is the ethane conversion [%],

$n_{C_2H_6,inlet}$ is the molar concentration of ethane in the inlet of the reactor [mol/m^3],

$n_{C_2H_6,outlet}$ is the molar concentration of ethane in the outlet of the reactor [mol/m^3].

The total outlet gas flow rate was monitored to account for potential volume changes. The volume expansion between the inlet and outlet is deemed negligible, so the molar concentration is assumed to be consistent with the number of moles flowing through the system [6].

The increase in ethane conversion with increasing H_2-removal rate can be explained following Le Chatelier's principle. When extracting hydrogen from the PCEC reactor by transferring it through the membrane, the partial pressure of hydrogen is lowered. A low partial pressure of hydrogen shifts the thermodynamic equilibrium of the reaction towards the product side, increasing ethane conversion [50]. Although high conversion is beneficial, achieving high selectivity is more valuable. A low single-pass conversion can be addressed by using a recycle stream, but improving selectivity is more challenging to accomplish. The definition of selectivity is given in Equation (3-6).

$$S_{C_2H_4} = \frac{n_{C_2H_4,outlet}}{n_{C_2H_6,inlet} - n_{C_2H_6,outlet}} * 100\% \quad (3\text{-}6)$$

Where:

$S_{C_2H_4}$ is the ethylene selectivity [%],

$n_{C_2H_4,outlet}$ is the molar concentration of ethane in the outlet of the reactor [mol/m^3].

A high H_2-removal rate impacts byproduct formation by continuously driving the equilibrium of the dehydrogenation reaction (Equation (3-2)) to the right. The reason for this is the increased ethylene production. The produced ethylene can further react with ethane or other ethylene molecules, forming heavier carbon chains [51]. This negatively impacts ethylene selectivity, which is defined in Equation (3-6). As more ethylene-consuming side reactions occur, $n_{C_2H_4,outlet}$ decreases, leading to a decrease in $S_{C_2H_4}$. The combination of ethane conversion and ethylene selectivity leads to the ethylene yield of the process (Equation (3-7)). This process parameter quantifies the fraction of the desired product to the ingoing feedstock.

$$Y_{C_2H_4} = X_{C_2H_6} * S_{C_2H_4} = \frac{n_{C_2H_4,outlet}}{n_{C_2H_6,inlet}} * 100\% \quad (3\text{-}7)$$

Where:

$Y_{C_2H_4}$ is the ethylene yield [%].

The different side reactions that take place in the PCEC reactor will be discussed in further detail in Section 3.6.2. Here, the mechanism of ethylene consumption through side reaction is displayed in Figure 3-12. Finally, the rate of coke formation increases with increasing hydrogen removal rate. This leads to a faster accumulation of coke in the reactor, requiring shorter times between catalyst regenerations cycles [49].

Sattler et al. found that operating at a hydrogen removal rate of close to 100% led to a decrease in ethylene yield. They attributed this reduction of ethylene yield to increased coking, which leads to catalyst poisoning, resulting in suppressed ethylene yield. In addition, increased coking rates lead to the decomposition of hydrocarbons into hydrogen and coke (Equation (3-8)), which facilitates the hydrogenation of ethylene [31]. This is the reverse reaction of the desired reaction and therefore unwanted (Equation (3-9)).

$$CH_4 \leftrightarrow C + 2H_2 \tag{3-8}$$

$$C_2H_4 + H_2 \rightarrow C_2H_6 \tag{3-9}$$

This observation stresses the fact that maintaining a hydrogen removal rate that approaches 100% is not desirable. A slight reduction in this rate to 95% resulted in an enhancement in ethane conversions, surpassing the equilibrium conversion at the specified operating conditions of 600 °C temperature and 5 atm pressure [31].

3.2.2. Faradaic Efficiency

The hydrogen removal rate depends on the proton flux through the membrane, a process driven by the supply of electrons through an electrical circuit. The FE (Faradaic Efficiency), as introduced in Section 2.3.6 (Equation (2-22)) quantifies the fraction of electrons that are effectively utilised for proton migration through the electrolyte compared to the total amount of electrons consumed by the system. Consequently, the electrons that contribute to the FE participate in the hydrogen splitting reaction (Equation (3-10)).

$$H_2 \rightarrow 2H^+ + 2e^- \tag{3-10}$$

In an ideal scenario (where FE = 100%), there would be two reactions – the thermochemical dehydrogenation of ethane and the electrochemical splitting of H_2. However, some phenomena can cause the FE to decrease.

Most protonic-ceramic electrolytes are Mixed Ionic-Electronic Conductors (MIECs). As a result, a certain level of 'electronic leakage' is observed that decreases the Faradaic Efficiency (FE). This suggests that part of the applied electrical current can be conducted through the membrane without generating a proton flux, and consequently, a hydrogen flux. This, in turn, leads to a decrease in FE [52].

Figure 3-3 shows the FE for different operating temperatures and applied current densities [6]. The dotted line represents the FE, while the solid line displays the H_2 evolution rate at the cathode of the PCEC. The H_2 evolution rate is proportional to the FE, as shown in Equation (2-22) in Section 2.3.6.

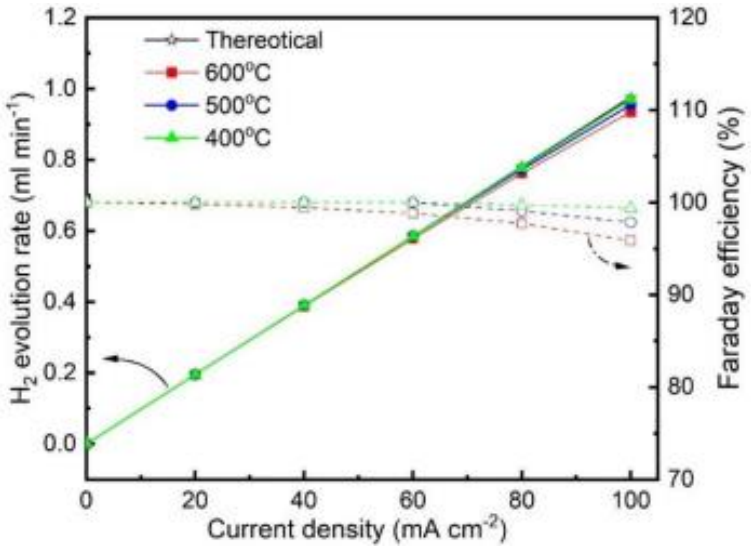

Figure 3-3: Faradaic efficiency for different operating temperatures, plotted against current density [6].

The FE decreases with increasing temperature and increasing current density. This stems from two interrelated underlying causes:

- In protonic-ceramic membranes like BZCYYb, used in this project, increasing Cerium content leads to an increase in FE. This increase in FE is attributed to a reduction in the ionic conductivity of the electrolyte. Nevertheless, when the temperature is elevated beyond 550 °C, an increase in anionic conductivity is observed. This anionic conductivity competes with proton diffusion across the membrane and could decrease the FE [52].
- An increase in current density increases resistive heating through Joule's law ((3-11). As a result, the local electrolyte temperature can be significantly higher than the PCEC reactor temperature of 550 °C. Relating this to the above-mentioned negative influence of temperature increases above 550 °C, this could explain the decrease of FE with increasing current density [52].

$$Q = I^2Rt \tag{3-11}$$

Where:

Q	is the heat generated [J],
I	is the current [A],
R	is the resistance of the PCEC [Ω],
T	is the time [s].

Wu et al. conducted an experiment that yielded empirical data on FE, as illustrated in Figure 3-3. The experiment was performed under conditions involving a current density of 40 mA/cm^2, a temperature of 550 °C, and a pressure of 1 bar, although note that these specific conditions are not explicitly stated in Figure 3-3. The hydrogen evolution rate in Figure 3-3 represents the protons diffusing through the membrane. Since there is no proton

flux over the membrane at zero current density, the resulting H_2 evolution rate is also zero. The hydrogen flow ($n_{H_2,actual}$) in Equation (2-22) is proportional to the applied current density. This can be observed in Figure 3-3 as the linear increase in H_2 evolution rate with increasing current density at low applied current densities. At higher applied current densities, the effect of a decreasing FE becomes visible as the H_2 evolution rate starts deviating from a purely linear line.

The data on fractional conversions for the different reactions within the PCEC reactor, extracted from this study, will be used later in this research. For the detailed Aspen Plus flowsheet of this process, please refer to APPENDIX G. From the given conditions, the FE was estimated to be 99.5%. The goal of the WINNER consortium is to eventually reach a current density of 1 A/cm^2 since a higher current density enables the reactor dimensions and thus CAPEX to come down. However, it should be noted that from the data available, it is not feasible to extrapolate the FE to a current density of 1 A/cm^2. As a solution to the unknown FE of the process at higher current densities, one of the KPIs of the WINNER consortium is taken as a reference. They aim for a FE of 95% at a current density of 1 A/cm^2 (Section 2.3.6). Therefore, the assumption is made that it will be feasible, in due course, to achieve a FE of 95% at a temperature of 550°C and a current density of 1 A/cm^2. This will require significant technological progress in terms of Research and Development (R&D) on materials engineering in the coming years.

Table 3-4 lists an overview of the cell voltages and FE at different current densities at a pressure of 1 bar and a temperature of 550°C. It considers two different scenarios – the experimental scenario from the lab-scale results of Wu et al. [6] and the goals of the WINNER consortium [8].

Table 3-4: Cell voltages and FE at different current densities [53].

Parameter	Wu et al. experiment	WINNER project goals
Current density (j)	j = 0.040 A/cm^2	j = 1.0 A/cm^2
Standard Potential (E^0)	0 V	0 V
Open Circuit Voltage (E_{OCV})	0.14 V	0.14 V
Overpotential (E_{OP})	0.04 V	1.0 V
Applied Voltage (V_{app})	0.18 V	1.14 V
Faradaic efficiency	99.5%	95%

3.3. Feed source

Electrochemically enhanced ethylene production requires the use of ethane as the primary feedstock. Before its use, ethane must be extracted from natural gas (NG) via a process known as natural gas liquids (NGL) recovery. The composition of the hydrocarbon feed

after NGL recovery is shown in Table 3-5, based on ethane purity specifications of multiple references for cryogenic ethane recovery processes [54-56]. These have been combined with feedstock data from Shell's Monaca ethane steam cracker. This ensures consistency in the feedstock between the benchmark and the PCEC system. It is assumed that the feed contains no further contaminants.

Table 3-5: Ethane feed composition.

Conditions	Value
Methane concentration	1.8 wt%
Ethane concentration	96.2 wt%
Propane concentration	2.0 wt%
Temperature	25 °C
Pressure	1 bar

In real-world applications, ethane derived from natural gas liquids (NGLs) recovery procedures typically enters the system under pressures ranging from 30 to 60 bar [57]. Consequently, this ethane feed must undergo depressurization to align with the PCEC reactor's operational pressure of 1 bar. This pressure reduction process results in a substantial cooling effect on the feed. However, this cooled feed could be utilised to reduce the temperature of the product stream exiting the PCEC reactor through a heat exchanger. Nonetheless, it is assumed that the ethane feed enters the process at a pressure of 1 bar in the current process design.

In addition to the ethane feed, water should be mixed with the incoming hydrocarbon feed. This is required to hydrate the protonic-ceramic membrane, which then conducts protons via the Grotthuss mechanism [58]. Under this mechanism, hydrogen molecules that are ionized into protons at the hydrocarbon electrode form bonds with water molecules within the ceramic membrane, creating hydronium ions (H_3O^+). These hydronium ions subsequently pass their proton to an adjacent water molecule, converting it into another hydronium molecule. This sequence repeats itself until the protons at the hydrogen electrode (cathode) recombine with electrons to generate hydrogen [59].

This thesis does not develop a kinetic reactor model. Thus, obtaining reliable data on the internal reactor process is crucial. Essential process parameters at the specified reaction conditions (T=550 °C, p=1 bar) are outlined in the paper and supplementary information by Wu et al. [6]. Their base experiments use a feedstock with a 10/90 molar ratio of ethane/argon (Ar) and a flow rate of 60 mL/min. A schematic representation of their experimental setup is illustrated in Figure 3-4. For the detailed Aspen Plus flowsheet, please refer to APPENDIX G.

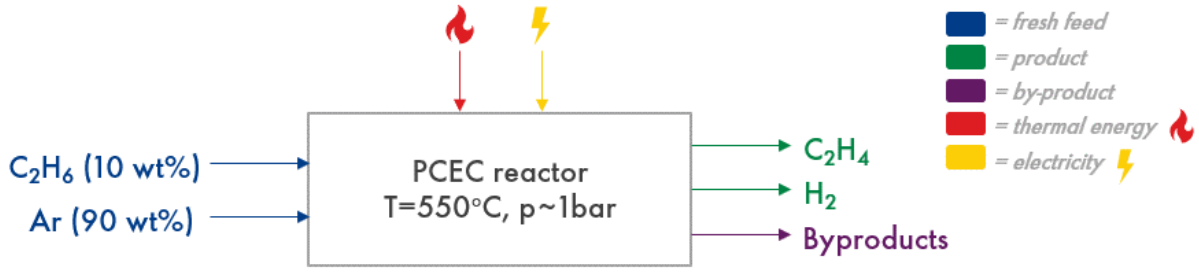

Figure 3-4: Schematic representation of the experimental setup by Wu et al. [6].

The use of argon (Ar), a noble and inert gas, is common in electrochemical experiments for its several advantages. It assists in reaction control, acts as a carrier gas, and helps regulate pressure. Including Ar in the feedstock can reduce the partial pressure of ethane, which can enhance selectivity. Additionally, it can improve electrode stability and reduce the risk of flammability hazards [60]. By purging out reactive gases from the reaction environment, an inert gas like Ar can increase selectivity by minimizing unwanted side reactions. Furthermore, using Ar in the feedstock can mitigate coking and lower unwanted side reactions, thereby enhancing ethylene selectivity.

In an industrial process, however, using Ar in the feedstock is unfavourable, as it increases the required reactor volume by increasing the volume of inert gas flowing through the reactor. Figure 3-5 illustrates the influence of an increase in ethane concentration in the feedstock on ethane conversion (X_{C2H6}), ethylene selectivity (S_{C2H4}), and ethylene yield (Y_{C2H4}) as defined in Equations (3-5) - (3-7). The figure contains a logarithmic x-axis and measured data points for 1/99, 10/90, and 100/0 molar feedstock compositions of ethane/Ar.

When ethane is dissolved in inert Ar within the feedstock, fractional ethane conversion [%] increases, using the conversion definition from Equation (3-12). A decrease in the molar concentration of ethane in the feedstock leads to a decrease in both $n_{C_2H_6,inlet}$ and $n_{C_2H_6,outlet}$. These lower molar concentrations cause a reduction of competing side reactions (Section 3.6.2). For example, a higher concentration of ethane may encourage dimerization reactions in adjacent catalyst sites rather than the dehydrogenation reaction of single molecules, which is the desired reaction.

$$X_{C_2H_6} = \frac{n_{C_2H_6,inlet} - n_{C_2H_6,outlet}}{n_{C_2H_6,inlet}} * 100\% \quad (3\text{-}12)$$

Conversely, increasing the ethane concentration in the feed leads to a decrease in selectivity, conversion, and subsequently yield. Figure 3-5 visualizes this, as a higher concentration of incoming ethane results in a smaller fraction being converted (indicated by the black line). The red line represents a decrease in ethylene selectivity with the rising ethane feed concentration. As the ethylene yield is a product of the conversion of ethane and ethylene selectivity, the blue line also declines with an increased concentration of ethane in the feed.

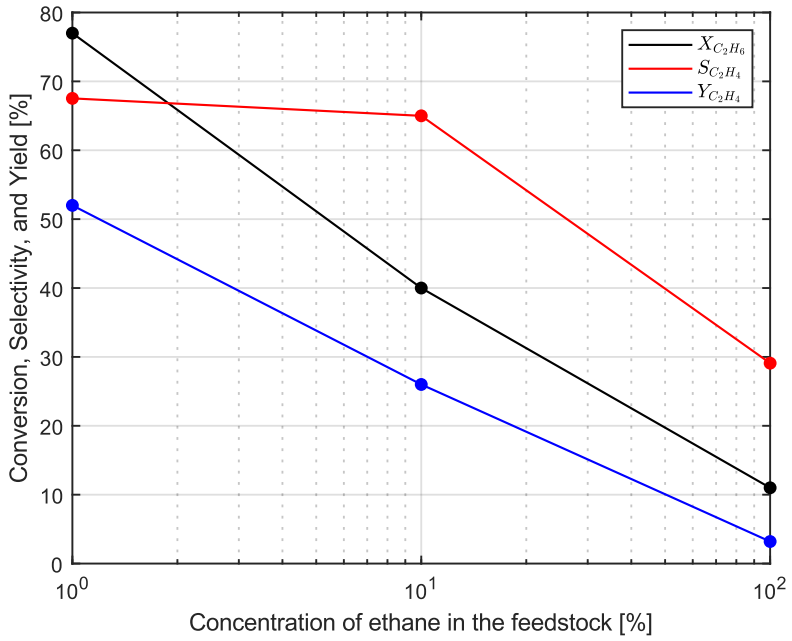

Figure 3-5: Conversion, Selectivity, and Yield using 1/99, 10/90, and 100/0 mol% feedstock compositions of ethane/Ar on a logarithmic scale (j = 40 mA/cm², p = 1 bar).

Even though the fractional conversion of ethane decreases with higher concentrations of ethane in the feed (as shown in Figure 3-5), Figure 3-6 shows that the absolute rates of ethane conversion [mol/min] and ethylene production [mol/min] increase with increasing ethane concentration in the feed. This is attributed to the fact that the flow of ethane grows by a factor of 10 and 100 when the ethane concentration shifts from 1% to 10% or 100%, respectively. However, the increase in the rate of ethane conversion and ethylene production does not correspond proportionally to the increase in the quantity of ethane supplied to the PCEC. For example, when moving from a 1% to 100% ethane concentration, the input moles of ethane rise by a factor of 100. In contrast, the rate of ethane conversion and ethylene production only increase by factors of 14 and 6, respectively. This is most likely a result of a decreasing kinetic rate due to catalyst deactivation caused by coke blocking active catalyst sites. It adheres to the negative implications of increasing the ethane concentration, as visualized in Figure 3-5.

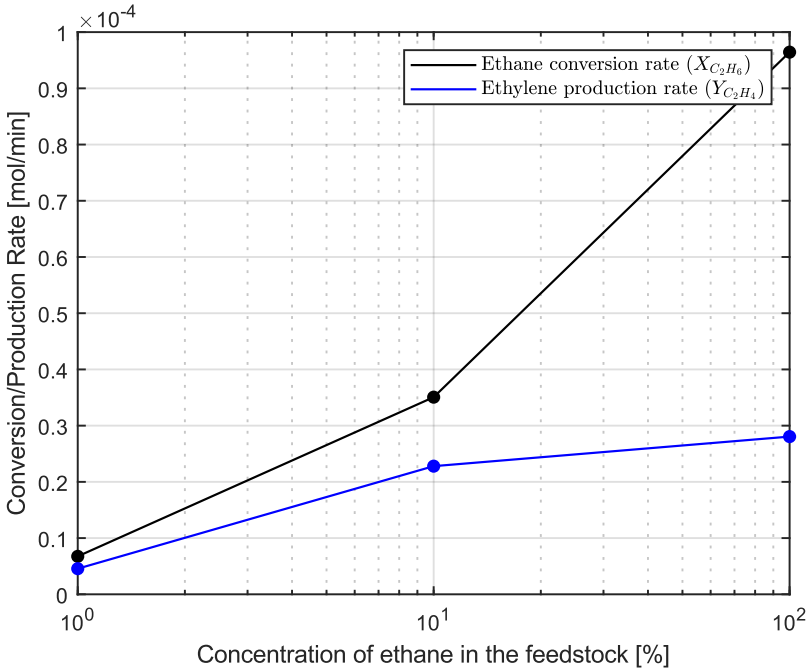

Figure 3-6: *Ethane conversion rate and ethylene production rate in mol/min using 1/99, 10/90, and 100/0 mol% feedstock compositions of ethane/Ar on a logarithmic scale (j = 40 mA/cm², p = 1 bar).*

In practical applications, the feedstock for the process design will contain close to 100% ethane. The resulting low ethylene yield, linked to the choice of a 100% ethane feedstock concentration, requires careful consideration in the process design and subsequent analyses. This is because it seems Wu et al. neglected the influence of increasing ethane concentration in the feed on fractional conversions. These fractional conversions were obtained from experiments with an ethane/Ar concentration of 10/90, whereas values are used in their process design using a 100% ethane feedstock [6]. This poses a risk of assuming overly optimistic values for the fractional conversions of the NODH reaction and associated side-reactions (Section 3.6.2). Section 4.5.1 mitigates this risk by designing different scenarios of fractional conversion. The definitions of conversion, selectivity and yield are similar to those defined in Equation (3-5) - (3-7). Experimental data from an experiment conducted by Wu et al. is used to model the process [6].

Figure 3-7 shows the ethane conversion, ethylene selectivity, and ethylene yield for different applied current densities, using a 100% ethane feedstock. The values for an applied current density of 40 mA/cm² correspond to the data points for a 100% ethane concentration in Figure 3-5 and Figure 3-6.

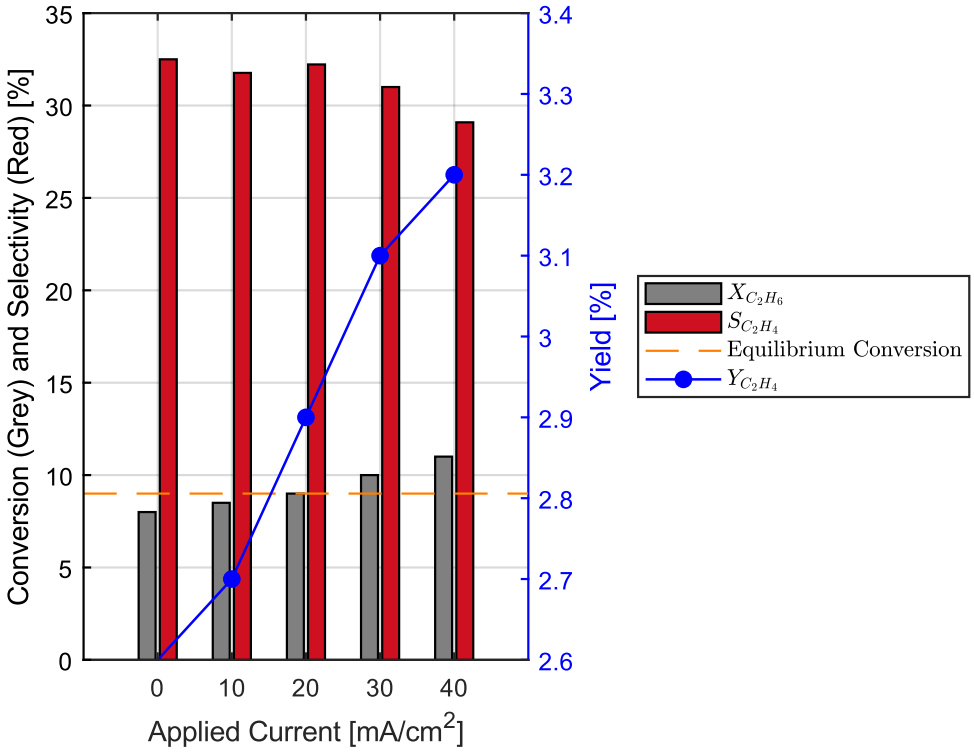

Figure 3-7: Conversion, Selectivity, and Yield for different applied currents using a 100% ethane feedstock at T = 550 °C, p = 1 bar.

At zero applied current, ethane conversion is 8%, whereas the equilibrium conversion of the NODH reaction is 9% (Section 2.2.2). This equilibrium conversion is shown by the dashed orange horizontal line at 9%. As the current density rises, ethane conversion increases to 11% at an applied current of 40 mA/cm^2, surpassing the NODH equilibrium conversion. This really shows the proof of concept of the electrochemical enhancement of conversion by making use of the protonic-ceramic membrane. Yet, ethylene selectivity decreases. This drop in ethylene selectivity is caused by increased selectivity towards higher (C_{3+}) hydrocarbons. This increase in C_{3+} selectivity stems from side reactions, such as the coupling of produced ethylene and its derivatives [6]. Two possible reasons for this are:

- Enhanced current density results in increased resistive heating, in line with Joule's law (Equation (3-13)).

This leads to elevated local temperatures in the PCEC, promoting side reactions that generate higher hydrocarbons. The process of forming higher hydrocarbons is typically facilitated by higher temperatures since the kinetic energy of the reactants is higher in these cases. This leads to more frequent collisions with greater energy, leading to increased reaction rates [61].

- Enhanced surface adsorption at higher current densities could result in a higher concentration of intermediate species on the electrode surface. This increases the likelihood of secondary reactions between intermediate species, potentially boosting the conversion of ethane, but decreasing the selectivity towards ethylene [6].

The catalyst, PtGa/ZSM-5, is not situated within a packed-bed reactor but is integrated within the 3D ultra-porous perovskite (PBFM) anode, as outlined in Table 3-1. This catalyst performs a dual role, facilitating both the thermochemical dehydrogenation of ethane and the electrochemical splitting of hydrogen. The integration of the catalyst within the PCEC anode provides a distinct advantage: it promotes the conversion of ethane by enabling the diffusion of hydrogen across the membrane.

An increased current density directly results in a higher proton flux over the membrane, thereby increasing the extraction of hydrogen from the hydrocarbon side of the PCEC. This enhanced hydrogen extraction positively influences the conversion of ethane. However, it is important to note that this effect may likely have a negative impact on the selectivity of ethylene. The reason being, alongside the desired ethylene, the process may also yield an increased quantity of unwanted byproducts, like coke (Table 3-3).

3.4. Separation Conditions

In the PCEC reactor, ethane feedstock reacts to form ethylene and byproducts. Part of the hydrogen permeates through the electrolytic membrane, as explained in Section 3.2.1, and is recovered at the hydrogen electrode of the reactor. However, the mixed product stream – which consists of ethylene, hydrogen, unreacted ethane, and other byproducts – that leaves the hydrocarbon electrode requires further downstream separation. Required product specifications, such as ethylene purity, prescribe the downstream separation and purification requirements. The requirements for polymer-grade ethylene purity are listed in Table 3-6.

Table 3-6: Polymer-grade ethylene specifications [62].

Component	Limits	Specification
Ethylene	% mole min	99.95
Methane + Ethane	ppm mole max	500
Hydrogen	ppm mole max	5
C_3 and heavier	ppm mole max	3

The conditions for separation depend on the different boiling points for the species in the product stream at different pressures. Section 3.6.2 gives an overview of the reactions and

side reactions that take place in the PCEC reactor and describes the associated mechanism. A schematic representation of the anodic and cathodic product streams is displayed in Figure 3-8. The downstream separation requirements stem from the mixed anodic product stream illustrated in blue.

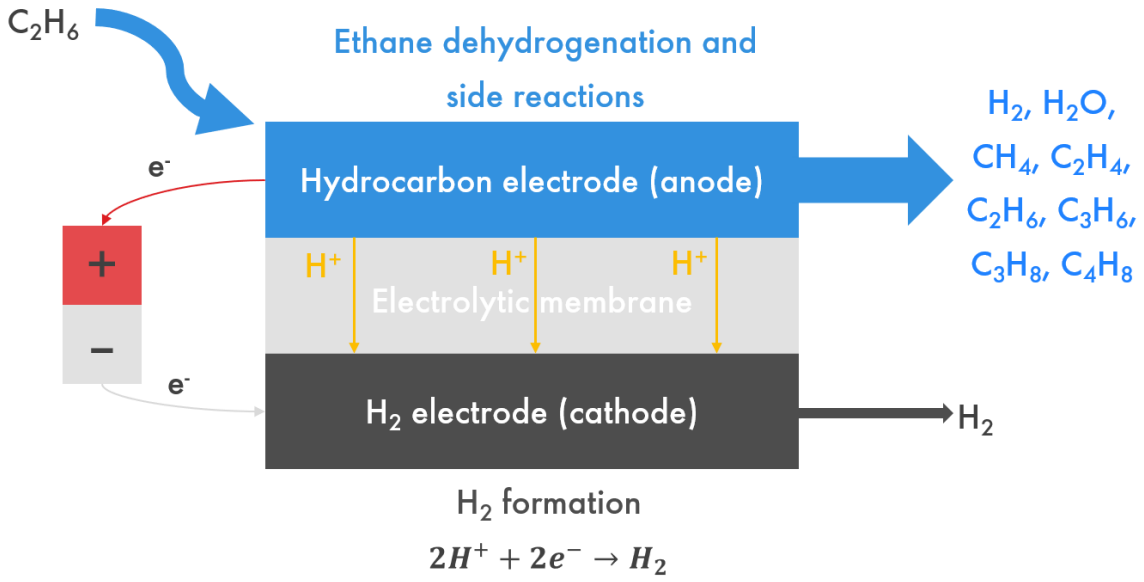

Figure 3-8: Anodic and cathodic product streams coming out of the PCEC reactor.

The mixed product stream from the reactor consists of several species, each with a unique boiling point under atmospheric pressure, as shown in Table 3-7. To enable later benchmark comparison, a similar separation method of cryogenic separation is chosen. Section 3.6.5 specifies the operating conditions, column specifications, input streams and output streams of the individual cryogenic distillation columns.

Table 3-7: Boiling points of product stream components [63].

Product components	Boiling Point [°C]
Hydrogen	-253
Methane	-162
Ethane	-89
Ethylene	-104
Propane	-42
Propylene	-48
Butene	-6

3.5. Process Flow Diagram

When performing process simulations with Aspen Plus, it is critical to choose the appropriate property method. The property methods in Aspen Plus correspond to distinct equations of state (EOS). An EOS is a mathematical model that characterizes the state of matter under specified physical conditions. The most well-known EOS is the Ideal Gas Law, represented by Equation (3-3) in Section 3.1.2, which provides a reliable approximation under ideal circumstances for gases.

However, to account for real-world phenomena like intermolecular phase-change interactions and the finite size of molecules, more complex equations are required [64]. This led to the choice of the Peng-Robinson (PENG-ROB) EOS. For the consulted decision tree and associated EOS, refer to APPENDIX H [65]. The PENG-ROB method was selected using the property method selection by Aspen Plus. This choice aligns with the property method selection of the simulations from which data was extracted [6, 66], and also adheres to guidelines found in Aspen Plus manuals [67].

Figure 3-9 shows the Aspen Plus flowsheet, broken down into various process areas. For a plain flowsheet with larger dimensions, refer to APPENDIX I.

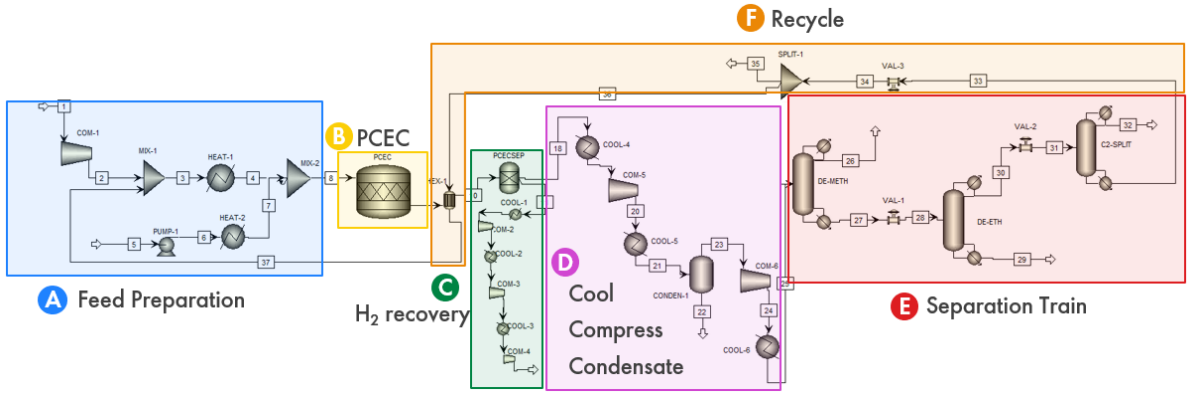

Figure 3-9: Aspen Plus flowsheet highlighting different process areas.

Each process area in the Aspen Plus flowsheet is indicated by a letter, and their corresponding functions are outlined in Table 3-8. The separate process units and streams will be discussed in Section 3.6. An overview of process design choices and assumptions is given in APPENDIX J.

Table 3-8: Function of the different process areas.

Letter & Name	Function
A – Feed preparation	Heat ethane feed to T = 550 °C and combine with steam (2 wt%) to keep the membrane hydrated.
B – PCEC	Perform non-oxidative dehydrogenation of ethane and side-reactions.
C – H_2 recovery	Mimic the function of the electrolytic membrane in Aspen Plus to separate and pressurize H_2 to p=50 bar.
D – Cool, compress, condensate	Prepare product stream for cryogenic separation (T = –50 °C, p = 35 bar) and remove water through condensation.
E – Separation train	Separate product stream in three stages to eventually recover ethylene, byproducts, and ethane for recycling.
F – Recycle	Recycle the unreacted ethane back into the process and purge 1% of this stream to prevent product accumulation. In addition, it uses heat to pre-heat the recycled ethane.

3.6. Process units

This section delves into the details of individual process units as they are modelled in Aspen Plus. To gain a comprehensive overview of each process stream and unit, refer to Table 0-2 in APPENDIX K.

3.6.1. Feed Preparation (A)

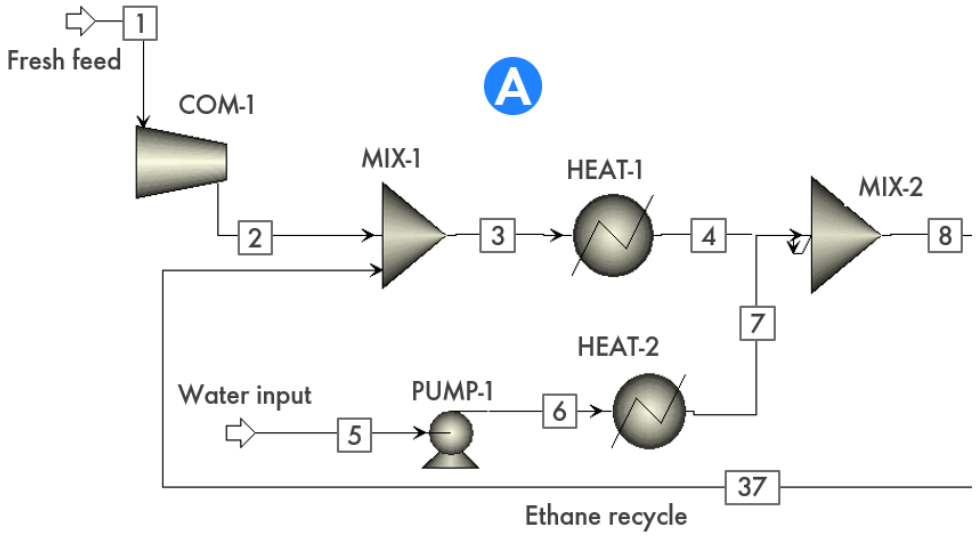

Figure 3-10: Feed Preparation process area (A), which heats the incoming ethane feed and combines it with steam to keep the reactor membrane hydrated.

The feed preparation section, as depicted in Figure 3-10, blends the fresh ethane feed (1) with steam (7) and recycled ethane (37). In the scenario where the operating pressure

within the PCEC reactor is 1 bar, the input and output pressures of both COM-1 and PUMP-1 are identical. As a result, these units could be skipped from the process in the base case (T = 550°C and p = 1 bar). However, they are intentionally included in the design to facilitate future pressure changes in a sensitivity analysis. Key considerations and observations for this stage include:

- Water is introduced at 2 wt% of the fresh ethane feed.
- The input and output pressures of COM-1 and PUMP-1 for the base case are equal.
- The ethane recycle (37) has been pre-heated by a heat exchanger to T=542°C.

3.6.2. PCEC reactor (B)

The PCEC reactor is modelled as a stoichiometric reactor, operating at 550°C and 1 bar. By default, these reactors run isothermally, so the outgoing stream (9) has the same temperature as the ingoing stream (8). The energy required to sustain the endothermic reactions and therefore maintain the PCEC reactor at a constant temperature of 550°C is obtained by combusting the produced fuel gas (Section 4.3.1). The PCEC reactor is shown in Figure 3-11.

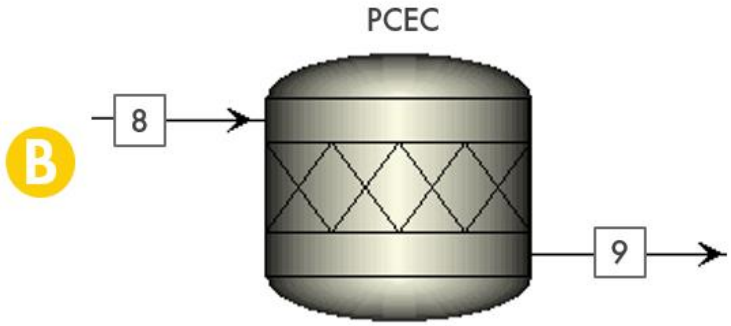

Figure 3-11: PCEC reactor process area (B), which carries out the NODH of ethane and associated side reactions at a temperature of 550°C and a pressure of 1 bar.

The six reactions outlined in Table 3-9 describe the kinetic reactions within the PCEC reactor [66]:

- Reaction 1 constitutes the primary route for ethylene production, involving the non-oxidative dehydrogenation of ethane. In this reaction, ethane is produced at the anode (hydrocarbon electrode), while hydrogen is generated at the cathode (hydrogen electrode) (refer to Figure 3-2).
- Reactions 2 and 3 are considered side reactions. They occur at the hydrocarbon electrode but do not consume any of the ethylene produced in reaction 1.
- Reactions 4 and 5, also taking place at the hydrocarbon electrode, are side reactions as well. However, these reactions consume a portion of the ethylene that was produced in Reaction 1.
- Lastly, reaction 6 characterizes the coking mechanism that causes catalyst deactivation and electrode surface contamination. This reaction is shaded to

indicate that the coking mechanism is not within the scope of this study, as will be explained hereafter.

Table 3-9: Reactions and corresponding conversions inside the PCEC reactor [66].

#	Stoichiometry	Fractional conversion	Limiting reactant
1	$C_2H_6 \leftrightarrow C_2H_4(anode) + H_2(cathode)$	0.363	Ethane
2	$2C_2H_6 \leftrightarrow C_3H_8 + CH_4$	0.02	Ethane
3	$C_3H_8 \leftrightarrow C_3H_6 + H_2$	0.8	Propane
4	$2C_2H_4 \leftrightarrow C_4H_8$	0.23	Ethylene
5	$C_2H_6 + C_2H_4 \leftrightarrow C_3H_6 + CH_4$	0.032	Ethylene
6	$CH_4 \leftrightarrow C + 2H_2$ $(Coke\ formation)$	0.07	Methane

While Wu et al. assumed the coking reaction (6) to follow Equation (3-13), other coking reactions, besides the dehydrogenation of methane, could likely occur. For instance, the cracking of ethylene (Equation (3-14)), and the polymerization of ethylene to butene and subsequent cracking into coke (Equation (3-15)) are potential additional coking reactions [68]:

$$CH_4 \leftrightarrow C + 2H_2 \quad (3\text{-}13)$$

$$C_2H_4 \leftrightarrow 2C + 2H_2 \quad (3\text{-}14)$$

$$2C_2H_4 \leftrightarrow C_4H_8 \quad C_4H_8 \leftrightarrow 4C + 4H_2 \quad (3\text{-}15)$$

To scope this research, the coking mechanism is not considered when simulating the process. However, for future studies it is an important aspect to consider, since it can affect the regeneration requirements of the process, fractional conversions, and catalyst lifetime.

Figure 3-12 visualizes the reaction mechanism taking place in the PCEC reactor. Side reactions 4 and 5 consume part of the ethylene, which is initially produced in Reaction 1. This partial consumption of produced ethylene is accounted for by scaling up the plant to ultimately reach a 100KTA polymer-grade ethylene output. The PCEC reactor is programmed such that the reactions in Table 3-9 occur sequentially.

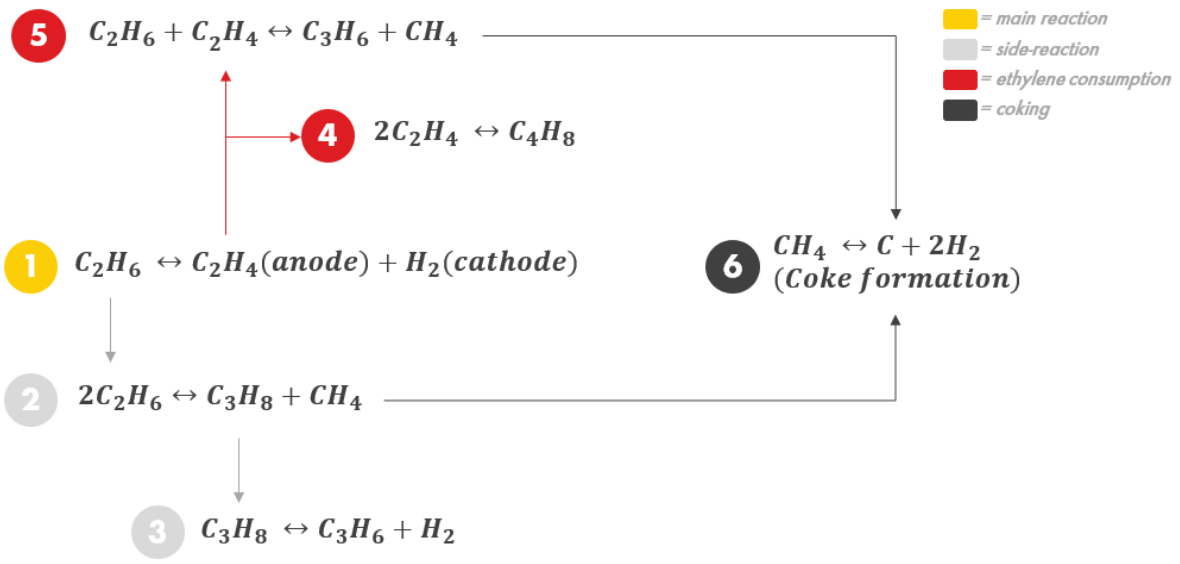

Figure 3-12: Main reaction and side reactions occurring inside the PCEC reactor.

The assumption that Steam Methane Reforming (SMR) does not occur in the PCEC reactor is substantiated in APPENDIX L. It also explains the reason behind the absence of both CO_2 and CO in the product stream.

3.6.3. Hydrogen Recovery (C)

Following the reactor, a separation unit is deployed. Since a PCEC with the ability to selectively let hydrogen diffuse through a membrane is not a pre-defined unit in the model palette of AspenPlus, the separation unit (PCECSEP) mimics the effect of hydrogen removal in the reactor. After the separation of hydrogen, it needs to be cooled down and compressed to mimic the electrochemical hydrogen compression function of the membrane. This is done by interstage cooling (COOL-1, COOL-2, and COOL-3) and compression (COM-2, COM-3, COM-4). Figure 3-13 shows the hydrogen recovery process area.

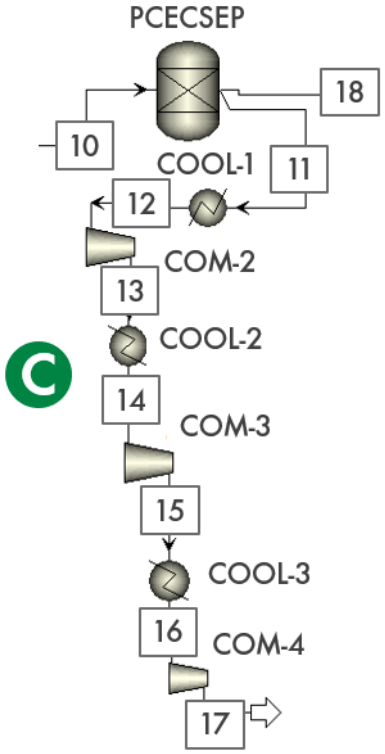

Figure 3-13: Hydrogen Recovery process area (C), which mimics the function of the electrolytic membrane in AspenPlus to separate 95% of the produced hydrogen and pressurize it to p=50 bar.

Table 3-3 in Section 3.2.1 explains the effects of hydrogen removal om multiple process parameters. Here the experiment of Sattler et al. was also mentioned, highlighting that a hydrogen removal rate that approaches 100% is not desirable [31]. Therefore, a hydrogen removal rate of 95% is assumed. As a result, the PCECSEP separates 95% of the hydrogen in the incoming product stream (10) towards the interstage cooling and compression system, where the hydrogen is cooled and compressed to a pressure of 50 bar. In reality, the proton-conducting membrane serves as a means for electrochemical membrane compression [53]. The calculation for the electrical energy requirement for hydrogen compression is done in APPENDIX E and results in a duty of 8.5 MW for 100 KTA ethylene capacity and 58.9 MW for 1500 KTA capacity. Key considerations and observations for the hydrogen recovery stage include:

- Hydrogen removal rate (R_{H2}) = 95%.
- PCECSEP mimics the function of the BZCYYb protonic-ceramic membrane.
- Duties of PCECSEP, COOL-1, COOL-2, COOL-3, COM-2, COM-3, and COM-4 can be replaced by the calculation of the electrical energy requirement of electrochemical compression. This leads to a value of 8.5 MW for 100 KTA ethylene capacity and 58.9 MW for 1500 KTA ethylene capacity (APPENDIX E).

3.6.4. Cool, Compress, Condensate (D)

The residual product stream coming out of the PCECSEP proceeds towards the interstage cooling, compression, and condensation process area, illustrated in Figure 3-14. The goal of this sequence of process units is to prepare the product stream for cryogenic separation by eliminating water from the stream through condensation, by cooling to a temperature of -50 °C, and by compressing to a pressure of 35 bar. Water should be removed from the product stream before cooling to temperatures below 0 °C to prevent ice formation. Key considerations and observations for the cool, compress, and condensate stage include:

- Additional condensers and/or drying units could be introduced in future designs to eliminate more H_2O from the product stream and minimize the change of ice formation.
- Compressors are modelled as isentropic compressors with an efficiency of 72%.

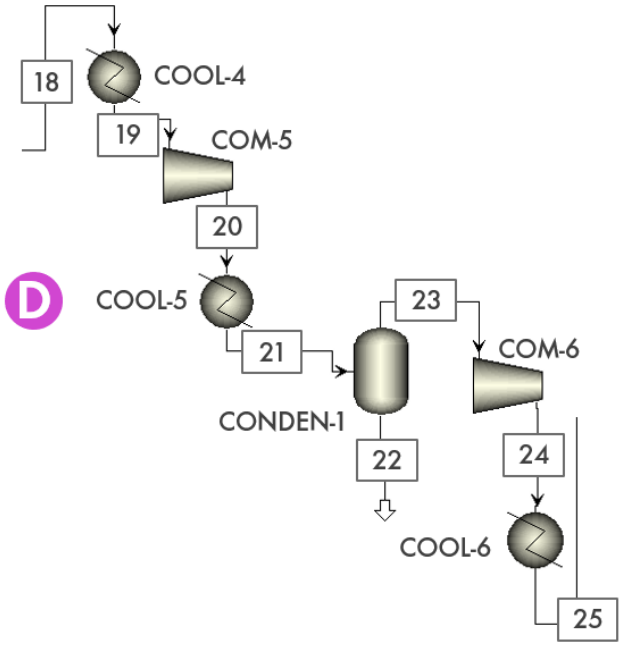

Figure 3-14: Interstage cooling, compression, and condensation process area (D), which prepares the product stream for cryogenic separation (T=-50 °C, p=50 bar) and removes water through condensation.

3.6.5. Separation Train (E)

The objective of the separation train is to recover the individual products with a defined purity level to be able to sell or further process them. This is accomplished via cryogenic distillation, explained in APPENDIX M. The separation train, shown in Figure 3-15, consists of a demethanizer, a de-ethanizer, and a C_2-splitter. For detailed specifications of each distillation column and an explanation of the role of the Light Key (LK) and Heavy Key (HK) in the separation process, refer to APPENDIX N.

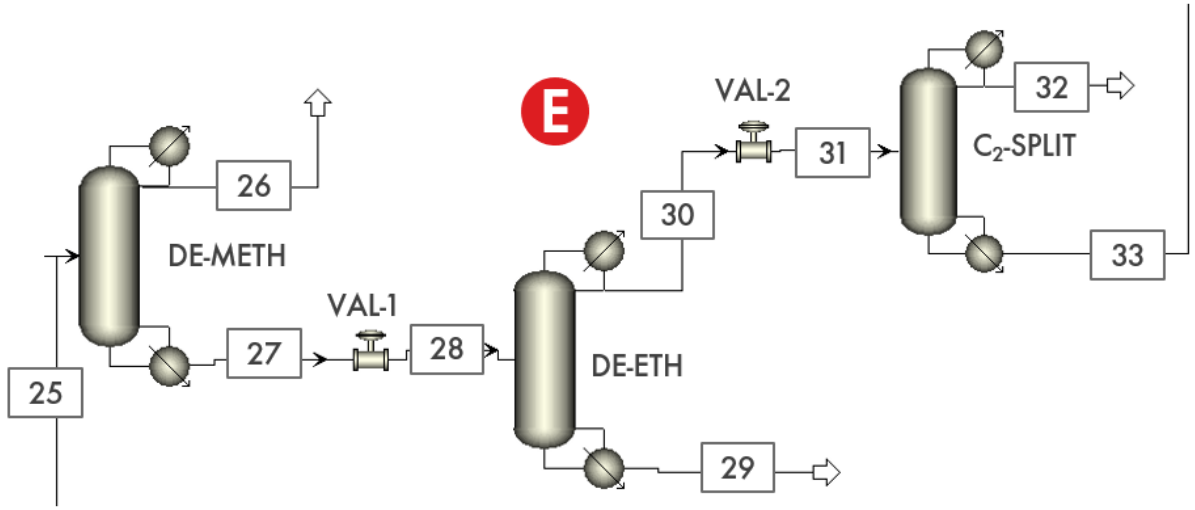

Figure 3-15: Separation Train process area (E), which separates the product stream in three stages to recover ethylene, byproducts, and ethane for recycling.

Different configurations in terms of the order of separation units can be selected based on process requirements and energy efficiency. The choice and underlying rationale for the order of distillation columns are described below. Key considerations and observations for the hydrogen recovery stage include:

- The separation units are modelled as Distillation Shortcut With Rigorous Thermodynamics (DSTWU) columns. This method enables a preliminary design without the need for a rigorous simulation.
- All distillation columns are placed after the PCEC reactor due to pressure advantages: all separation units operate under high pressures. An alternative configuration could place a de-ethanizer before the PCEC reactor to remove the C_{3+} components before entering the reactor. However, this would require an increase and subsequent decrease in pressure before reactor entry.
- Components are separated in a light-to-heavy sequence in the order of demethanizer, de-ethanizer, and C_2-splitter. This conventional approach (front-end demethanizer) is selected as lighter components have lower boiling points, and rearranging the sequence of distillation columns would require interstage cooling.
- A potential drawback of the current configuration is the relatively small volume of the light component stream (26) when compared to the C_{3+} components (29). Reversing the sequence (i.e., front-end de-ethanizer) could reduce equipment size as a larger stream would be segregated early in the separation train.
- Stream 26 is a mix of roughly 60 mol% CH_4 and 40 mol% H_2. Steam 29 is a mix of approximately 5 mol% C_3H_6, 29 mol% C_3H_8, and 65 mol% C_4H_8. To be able to sell the individual products, these should be further separated. In the case of stream 26, this can be done through membrane separation of H_2 and CH_4. In the case of stream 29, this can be achieved through a depropanizer and subsequent C_3-splitter. However the current configuration of the separation train is intentionally

chosen to be consistent with the Monaca benchmark, which will be used for quantitative comparison in Chapters 4 and 5.

3.6.6. Recycle (F)

Since the single-pass fractional conversion of ethane to ethylene is only 0.363 (see Table 3-9), the product stream contains significant amounts of unreacted ethane. The purpose of the recycling, illustrated in Figure 3-16, is to feed this unreacted ethane back into the system. Key considerations and observations for the recycle include:

- 1% of the ethane recycle is purged to prevent the accumulation of contaminants in the cycle (35).
- The temperature of the ethane recycle is lowered to 1 bar through a valve (VAL-3) to match the operating pressure of the PCEC reactor.
- A heat exchanger is used to pre-heat the cooled down ethane recycle (36) with latent reactor heat. This leads to a temperature of 542 °C of the ethane recycle (37), which almost matches the reactor temperature of 550 °C.

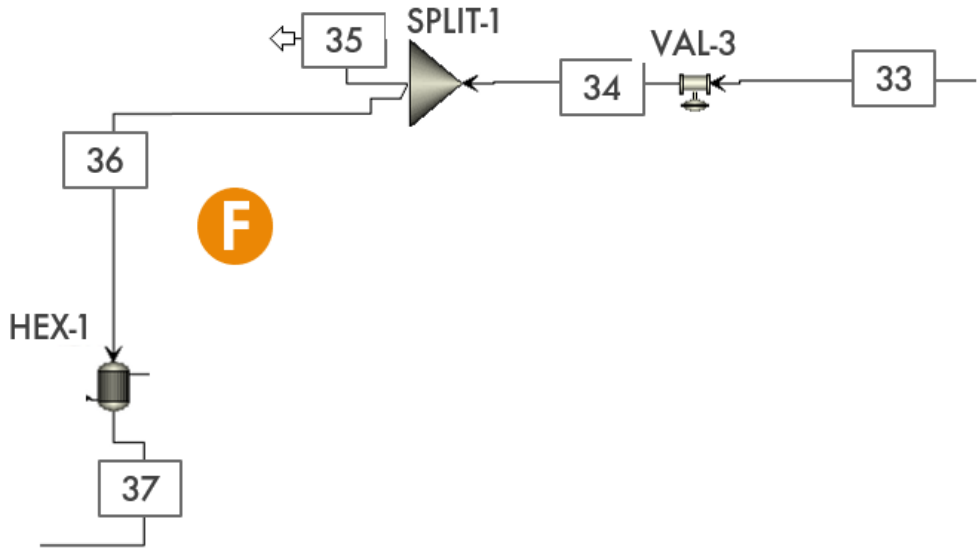

Figure 3-16: Recycle process area (F), which recycles the unreacted ethane back into the process and purges 1% of this stream to prevent product accumulation. In addition, it uses the heat from the PCEC reactor product stream to pre-heat the recycled ethane.

4. Process Simulations

This chapter outlines the results of the AspenPlus process simulations, focusing on energy consumption, product outputs, and highlighting the key assumptions made. The base case is slightly adjusted to enable a fair comparison between the WINNER process and the Monaca benchmark in the TEA (techno-economic analysis) in Chapter 5. Section 4.1 introduces the base case scenario, its associated assumptions, and outcomes in terms of process duties and product outputs. Section 4.2 presents the process duties and product outputs for the Monaca benchmark, while Section 4.3 compares both processes. This comparison stresses the need to introduce some process analysis adjustments, detailed in Section 4.4. Finally, Section 4.5 presents a scenario related to fractional conversions and another scenario considering e-cracking.

4.1. Base case scenario

4.1.1. Assumptions

Table 4-1 gives an overview of the assumptions made and the calculated values used for the process parameters in the conceptual process design.

Table 4-1: Overview of assumed and calculated process parameters.

Process parameter	Assumption/Value	Unit	Reference
Capacity (polymer-grade ethylene)	100	KTA	N/a
Reactor temperature	550	°C	[6]
Reactor pressure	1	bar	[6]
Current density (j)	40	mA/cm^2	[6]
Faradaic Efficiency (FE)	99.5	%	[6]
Area Specific Resistance (ASR)	1	Ω/cm^2	[8]
Open circuit voltage (V_{OCV})	0.14	V	[53]
Overpotential ($V_{Overpotential}$)	0.04	V	[53]
Cell voltage (V_{cell})	0.18	V	[53]
Operating year	8410	hours/year	N/a

In evaluating the potential performance of the non-oxidative dehydrogenation of ethane in PCECs, several assumptions regarding process parameters have been made. The system operates with a capacity of 100 KTA polymer-grade ethylene and under specific conditions: a temperature of 550°C, a pressure of 1 bar, and a current density of 40

mA/cm^2. The process assumes a FE of 99.5% and an Area-Specific Resistance (ASR) of 1 Ω/cm^2. The Open Circuit Voltage (OCV), overpotential, and cell voltage are 0.14V, 0.04V, and 0.18V respectively. These parameters are considered in the scenario of a plant operating for 8410 hours per year. The assumption regarding the operating year of the plant is substantiated in Section 5.1. In addition to the process parameters, assumptions have also been made regarding the associated energy consumption analysis.

Table 4-2: Overview of assumptions used for energy consumption analysis.

Process	Type of energy consumption
Cooling processes (T > 25°C)	Cooling water
Cooling processes (T < 25°C)	Refrigerants, which consume electricity
Heating processes	(1) Priority: produced fuel gas (2) Else: external Standard Refinery Fuel (SRF)
Demethanizer (DM) duties	Reboiler + condenser: electricity
De-ethanizer (DE) duties	Reboiler: cooling water Condenser: electricity
C_2-splitter duties	Reboiler + condenser: electricity

Several assumptions are made regarding heating and cooling processes in the energy consumption analysis. For cooling processes above 25°C, cooling water is utilized, while electricity-consuming refrigerants are used for temperatures below 25°C. Heating processes prioritize the use of produced fuel gas before switching to external Standard Refinery Fuel (SRF).

Distillation column process duties are selected based on operating temperatures. If reboilers and condensers operate above 25°C, they use cooling water. Conversely, for temperatures below 25°C, they use electricity-consuming refrigerants. As a result, the DM (demethanizer) unit employs electricity for both the reboiler and condenser. The DE (de-ethanizer) unit uses cooling water for the reboiler and electricity for the condenser. All duties in the C_2-splitter are fulfilled by electricity. For detailed information, refer to APPENDIX K and APPENDIX N.

4.1.2. Duties

In the base case scenario simulated through AspenPlus, the process duties – categorized as cooling water, heating, and several electrical duties – have been identified to produce 100 kton ethylene annually. Figure 4-1 visualizes these duties, broken down as follows:

- Cooling water - Cooling processes above a temperature of 25°C, assumed to consume cooling water, stem from coolers involved in interstage cooling and

compression after the reactor (Section 3.6.4) and the reboiler in the DE (Section 3.6.5).

- Heating – Heating duties prioritize the consumption of produced fuel gas before utilizing Standard Refinery Fuel (SRF). These heating requirements are attributed to the furnaces that heat the incoming feed and supply the thermal energy required for the endothermic reaction in the PCEC reactor (Section 3.6.1).

- Electricity (Reactor) – Electrical energy requirements for electrochemical hydrogen splitting, diffusion, and compression within the PCEC reactor. Section 3.6.3 explains these phenomena and APPENDIX E provides the equations for the electrical energy requirements for hydrogen compression.

- Electricity (BoP) – Electrical energy requirements attributed to the use of compressors in the process.

- Electricity (Cry. Sep.) – Cooling processes below a temperature of 25°C consume refrigerants. These relate to the reboilers and condensers in the cryogenic distillation columns used in the product separation sections (Section 3.6.5) as well as the coolers operating at a temperature below 25°C. Refrigerated cooling processes are assumed to exclusively consume electricity during the compression required to eventually cool the refrigerants through expansion.

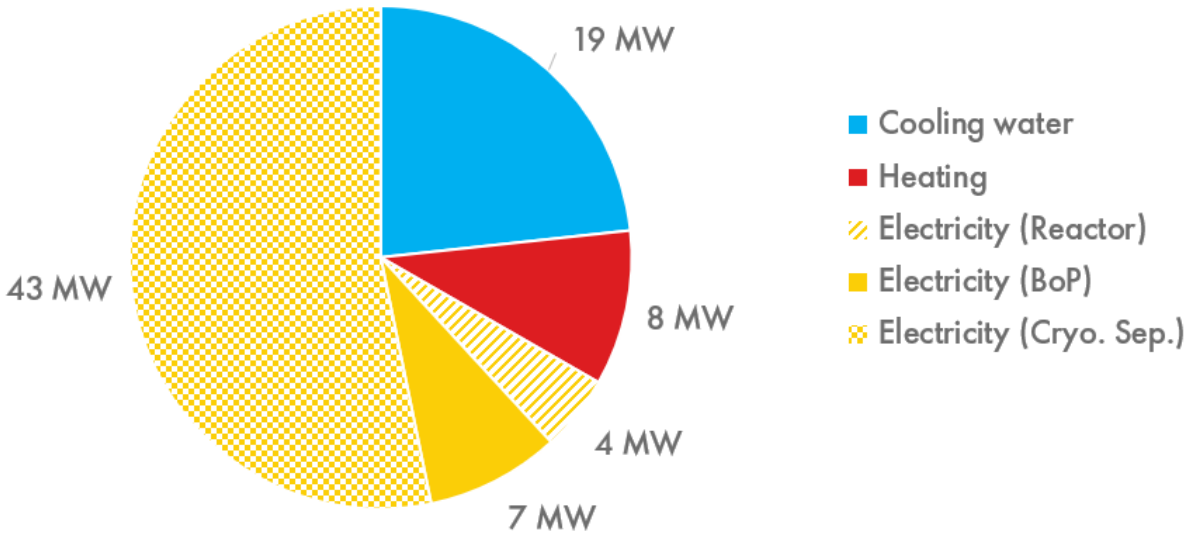

Figure 4-1: Process duties for the base case scenario (100 KTA) in MW, broken down into cooling water, heating and several electrical energy consumptions.

Most of the energy requirements in the process relate to electrical consumption, comprising 67% of the total (81 MW). This is primarily due to the use of refrigerants in the cryogenic separation process (Cryo. Sep.). Cooling water requirements account for 23%

of the process's total energy consumption. Interestingly, the duty for the PCEC reactor only accounts for 5% of the overall process duties. As such, the most significant contributor to the total energy requirements of the process is the downstream product separation that occurs post the PCEC reactor, which covers more than half of the tot process duties.

Figure 4-2 shows the accumulated process duties, broken down into the different categories of process equipment.

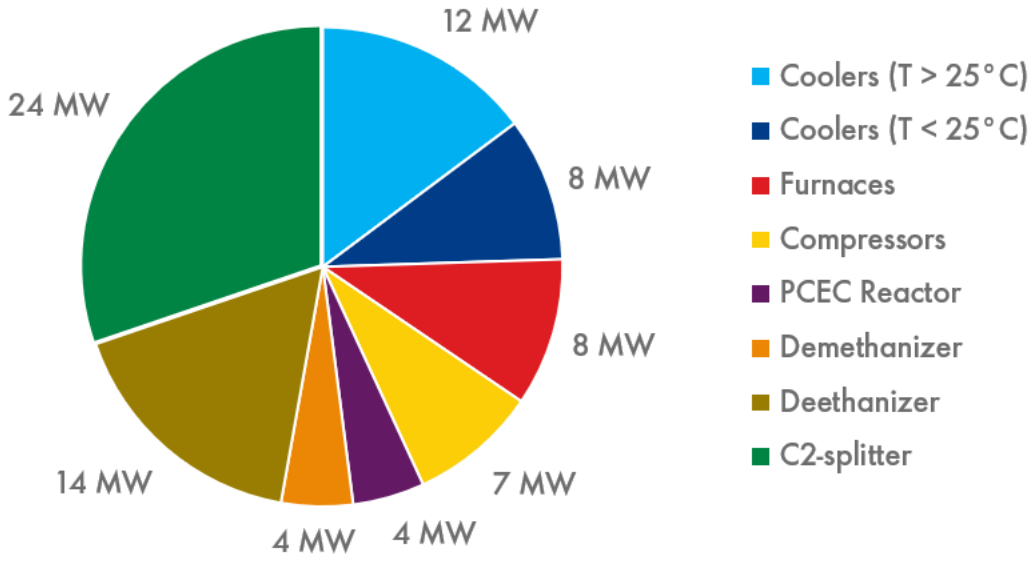

Figure 4-2: Accumulated unit component duties for the base case scenario (100 KTA) in MW.

Among all the process units, the C_2-splitter consumes the most energy, at 24 MW, accounting for 30% of the total process energy requirements. This significant energy demand is understandable, given the challenge of separating ethane and ethylene, which have only minor differences in their boiling points (as referred to in Table 3-7). Moreover, the DE (de-ethanizer) is another major energy consumer, responsible for 17% of total process duties. Lastly, coolers operating above 25°C also have a substantial energy impact, making up 15% of the overall process duties.

4.1.3. Material Balance

Table 4-3 shows the material mass balance for the base case simulation of the electrochemically enhanced NODH (non-oxidative dehydrogenation of ethane). The process output is visualized in the product slate in Figure 4-3 and is referred to as WINNER.

Table 4-3: Material mass balance for the WINNER process base case simulation with 100 KTA ethylene capacity.

Commodity	Input [KTA]	Output [KTA]
Methane	3.0	6.1
Ethane	155.2	2.5
Propane	3.2	1.4
Hydrogen	0	10.0
Ethylene	0	100.0
Propylene	0	10.4
Butene	0	31
Total	**161.4**	**161.4**

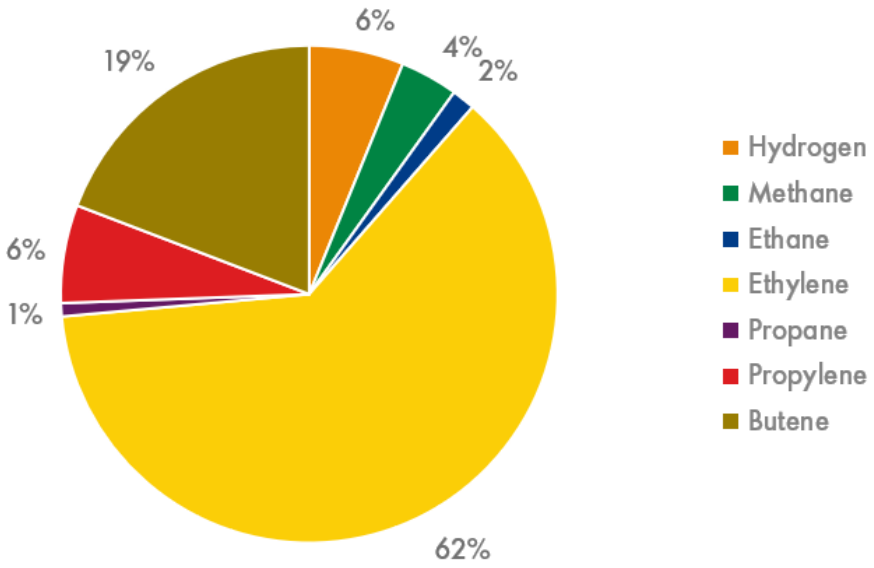

Figure 4-3: Annual product slate for the base case scenario (100 KTA).

The process demonstrates an ethylene selectivity of 62%. Moreover, it exhibits a high selectivity towards butene (19%), propylene (6%), and hydrogen (6%). However, as explained in Section 3.6.5, not all these commodities are individually recovered in the separation train as this would require the use of additional distillation columns. To keep consistency between the separation train of the WINNER process and the Monaca benchmark, the following four products are recovered at process level:

- Polymer-grade ethylene (99.95% purity)
- Hydrogen recovered at PCEC cathode side (99.97% purity and p = 50 bar)
- Ethane purged in the recycle stage (Section 3.6.6)

- Fuel gas (mixture of hydrogen from the PCEC anode, methane, propane, propylene, and butene)

Figure 4-4 presents the annual product slate for the WINNER process base case scenario, taking into account the aforementioned product recovery considerations. As a result, Figure 4-4 is a simplification of Figure 4-3, based on the ability of the DM, DE, and C_2-splitter to recover individual products.

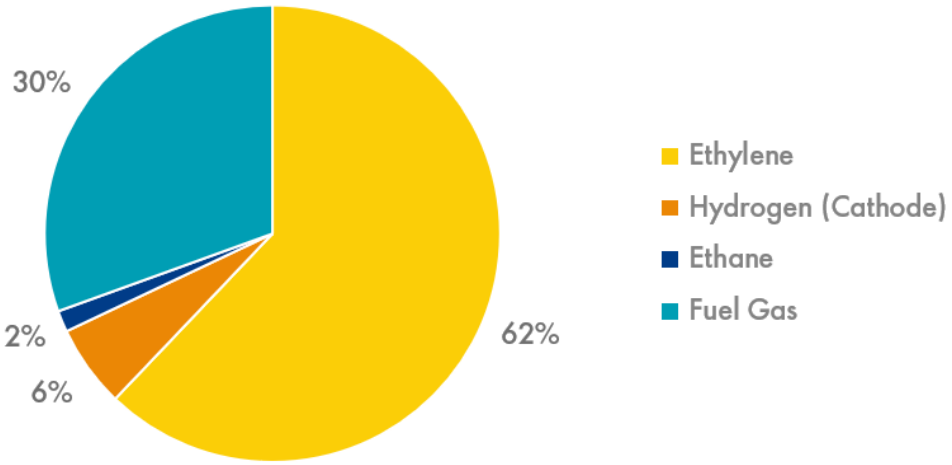

Figure 4-4: WINNER process product slate indicating individually recovered products.

4.2. Benchmark

4.2.1. Selection

The benchmark selected for comparison is the Shell Polymers Monaca plant located in Pittsburgh, Pennsylvania. This facility houses both an ethylene cracker and a polyethylene derivatives unit. However, for this study, only the ethylene cracker (ethane steam cracker) component is considered. The ethylene cracker unit has a production capacity of 1500 kton polymer-grade ethylene per year and capitalizes on low-cost ethane supplied by shale gas producers in the Marcellus and Utica basins [69]. The benchmark results are simulated by making use of Shell's Ethylene Cracker Unit (ECU) model.

4.2.2. Duties

Figure 4-5 illustrates the process duties for the Monaca steam cracker, indicating a 45% contribution from heating requirements and a 42% contribution from electrical energy requirements. Unfortunately, the electrical energy requirements cannot be subdivided into the same categories as shown in Figure 4-1, since this granularity is not shown in the ECU model regarding electricity consumption.

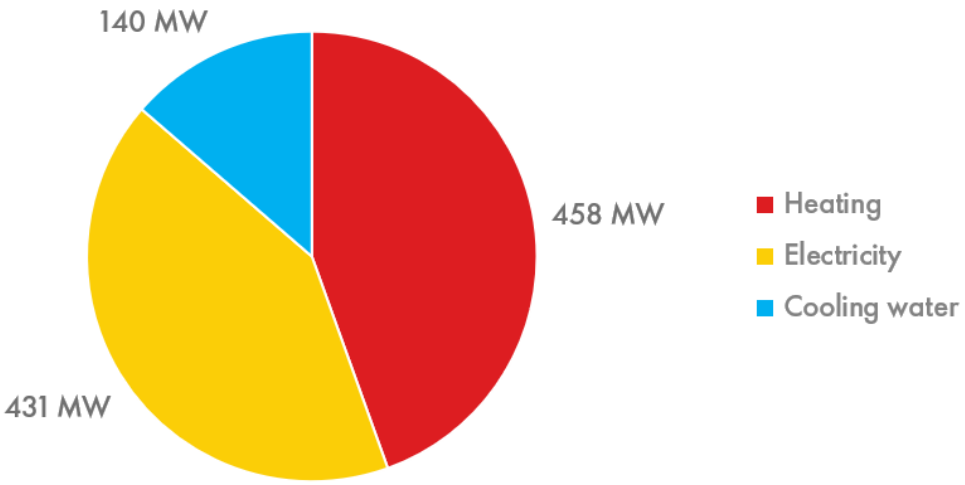

Figure 4-5: Accumulated process duties in MW for Monaca benchmark (1500 KTA).

4.2.3. Material Balance

Table 4-4 shows the material mass balance for the Monaca benchmark. The process output is visualized in the product slate in Figure 4-6.

Table 4-4: Material mass balance for the Monaca ethylene cracker benchmark.

Commodity	Input [KTA]	Output [KTA]
Methane	35.3	0
Ethane	1852.3	0
Propane	38.7	0
Fuel gas	0	426.4
Ethylene	0	1500.0
Total	**1926.3**	**1926.3**

In terms of ethylene selectivity, the benchmark process outperforms the WINNER process by achieving a selectivity of 78% (Figure 4-6), compared to 62% for the WINNER process (Figure 4-4). The benchmark process also shows a selectivity of 22% for fuel gas, which is a mixture of combustible compounds such as hydrocarbons and hydrogen [70]. This generated fuel gas can cover the furnace heating requirements, thereby reducing the net heating duties of the process. However, it also decreases the potential revenue from selling H_2, CH_4, C_2H_6, and C_3H_8. The decision to burn the fuel gas or sell it as a mixed stream is driven by the fact that additional separation steps to recover individual products would lead to added costs for distillation column equipment and associated process duties. It is critical to highlight the higher ethylene selectivity in the benchmark process compared to the WINNER process. Since, when assessing process energy consumption normalized

against a gravimetric unit of ethylene (e.g., MWh/tC_2=), the benchmark process will inherently be favored due to its higher ethylene selectivity. Because, when calculating the SEC (Specific Energy Consumption) in MWh/tC_2= for capacity of ethylene production, the calculation considers greater byproduct production in the WINNER process. The production of these byproducts also consumes energy, but this is not accounted for when dividing the total process duty by the amount of ethylene produced.

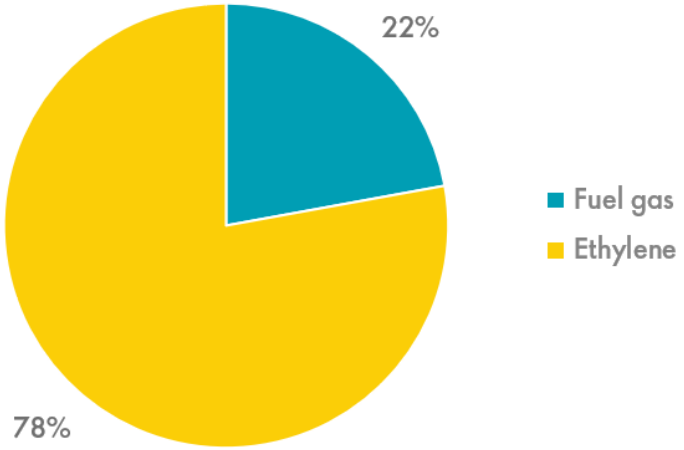

Figure 4-6: Monaca ethylene cracker product slate indicating individually recovered products.

4.3. Comparison

For a fair comparison between the WINNER process and the Monaca benchmark, production capacities are matched. Accordingly, the WINNER process is scaled up to match the capacity of the Monaca SC of 1500 KTA of ethylene. This ensures that energy efficiency, emissions, costs, and other metrics for both processes can be compared on a like-for-like basis.

4.3.1. Product Yield

The WINNER process is simulated at a capacity of 1500 KTA ethylene to match the capacity of the Monaca benchmark. Figure 4-7 illustrates the resulting product outputs for both processes.

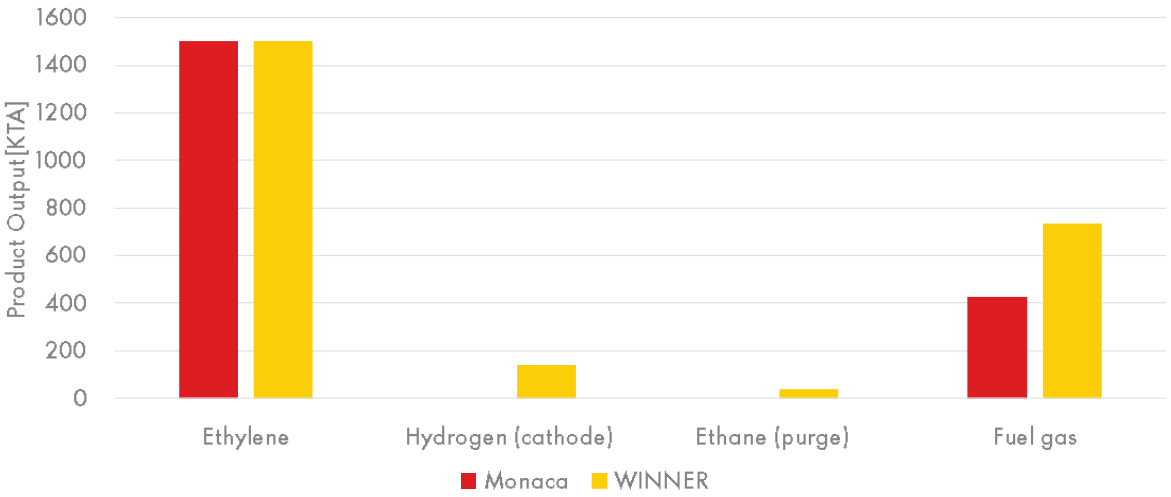

Figure 4-7: Product output comparison for the WINNER process and the Monaca benchmark, matched at a capacity of 1500 KTA ethylene (1/2).

One of the main advantages of the WINNER process over the ethane stream cracking process is the production of high-value, 99.97% pure hydrogen at a pressure of 50 bar. The hydrogen production shown in Figure 4-7 solely refers to the hydrogen produced at the hydrogen electrode (cathode) of the PCEC reactor. In the Monaca benchmark, the produced H_2 is recovered within the fuel gas stream. For a plant size of 1500 KTA ethylene, the WINNER process produces 141 KTA pressurized hydrogen. This has a significant positive influence on the economic evaluation of the process. Since other byproducts, such as methane, propane, propylene, and butene are not individually recovered in the separation process, these are bundled in fuel gas, as explained in Section 4.1.3. The compositions of the fuel gases recovered from both processes slightly differ from each other. This difference has been accounted for by calculating the calorific values of the fuel gas streams. The produced fuel gas is used to fuel the furnaces in both processes. The residual fuel gas is sold according to its calorific value.

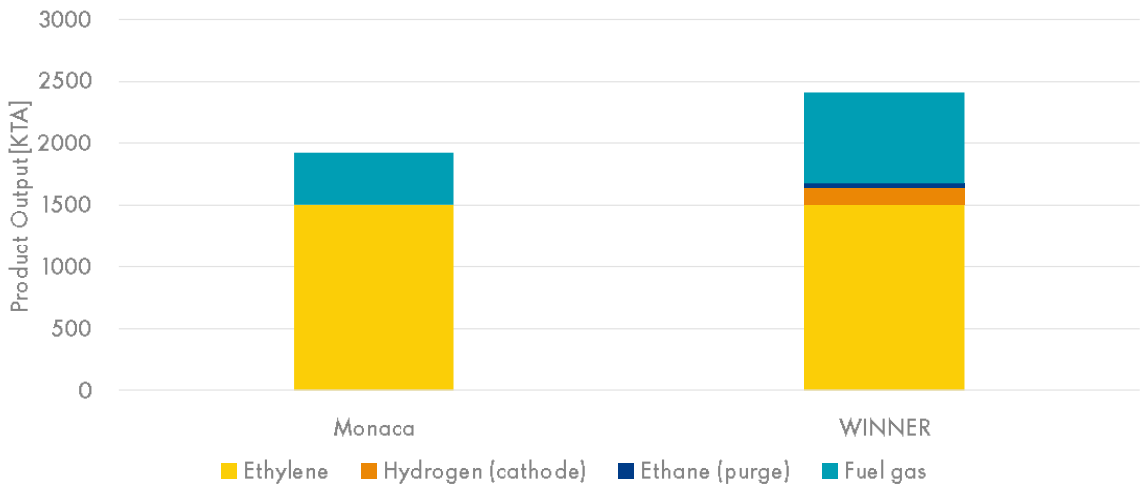

Figure 4-8: Product output comparison for the WINNER process and the Monaca benchmark, matched at a capacity of 1500 KTA ethylene (2/2).

Figure 4-8 shows a different representation of the produced product in the form of a stacked column chart. It clearly illustrates that the total product output in the WINNER process surpasses that of the benchmark (1926 vs. 2414 KTA) when producing an equivalent amount of ethylene.

4.3.2. Duties

Figure 4-9 presents the normalized process duties for both processes operating at a capacity of 1500 KTA. One notable difference between the duties of both processes is the substantial heating requirement of the Monaca benchmark (458 MW) compared to the WINNER process (121 MW). This difference stems from the significantly higher temperature of the cracking process in the Monaca benchmark (850°C) compared to the operating temperature in WINNER's PCEC reactor (550°C).

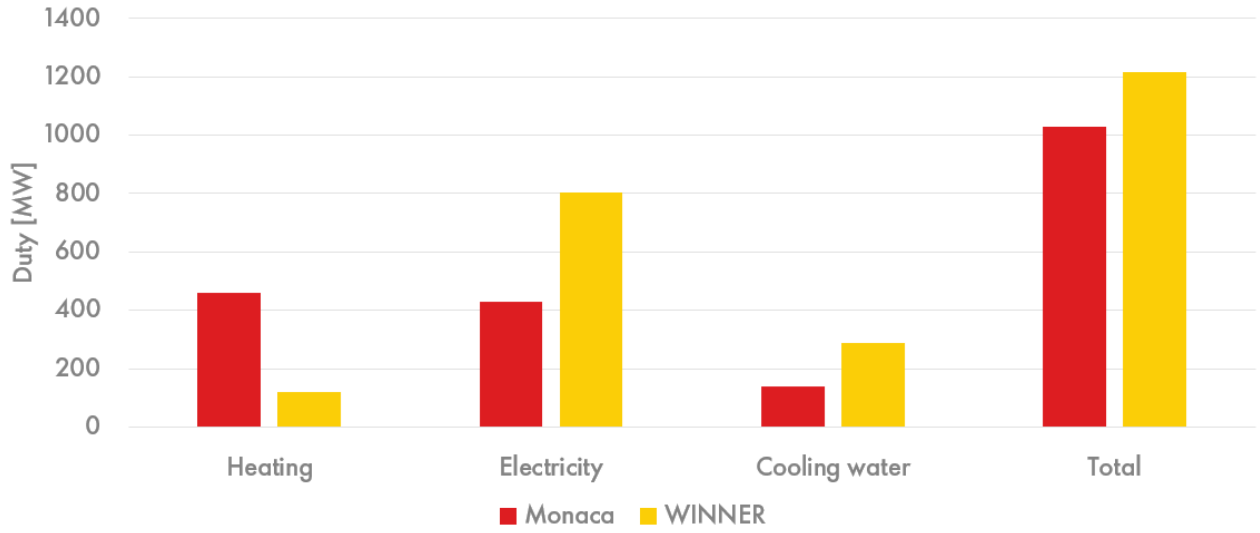

Figure 4-9: Normalized process duties comparison for the WINNER process and the Monaca benchmark, matched at a capacity of 1500 KTA ethylene.

In the WINNER process, the reduction in heating requirements is partly offset by increased electricity consumption, with the PCEC reactor requiring 59 MW for hydrogen splitting, diffusion, and compression. Other electrical energy requirements stem from compressor duties and cryogenic separation, as explained in Section 4.1.2. As explained in Table 3-4, the overpotential of the PCEC is 0.04 V, concerning an open circuit voltage of 0.14 V. With the assumption that all overpotential leads to resistive heating in the PCEC, approximately 19 MW of electrically generated heat can be subtracted from the thermal energy requirement of the PCEC furnace. It is a recommendation for further research to take this into account when evaluating the duty of the PCEC reactor furnace.

Cooling water requirements in the WINNER process roughly double compared to the Monaca benchmark, whereas the WINNER process operates at lower temperatures. This indicates a difference in the degree of heat integration and optimization between the two models used in the simulations and offers room for further improvement (see discussion

below). The Monaca benchmark uses a model representing a well-integrated process in terms of energy efficiency. At the same time, the CPD (Conceptual Process Design) as presented in Sections 3.5 and 3.6 does not contain this same level of heat integration. To resolve this discrepancy, an "Adapted heat integration" scenario will be introduced in Section 4.4.1.

When considering various types of energy demands, including heating, electricity, and cooling water, it is crucial to realize that a mere energy analysis does not fully encompass the energy inefficiencies that lead to thermodynamic losses. To properly address this, an exergy analysis should be conducted. Exergy analysis is a thermodynamic technique that evaluates the quality or usability of energy. It is based on the second law of thermodynamics, which states that not all energy in a system is available to do work. Exergy represents the maximum achievable useful work that can be obtained from a system as it reaches equilibrium with its surroundings. Although this specific research does not encompass an exergy analysis due to its defined scope, future research would benefit from conducting such an analysis. This would enable the evaluation of energy efficiency and its outcome could be used to further optimize the energy system [71].

4.4. Process Analysis Adjustments

For a fair assessment of the potential of the electrochemically enhanced NODH process in comparison to the ethylene cracker benchmark, several adjustments are made. As discussed in Section 4.3.2, discrepancies in heat integration and plant capacity make the comparison biased. Sections 4.4.1 and 4.4.2 will address these biases and implement the adjustments for future scenario simulations (Section 4.5).

4.4.1. Adapted Heat Integration

This process adjustment adapts the WINNER process duties to simulate the same level of heat integration seen in the benchmark process. It involves using an AspenPlus model of the Rhineland SC (steam cracker) separation train combined with the Aspen Energy Analyzer (AEA). The Rhineland SC is used instead of the Monaca SC due to the availability of an AspenPlus model of the former. Assuming the Rhineland steam cracker demonstrates similar heat integration to the Monaca benchmark, this model offers an appropriate reference point. The Rhineland SC model is simulated and the outcomes of the AspenPlus simulations are analyzed and integrated into the energy consumption of the WINNER process. (Unfortunately, the Rhineland SC model cannot be shared in the Appendix due to confidentiality considerations.) The AEA employs pinch technology and utility planning tools to predict and eliminate energy waste [72]. The goal of pinch technology is to assess all heat transfers within a plant and reorganize them to minimize total energy consumption [73]. This approach provides an estimate of potential heating and cooling utility savings in terms of percentages. These savings translate into potential reductions for the WINNER process, as visualized in Figure 4-10. The indicated

percentages represent the adapted savings transitioning from the current process to the adjusted scenario, assuming the same level of heat integration as the Monaca benchmark. For a more detailed explanation of the methodology used to adapt heat integration, please refer to APPENDIX O.

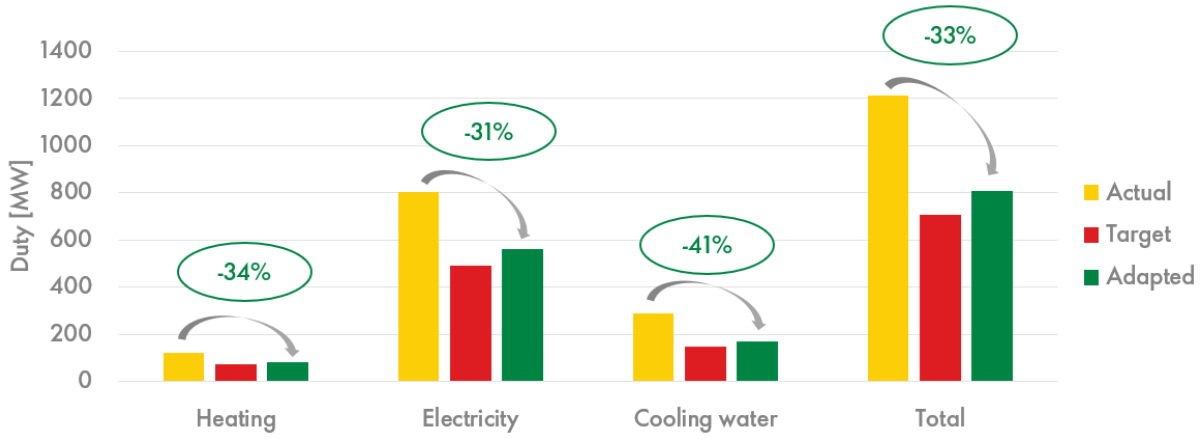

Figure 4-10: WINNER process duties (1500 KTA) after adaptation for heat integration.

Figure 4-10 primarily demonstrates that the "adapted" scenario has higher process duties compared to the "target" scenario as indicated by the AEA, but considerably lower than the "actual" scenario. This approach of adapted heat integration is a workaround to enable a fair comparison. For a future study, the recommendation is to further optimise the process design to arrive at the same level of heat integration. This can be done by using an existing separation train of an ethylene cracker and connecting it to the PCEC reactor. In theory, the adaptation for heat integration methodology mimics this procedure.

4.4.2. Matching Capacities

The original sizing of the 100 KTA process unit was based on WINNER's initial sizing predictions [8]. In the case of novel technologies, plants often begin with small-scale units that gradually scale up over time. However, for a fair comparison, the WINNER process is simulated at a capacity of 1500 KTA.

"Bigger is better" is one of the fundamental principles of chemical engineering [74]. This phenomenon is also referred to as economies of scale and describes the cost advantage that a business obtains due to expansion. Besides economic advantages, increasing plant size can also improve process efficiency as large-scale operations allow for more efficient use of equipment and energy [74]. Some of the advantages of economies of scale are listed below:

- Cost spreading of CAPEX and fixed OPEX (e.g., O&M, labour) over a larger output.
- Enhanced process efficiency (e.g., improved heat transfer due to the square-cube law relating surface to volume in reactors and heat exchangers).
- Bulk buying of resources and feedstock.

- Efficiency improvements in material handling.

Economies of scale may not be as prominent in electrochemical reactors as in traditional thermal plants. Even though the modular design of electrochemical systems offers increased flexibility in scaling, the cost advantages related to equipment scaling might not be as significant as those seen in thermal operations. This is primarily due to the complex structure of electrochemical cells, the expensive materials required, and the substantial costs related to power supply infrastructure [75]. These factors collectively may limit the cost reductions typically observed with scaling in conventional thermal plants.

Figure 4-11 visualizes the SEC (Specific Energy Consumption) per ton of ethylene produced for the WINNER process and the Monaca benchmark. Red figures indicate a negative development of the WINNER process with respect to the Monaca benchmark, whereas green figures indicate a positive comparison. This convention is used throughout the rest of this report. The simulation is run with the implementation of the adapted heat integration discussed in Section 4.4.1 and an equal capacity of 1500 KTA ethylene. The percentages represent the percentual change of the WINNER process compared to the Monaca benchmark. Green indicates a decrease in SEC (Specific Energy Consumption), which is desirable, whereas red indicates an unfavourable increase in SEC.

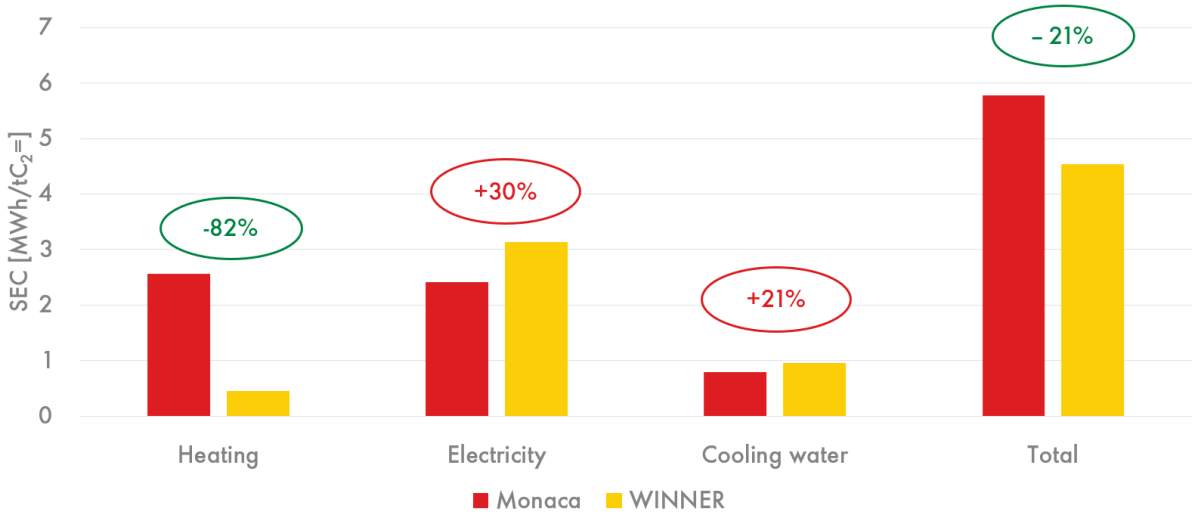

Figure 4-11: Specific Energy Consumption for 1500 KTA plants with adapted heat integration. Red figures indicate a negative development of the WINNER process with respect to the Monaca benchmark. Green figures indicate a positive development.

Based on this base case scenario with heat integration adaptation and matching capacities, the following conclusions about SEC can be drawn:

- The WINNER process has the potential to decrease total SEC (in MWh/tC_2=) by ~21%.

- The WINNER process curtails thermal energy needs by making use of electrical energy in the PCEC reactor, shifting from heat to electricity.
  - Thermal energy consumption decreases by ~82%
  - Electrical energy consumption increases by ~30%
- Cooling water consumption increases by ~21%, indicating room for further improvement of the integration of cold product streams in the interstage cooling process.

It is worth noting that the comparison of the SEC of both processes uses a unit of MWh/tC_2=. As explained earlier (Section 4.2.3) the ethylene selectivity of the WINNER process is lower compared to the Monaca benchmark (62% vs 78% as outlined in Section 4.2.3), the outcomes of the MWh/tC_2= comparison favour the Monaca benchmark. This is due to the WINNER process also consuming feedstock and electricity to produce byproducts, whereas these are not considered when calculating the SEC based on ethylene output. Despite this, the WINNER process holds a potential advantage: it produces a larger number of byproducts within the same calculated energy budget. This could lead to even more favourable outcomes if these byproducts were accounted for by individually recovering them through additional distillation columns.

4.5. Scenarios

Besides heat integration, the WINNER process exhibits lower process efficiencies due to its low TRL. Hence, to address these possibilities for improvement, Section 4.5.1 introduces a scenario with different fractional conversions in the PCEC reactor. Further, considering ongoing technological advancements in ethane steam cracking, an e-cracking scenario is discussed in Section 4.5.2.

4.5.1. Fractional Conversions

This section addresses the uncertainties in fractional conversion assumptions by creating three distinct scenarios:

A. Conservative (Conser.) Scenario, using the analysis on concentration dependence in Section 3.3.

The Conservative Scenario is derived from the analysis in Section 3.3 regarding the influence of ethane concentration in the feedstock on conversion, selectivity, and yield. It specifically adheres to Figure 3-5, in which a decrease in ethane conversion from 40% to 11% when moving from a 10 wt% to a 100 wt% ethane concentration in the feed is observed. This observation is implemented into the Conservative Scenario by scaling reaction 1 with a factor $\frac{11}{40}$. The fractional conversions of the other side reactions are presumed to be consistent with the base case Scenario.

B. Base case (BC) scenario, consistent with the assumption made in previous process simulations and discussions in this report.

The base case Scenario uses the fractional conversions from the reactions mentioned in Section 3.6.2, adapted from the literature [6, 66]. This base case Scenario represents a currently plausible scenario, based on lab-scale technology.

C. Future Scenario, projecting an increase in fractional conversions due to future technological advancements.

The Future Scenario describes a potential scenario where advances in technology will have driven an increase in fractional conversions in the PCEC reactor. This scenario is hypothetical and assumes performance improvements in the electrochemically enhanced NODH process due to technological and process advancements. Three main areas with technological challenges and associated possibilities for increased performance are identified:

- Electrocatalyst advancements – For achieving improved thermal activity in electrocatalysts, it is vital to innovate and design new versions that optimize electron transfer and promote intended reactions effectively. By doing this, a more robust electrocatalytic process can be realized, boosting ethane conversion while keeping side reactions, catalyst deactivation, and coking minimal at lower temperatures [66].

- Enhanced cell components – A technical opportunity is to increase the proton-transference capacity of the electrolyte to increase the FE. This would pave the way for operation at higher current densities, thanks to a sufficient proton flux, generating more hydrogen at the cathode side and reducing separation costs of the hydrogen produced at the anode side [66].

- Overall process improvement – Besides materials and catalyst improvements, it is essential to understand the influence of different operating conditions on ethylene yield and durability. Key considerations include EC cell and stack design, scalability, modularity, and the engineering of feedstock and downstream distribution for economical operations [66].

The future fractional conversions in the PCEC reactor are extracted from data gathered from a reference steam cracking process and a study by Hu et al. [22, 66]. The main difference is the increased conversion of ethane in the primary reaction 1, which significantly impacts the single-pass ethylene yield. In addition, the fractional conversion of the dimerization reaction 4 decreases. Since reaction 4 consumes ethylene as a side

reaction (refer to Figure 3-12), this reduction in fractional conversion contributes to a higher ethylene yield.

Table 4-5 outlines the various reactions taking place within the PCEC reactor, along with their corresponding fractional conversions for the three scenarios.

Table 4-5: Fractional conversions within the PCEC reactor for the different scenarios [22, 66].

#	Stoichiometry	Fractional conversion			Limiting reactant
		Conser.	BC	Future	
1	$C_2H_6 \leftrightarrow C_2H_4(anode) + H_2(cathode)$	0.10	0.363	0.56	Ethane
2	$2C_2H_6 \leftrightarrow C_3H_8 + CH_4$	0.02	0.02	0.02	Ethane
3	$C_3H_8 \leftrightarrow C_3H_6 + H_2$	0.8	0.8	0.8	Propane
4	$2C_2H_4 \leftrightarrow C_4H_8$	0.23	0.23	0.05	Ethylene
5	$C_2H_6 + C_2H_4 \leftrightarrow C_3H_6 + CH_4$	0.032	0.032	0.07	Ethylene

The results of simulating these distinct scenarios and their impact on the KPIs of the process are presented in Section 5.6. This is intentionally done since the analysis will provide insight into the economic implications discussed in Chapter 5.

4.5.2. E-cracking scenario

Given the projected 15-year time-to-market for the WINNER process, it is essential to account for potential technological advancements in the current state-of-the-art ethane steam cracking technology over the same period. Shell and Dow have initiated an experimental unit to electrically heat steam cracker furnaces, marking a milestone in their joint efforts to electrify steam cracking furnaces (e-crackers). The objective is to retrofit current gas-fired steam cracker furnaces to be powered by renewable energy in the electricity grid. This will contribute to the decarbonization of the chemicals industry [76].

In this scenario, the furnaces in both the Monaca steam cracker and the WINNER process are fully electrified. This scenario is based on the promising advancements in e-cracking, anticipating industrial scale-up readiness within 15 years. This prospect is likely, given Shell and Dow's existing plans to design and build a multi-megawatt pilot plant, aiming for potential start-up in 2025 [76].

This scenario is elaborated upon in Section 5.5.1 on PCF (Product Carbon Footprint), since its impact on economic KPIs is relatively small. Yet it provides an opportunity for the Monaca benchmark to reduce carbon emissions through the electrification of process energy.

5. Techno-economic Analysis

This chapter provides a TEA (techno-economic analysis) of the electrochemically enhanced NODH process. The objective is to assess the economic performance and environmental impacts of the WINNER process in comparison to an ethylene cracker, accounting for uncertainties associated with input parameters. For a direct comparison with the Monaca steam cracker, a plant capacity of 1500 KTA of ethylene is utilised, in line with the adjustments made in Section 4.4. Considering the low TRL of the electrochemically enhanced NODH process, the techno-economic analysis must be extrapolated from a technology that has only been demonstrated at a laboratory scale. This requires making certain assumptions and acknowledging the inherent uncertainties involved in predicting the performance and costs of a large-scale, commercialized version of this process.

Figure 5-1 outlines the procedure for the TEA. Section 5.1 compares the WINNER process and the Monaca benchmark based on technical KPIs. Sections 5.2 and 5.3 then estimate the capital (CAPEX) and operational (OPEX) costs, respectively. These estimations are crucial for identifying the main cost drivers and facilitating a quantitative comparison of different process scenarios. Section 5.4 evaluates the plant's profitability by estimating revenues and contrasting this with the cost of manufacturing ethylene. As this profitability analysis relies on assumptions and predictions, they inherently carry some risk. Section 5.6 conducts a sensitivity analysis to accommodate these risks and to address the impact of these variables on the overall techno-economic analysis.

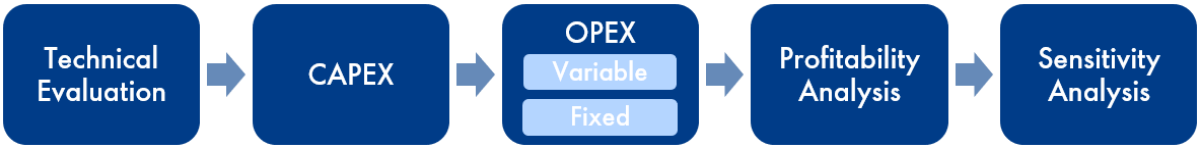

Figure 5-1: Techno-economic Analysis procedure.

5.1. Technical Evaluation

Table 5-1 compares the WINNER process to the Monaca benchmark based on technical KPIs (Key Performance Indicators). These KPIs relate to process efficiency (e.g., C_2= selectivity, conversion, and process yield) and SEC (Specific Energy Consumption).

An ethylene cracker typically operates approximately 8410 hours per year, accounting for a downtime period of roughly ten weeks every five years. The typical plant lifetime is 20 years. The same operational year and lifetime are assumed for the PCECs deployed in the electrochemically enhanced NODH process [66]. However, solid-oxide electrolytic cell (SOEC) stacks typically have a lifetime ranging from 40,000 to 80,000 operating hours [77]. By assuming an average SOEC cell stack lifespan of 60,000 operating hours, replacements would be required approximately every seven years. These costs are added as fixed operational costs to the WINNER process. The downtime in the WINNER process

primarily arises from the need for catalyst regeneration due to coking reactions. While the specifics of these degradation mechanisms are not extensively discussed, a 4% downtime (corresponding to two weeks of downtime per year) is accounted for.

Table 5-1: Overview of technical parameters for the WINNER process and the Monaca benchmark.

Parameter	Unit	WINNER process (Base case)	Monaca Benchmark
Annual C_2= production	KTA	1500	1500
Annual H_2 production	KTA	148	N/A
S_{C2H4}	%	65	84
Single-pass X_{C2H6}	%	34	60
Y_{C2H4}	%	64	81
$T_{Operating}$	°C	550	850
SEC	MWh/tC_2=	4.5	5.8
Heating duty	MWh/tC_2=	0.5	2.6
Electrical duty	MWh/tC_2=	3.1	2.4
Cooling duty	MWh/tC_2=	1.0	0.8
Operating hours	Hours	8410	8410
Plant lifetime	Years	20	20
PCEC stack lifetime	Operating h	60000	N/a

Table 5-1 indicates that the WINNER process is less efficient when converting ethane to ethylene compared to the Monaca benchmark. This is evident in the lower values for ethylene selectivity (65% vs. 84%), single-pass ethane conversion (34% vs. 60%), and ethylene yield (64% vs. 81%). The superior performance of the Monaca benchmark stems from its well-optimized ethane steam cracking process with a long track record of reliable operation and process optimization. Section 5.6 contains sensitivity analyses that address these differences in process maturity. On the other hand, the WINNER process operates at a lower temperature (550°C vs. 850°C) and has a reduced SEC (4.5 vs. 5.8 MWh/tC_2=). This implies a potential to cut carbon emissions linked to utility consumption. In addition, the WINNER process generates high-value, pressurized hydrogen (p = 50 bar) that can serve as an extra revenue stream.

5.2. Capital Expenditure (CAPEX)

The overall cost of designing, building, and installing a plant make up the fixed capital investment. The components of the fixed capital investment for an electrochemically enhanced NODH plant include [78]:

- The Inside Battery Limits (ISBL) - costs of the plant itself.
- The Outside Battery Limits (OSBL), also known as offsite costs - infrastructural modifications that need to be made before a plant can be constructed.
- Engineering and construction costs
- Contingency charges – extra costs to account for deviations from the cost estimate.

The word "battery" does not refer to the energy-storing device. Instead, it relates to the production unit of a chemical plant: in our case, the functional unit of the PCEC reactor plant for ethylene production with a capacity of 1500 KTA. Table 5-2 shows an overview of the assumptions made regarding CAPEX and their corresponding values.

Table 5-2: Overview of CAPEX estimation assumptions [78].

Cost component	Assumption	Value [$MM]	Reference
ISBL	AspenPlus output	137	N/a
OSBL	50% of ISBL	68	[78]
Engineering costs	20% of (ISBL + OSBL)	41	[78]
Contingency charges	50% of (ISBL + OSBL)	102	[78]
TCI	Sum of above	348	N/a

As previously discussed, the electrochemically enhanced NODH process is still in the early stages of research, with only lab-scale technology demonstration available. Consequently, the simulations are extrapolated, based on limited data from lab-scale systems. For estimation of the CAPEX, the electrochemically enhanced NODH process can be compared to high-temperature electrolysis (HTE) in SOECs (solid-oxide electrolytic cells). This comparison is justified based on the similarities between both processes. They both involve similar cell-stack constructions, reaction mechanisms, and operating conditions [66].

This section introduces four different scenarios for estimating the costs associated with the PCEC reactor, relying on comparisons drawn from SOEC systems. For further analysis, the Conservative Upscaling (2030) scenario has been selected. Despite the proposed process still being in its early stages, these comparisons offer a preliminary basis for understanding the potential cost structure at a larger scale.

5.2.1. Inside Battery Limits

The ISBL plant costs comprise the direct and indirect costs of sourcing and the installation of all process equipment that make up the new plant [78]. Table 5-3 shows the ISBL costs, broken down into different equipment categories. These categories relate to the CPD (conceptual process design) as outlined in Section 0 and 3.6. The category "other" represents the condenser, pump, and heat exchanger costs. All costs, except for the PCEC reactor costs, are derived from the Aspen Process Economic Analyzer (APEA), which uses the outcomes of the process simulation to give an ISBL estimate.

Table 5-3: ISBL costs per equipment category.

Equipment category	Cost [$MM]
PCEC Reactor	69
Coolers	5
Heaters	4
Compressors	39
Cryogenic Distillation	18
Other	2
Total ISBL equipment costs	**137**

Figure 5-2 presents a visual breakdown of the CAPEX equipment costs. In the Conservative Upscaling (2030) scenario, the PCEC reactor forms the most substantial cost component, accounting for half of the total installed equipment costs. The compressors are another significant cost factor, comprising approximately 30% of the total equipment costs. Conversely, the expenses associated with cryogenic distillation are relatively lower, making up around 13% of the total equipment costs. It is important to acknowledge that the estimates for the ISBL costs, especially for the PCEC reactor, involve a significant level of uncertainty. This will be demonstrated in the different CAPEX scenarios in Table 5-5 and Figure 5-3. However, an additional accuracy variation of approximately ±50% should be factored into these estimations.

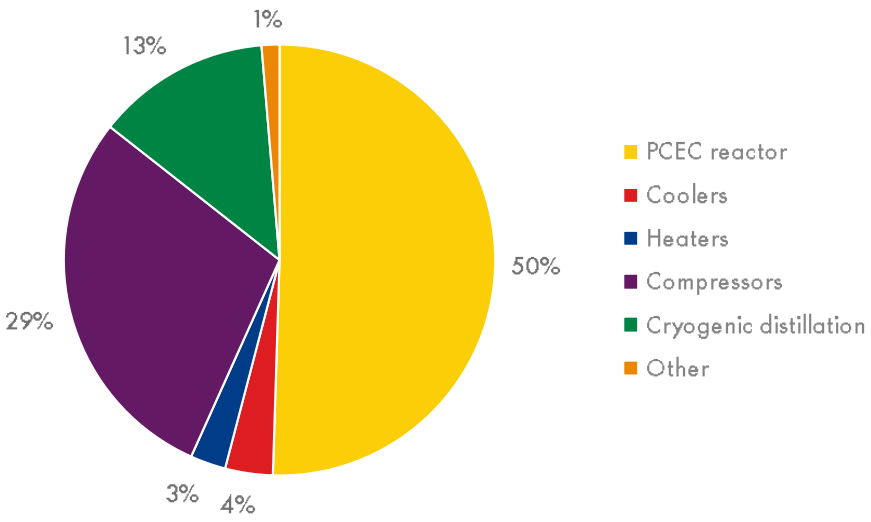

Figure 5-2: Upscaling (2030) conservative CAPEX equipment cost breakdown.

As explained earlier, for the PCEC reactor cost estimation, a comparison with SOECs is used. SOECs are in their scale-up phase, with the first multi-megawatt (2.6 MW) high-temperature SOEC *MultiPLHY* project currently being installed [79]. There are still a lot of uncertainties and differences in cost estimations for current SOEC projects, let alone future CAPEX estimations for these systems. Therefore, it was decided to combine data available in the literature on bottom-up CAPEX estimations of electrolyzer systems [80-82], into four different scenarios with corresponding total direct costs as presented in Table 5-4. This resulted in a cost estimation for the ISBL PCEC reactor costs based on a nominal capacity of 59 MW for hydrogen splitting and compression over the electrolytic membrane.

Table 5-4: SOEC cost scenarios and corresponding ISBL costs.

Scenario	SOEC direct costs [$/kW] [80-82]	PCEC reactor ISBL costs [$MM]
1: Current (2020) – Conservative	~3600	212
2: Current (2020) – Progressive	~1200	72
3: Upscaling (2030) – Conservative	~1200	69
4: Upscaling (2030) – Progressive	~450	27

It should be noted that SOEC studies underpinning these estimates anticipate an increase in current density in the cell from ~0.7 A/cm^2 to ~1.5 A/cm^2 in the Upscaling (2030) scenario. Contrastingly, the current data on fractional conversions within the PCEC reactor is based on a current density of 40 mA/cm^2. Given that the membrane area of the PCEC is inversely proportional to the current density of the cell (APPENDIX P, Equation (0-6)), it is a minimum requirement for industrial scale-up of the electrochemically enhanced NODH process that the current density increases to a value around 1 A/cm^2. This is an increase by

a factor of 25 and requires significant technological progress in R&D (research and development) on PCECs.

Table 5-5: Total Capital Investment (CAPEX) for the different scenarios.

Cost component	2020 – Conservative [$MM]	2020 – Progressive [$MM]	2030 – Conservative [$MM]	2030 – Progressive [$MM]
ISBL	280	139	137	94
OSBL	140	70	68	47
Engineering costs	84	42	41	28
Contingency charges	210	104	102	71
TCI	714	356	348	241

Table 5-5 presents the Total Capital Investment (TCI) for the PCEC reactor following the various scenarios. There are significant variations in the TCI values across these scenarios, highlighting the uncertainty around future capital expenditure forecasts for SOECs, and even more so for PCECs. For further analysis, the 2030 conservative scenario is selected. This scenario better adheres to the time-to-market of the WINNER process than the 2020 scenario, providing a more realistic picture of potential capital expenditures. In addition, adopting a conservative approach ensures the resulting techno-economic analysis does not produce an overly optimistic economic projection.

In order to make a CAPEX comparison with the benchmark, an FCI (Fixed Capital Investment) value of $871 million is used for an 830 KTA ethane steam cracker [22, 83]. This value is scaled up to represent a plant with a capacity of 1500 KTA, using Equation (5-1) [22].

$$FCI_B = FCI_A * \left(\frac{Capacity\ of\ B}{Capacity\ of\ A}\right)^n \quad (5\text{-}1)$$

Where:

$FCI_{A/B}$ is the fixed capital investment of plant A or B at their rated capacities,
n is a scaling factor, averaging ~0.6 across the entire chemical industry [78].

This calculation results in an FCI for the Monaca benchmark with a capacity of 1500 KTA of $1,242 million. Figure 5-3 visualizes this CAPEX comparison for the four scenarios for the WINNER process CAPEX compared to the Monaca benchmark. The selected scenario, Upscaling (2030) – Conservative, is bordered in green.

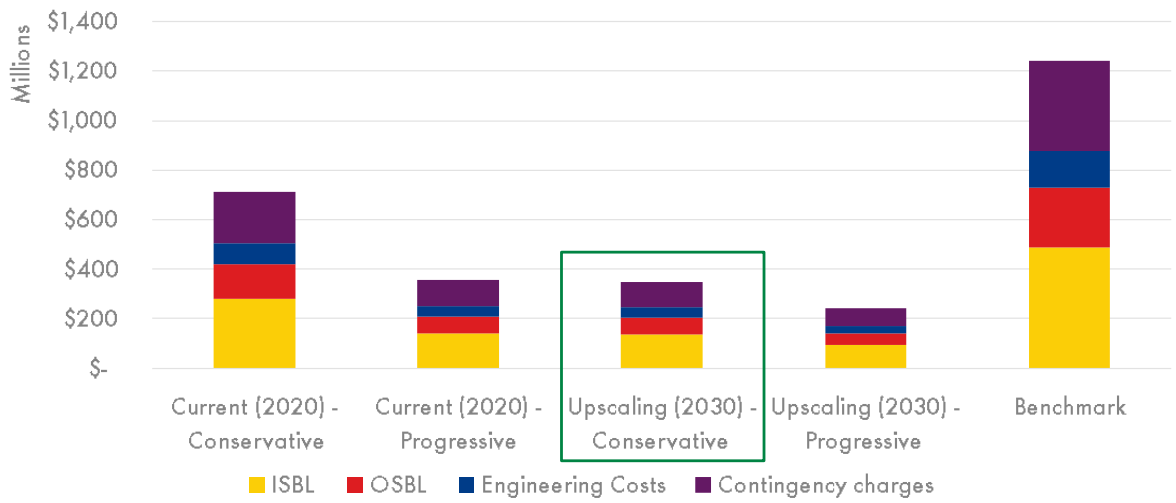

Figure 5-3: CAPEX cost estimations for the various scenarios compared to the Monaca benchmark.

The CAPEX for the steam cracking benchmark is more than three times as high compared to the WINNER process Upscaling (2030) - Conservative scenario (+257%). For a detailed overview of the CAPEX estimation of the PCEC Reactor, please refer to APPENDIX S.

5.2.2. Outside Battery Limits

The OSBL or offsite costs cover the costs of the site infrastructure upgrades required to accommodate the installation of a new plant or the expansion of an existing plant. In the early stages of design, OSBL expenses are often calculated as a percentage of ISBL costs. Typically, OSBL expenses range from 10% to 100% of ISBL expenditures, depending on the project's magnitude and the infrastructure impact on the site. Offsite costs for conventional chemical projects typically range from 20% to 50% of ISBL expenditures, with 40% serving as an initial estimate of unknown site specifics [78]. Note that the definition of "battery" as described at the beginning of Section 5.2 is used – the production unit of a chemical plant. However, OSBL expenses will be higher if the facility is built on a brand-new site location. WINNER's electrochemical process requires significant infrastructural improvements to be able to supply the necessary electricity. As a result, the initial estimate for the OSBL costs for this project will be set at the upper limit of 50% of ISBL costs.

5.2.3. Engineering Costs

The expense of detailed design and other technical services critical to complete the project is included in the engineering costs, often known as home office costs or contractor charges. For smaller projects, a general rule of thumb for engineering expenditures is 30% of ISBL plus OSBL cost, while for larger projects, 10% of ISBL plus OSBL cost. The upscaled WINNER process with a capacity of 1500 KTA can be regarded as large scale, but, as it

concerns a novel technology, slightly higher engineering costs are estimated. As a result, engineering expenses of 20% of ISBL + OSBL are set for this project [78].

5.2.4. Contingency Charges

Additional expenses, known as contingency charges, are applied to the project budget to account for deviations from the cost estimate. A contingency charge can be regarded as an additional fee levied by the Engineering, Procurement and Construction (EPC) firm to cover the possibility that the project will run over budget. Generally, a minimum contingency charge of 10% of ISBL + OSBL costs should be used on all projects [78]. However, for novel technologies like the WINNER process, higher contingency charges can reach up to 50%. Given the innovative nature of the WINNER process and the absence of its large-scale commercialization, a 50% contingency fee of ISBL and OSBL costs is applied to this project.

5.3. Operational Expenditure (OPEX)

Estimating the costs of manufacturing is a crucial stage in figuring out whether a process will be profitable. Moreover, regardless of the specifics of the process, understanding the breakdown of production costs is critical to process optimisation. Operational costs can be separated into variable and fixed costs of production [78].

5.3.1. Variable Costs

Variable operational costs proportionally change with production levels. They can often be minimized by efficient plant design or operation. Variable costs primarily depend on the selection of feedstock, process chemistry, and plant location. They typically make up 60 – 80% of total OPEX. The following are examples of variable production costs [78]:

- Raw material consumption
- Utilities
- Carbon costs

Raw material consumption

For this project, the geographical location is set as the United States, following the benchmark of Shell's Monaca ethylene cracker in the United States. Feedstock costs depend on the plant location, and Table 5-6 shows feedstock prices for different regions. Section 5.6 presents the results of a sensitivity analysis for different commodity prices since these economic inputs have a large influence on the project profitability while carrying a high degree of uncertainty.

Table 5-6: Feedstock prices across various regions from 2015 – 2019. North American feedstock prices, about the selected geographical location of the plant (U.S.), are highlighted within a frame.

Product	Europe [$/t]	North America [$/t]	Middle East [$/t]	Asia-Pacific [$/t]	Reference
Methane	450	150	150	200	[84]
Ethane	600	450	300	700	[85]
Propane	700	1000	700	950	[86]

Using these feedstock prices to estimate the raw material costs of the process poses some difficulties and risks:

- Commodity prices are highly volatile, influenced by supply and demand balance, oil and gas prices, geopolitical conflicts (like the recent Russian war), and the COVID-19 pandemic. Hence, the data used in this project is gathered within a timeframe between 2015 – 2019.
- Securing free, open-source data on chemical commodity prices can be challenging, and there is considerable variation in values from different sources. As a result, multiple references are combined to derive an average figure.
- Considering that the projected time-to-market of the PCECs in the WINNER process is approximately 10 – 15 years [8], commodity prices at around the year 2035 would be more relevant. However, as these predictions are not available in open-source references, prices from 2015 – 2019 prices are utilised.

In practice, the production of fuel gas exceeds the energy requirement of the pre-heater and furnace, so no external refinery fuel is consumed in the process. Figure 5-4 gives a visual representation of this. The total production of fuel gas (depicted in purple) surpasses the fuel gas consumption at the furnaces (shown in blue). Consequently, the net amount of fuel gas that can be exported is the difference between the total amount of fuel gas produced and consumed and is shown in red. The amount of exported fuel gas in the WINNER process is higher compared to the Monaca benchmark due to 1) a higher total fuel gas production and 2) a lower amount of consumed fuel gas at the furnaces. For the specific compositions and heating values of the fuel gas streams produced in both processes, please refer to APPENDIX Q.

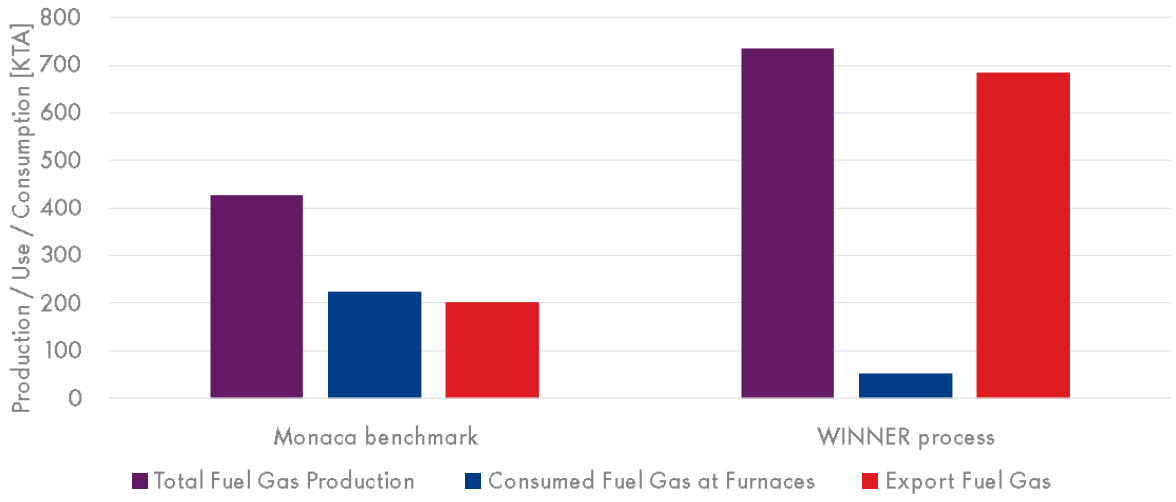

Figure 5-4: Fuel gas production, consumption, and export in the Monaca benchmark and the WINNER process.

Cooling duties above a temperature of 25°C are met using cooling water, of which the required mass flow is calculated by using Equation (5-2) [87]:

$$\dot{m} = \frac{Q}{C_p * \Delta T} \tag{5-2}$$

Where:

$\dot{m}$	is the mass flow of cooling water through the heat exchanger [kg/s],
Q	is the heat transferred [kW],
C_p	is the specific heat of water [=4.2 kJ/kg]
ΔT	is the temperature change between the in and outgoing cooling water [K]

The latter is assumed to be equal to 10 K since this represents an average value observed in the industry [87]. Electrical units like compressors are driven by grid electricity and refrigeration cycles are assumed to purely consume electricity. Table 5-7 specifies the different utility input parameters for refinery fuel, electricity, and cooling water. Carbon intensity refers to the amount of carbon emissions (in the form of CO_2) per unit of energy generated [88]. APPENDIX Q provides more detailed specifications on fuel and electricity inputs.

Table 5-7: Utility input parameters used for the techno-economic modelling of the WINNER process and the Monaca benchmark.

Parameter	Value	UOM	Reference
Refinery fuel price	18.40	$/MWh	[84], [85], [86]
Refinery fuel carbon intensity	0.098	tCO_2/MWh	[89, 90]
WINNER fuel gas carbon intensity	0.24	tCO_2/MWh	[89, 90]
Monaca fuel gas carbon intensity	0.14	tCO_2/MWh	[89, 90]
Average retail electricity price in industry	68.25	$/MWh	[91]
Electricity grid carbon intensity (U.S., 2020)	0.369	tCO_2/MWh	[88]
Cooling water price	0.1744	$/m^3$	[92]
Cooling water carbon intensity	0.026	tCO_2/MWh	[93]
Carbon price	51	$/$tCO_2$	[94]

It is crucial to note the large difference in carbon intensity between the refinery fuel carbon intensity and the electricity grid carbon intensity (0.098 vs. 0.369 tCO_2/MWh). This deviation primarily results from conversion losses in electricity generation. The weighted U.S. electricity production efficiency is approximately 40% [95]. The higher grid carbon intensity in the base case scenario implies that the electrification of a process leads to an increase in carbon emissions. As a result, the PCF (Product Carbon Footprint) and associated carbon costs increase. This aspect will be further elaborated upon in Section 5.6. Furthermore, the Monaca fuel gas carbon intensity is lower than the WINNER fuel gas carbon intensity (0.14 vs. 0.24 tCO_2/MWh). This difference in carbon intensity can be attributed to the fact that in the WINNER process, only 5% of the produced H_2 is present in the fuel gas, with the remaining 95% diffusing through the membrane in the PCEC reactor.

U.S. electricity markets have both wholesale and retail segments. The wholesale markets involve the sale of electricity among utility traders before it is sold to the end consumers, while the retail markets deal with the selling of electricity directly to consumers [96]. The retail price of electricity varies by state and sector. For this analysis, the average industrial retail electricity price from 2015 to 2020 is used. This time range is purposefully truncated at the start of the COVID-19 pandemic because electricity prices saw significant increases in response to the pandemic (an 8% increase in 2021 and 18% in 2022). Table 5-8 presents the average annual retail electricity price in the industrial sector in the U.S. from 2015 to 2020 [91]. The average retail electricity price in the industry in the United States between 2015 – 2020 was $68.25/MWh. The carbon intensity of electricity in the U.S. was 0.369 tCO_2/MWh in 2022 [88] (Table 5-7) because of burning NG and coal to generate electricity.

Table 5-8: Average annual retail electricity price in industry in the U.S. [91].

Year	2015	2016	2017	2018	2019	2020	Average
Average retail electricity price [$/MWh]	69.1	67.6	68.8	69.2	68.1	66.7	68.25

Carbon Costs

The market price of utilities often does not reflect the full cost of their usage as it fails to capture environmental impacts, such as climate change and air pollution. To address this inconsistency, the concept of carbon pricing has been introduced. It integrates these external costs into the market, ensuring a more comprehensive cost. By making polluting fuels, utilities, and products more expensive, carbon pricing encourages the adoption of cleaner energy alternatives and ensures that the entities emitting GHGs bear the associated costs [97]. This can be achieved through policies such as:

- Carbon taxes: These directly levy charges on the production of GHG emissions.
- Emission Trading Schemes (ETS) or 'cap and trade' systems: These establish a maximum pollution level and require that manufacturers hold permits for emitting GHGs.

The U.S. currently does not have a carbon tax. They have an ETS in place, of which the weighted carbon price in 2020 amounted to $1.01/t$CO_2$ [98]. There are other measures to internalize the cost of emitting GHGs, such as the Social Cost of Carbon (SCC). The SCC quantifies the economic damage associated with an increase in CO_2 emissions, typically expressed in $/t$CO_2$. Currently, the U.S. government uses a price of $51/t$CO_2$ emitted to monetize the SCC [94], while other studies indicate that this price should be $185/t$CO_2$ [99]. As a reference, the cost of emissions allowances in the EU in July 2023 were around €90/tCO_2 [100].

As becomes clear from the large differences in the cost of carbon, the U.S. is still struggling to monetize the cost of carbon emissions. For this research, the current price of carbon that the U.S. government uses for its cost calculations of 51$/t$CO_2$ was selected [94].

Figure 5-5 visualizes the variable costs for the WINNER process [1500 KTA], with adapted heat integration (Section 4.4.1) versus the Monaca benchmark. The red figures in Figure 5-5 indicate a negative development of the WINNER process with respect to the Monaca benchmark. In this case, an increase in costs. This convention will be used throughout the rest of this report. The variable operational costs depend on the feed and product prices. These commodity prices are listed in Table 0-13 in APPENDIX R.

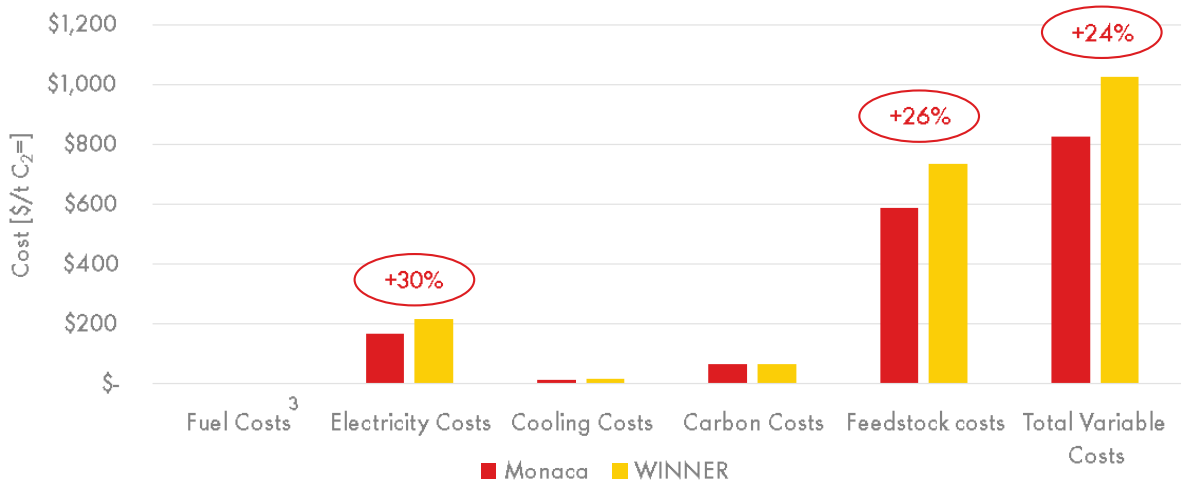

Figure 5-5: Comparison between the WINNER process and the Monaca benchmark of various variable cost components in $/tC$_2$= [3]. Red figures indicate a negative development of the WINNER process with respect to the Monaca benchmark.

The analysis of the variable costs yields several key insights. Notably, the Total Variable Costs (TVC) of the WINNER process exceed those of the Monaca benchmark by approximately 25%. This cost difference arises from higher feedstock costs, caused by the WINNER process's higher total product output compared to Monaca (2415 vs. 1926 KTA).

Furthermore, the WINNER process has about 30% higher electricity costs, which is a significant contributor to its overall higher operating costs. Conversely, the costs associated with cooling and carbon remain relatively low for both processes. The carbon costs for the two processes are roughly equivalent, despite the U.S. electricity grid's carbon intensity being approximately four times that of refinery fuel (0.37 vs. 0.10 tCO$_2$/MWh). These findings suggest opportunities for future cost reductions. As the electricity grid develops towards lower carbon intensity, the WINNER process, more dependent on grid electricity, will benefit more substantially. Consequently, a faster decrease in carbon costs in the WINNER process is anticipated. This highlights the advantages of the WINNER process in an increasingly decarbonized energy scenario.

5.3.2. Fixed Costs

Fixed operational costs are expenses that remain relatively stable, regardless of the level of production. These costs include depreciation, insurance, and the salaries of permanent

[3] In both processes, fuel costs are effectively zero as the production of fuel gas exceeds its consumption at the furnaces. The surplus fuel gas, which is produced but not burned in the furnaces, is sold.

staff. Table 5-9 gives an overview of the different components of the fixed OPEX, the associated assumption, and its corresponding value [101].

Table 5-9: Overview of annual fixed OPEX plant costs (table was constructed based on [101]).

Component	Assumption	Value [$MM/yr]	Value [$/tC$_2$=]
Operating labour	2 shift positions (4.8 operators/shift position)	0.5	0.3
Supervision	25% of labour	0.1	0.1
Direct salary overhead	50% of (operating labour + supervision)	0.3	0.2
Maintenance	4% of ISBL	5.5	3.6
Property taxes and insurance	1% of ISBL	1.4	0.9
Rent of land (and/or buildings)	1.5% of (ISBL + OSBL)	3.1	2.1
General plant overhead	1% of ISBL	1.4	0.9
Allocated environmental charges	1% of (ISBL + OSBL)	2.0	1.4
Capital charges	15% of TCI	52.2	34.8
PCEC cell stack replacement	Lifetime of 60,000 h	9.7	6.5
Total FC	**Sum of above**	**76.1**	**50.8**

When analyzing projects that are still in the early stages of research, particularly those at TRLs 1 or 2, making a detailed estimate of fixed costs can be challenging due to the high level of uncertainty around the assumptions. In such cases, a commonly applied approach within the Process Evaluations Department at Shell is to set the fixed annual OPEX as 3.5% of the CAPEX and include an additional 15% of the CAPEX as annual capital charge. This method simplifies the estimation process and provides a rough overview of the expected financial requirements. This assumption stems from personal communications with Luis Fernando Castro, a Process Evaluation Engineer at Shell [102]. Table 5-10 presents the outcomes of the fixed OPEX estimation with these assumptions.

Table 5-10: Fixed OPEX based on Shell Process Evaluations low TRL procedure [102].

Component	Assumption	Value [$MM]	Value [$/tC$_2$=]
Fixed OPEX (annual)	3.5% of CAPEX	12.2	8.1
Capital charge	15% of CAPEX	52.2	35.6
PCEC cells stack replacement	Lifetime of 60,000 h	9.7	6.5
Total FC	**Sum of above**	**75.2**	**50.1**

It becomes clear that both procedures, outlined in Table 5-9 and Table 5-10, lead to roughly the same outcome of approximately $75 million fixed annual OPEX (or $50/tC$_2$= produced). This value will be used in further analyses.

5.4. Profitability Analysis

5.4.1. Margin

Figure 5-6 visualizes various economic performance indicators for both the WINNER process and the Monaca benchmark. For specific values and a complete overview of these economic indicators, please refer to APPENDIX T.

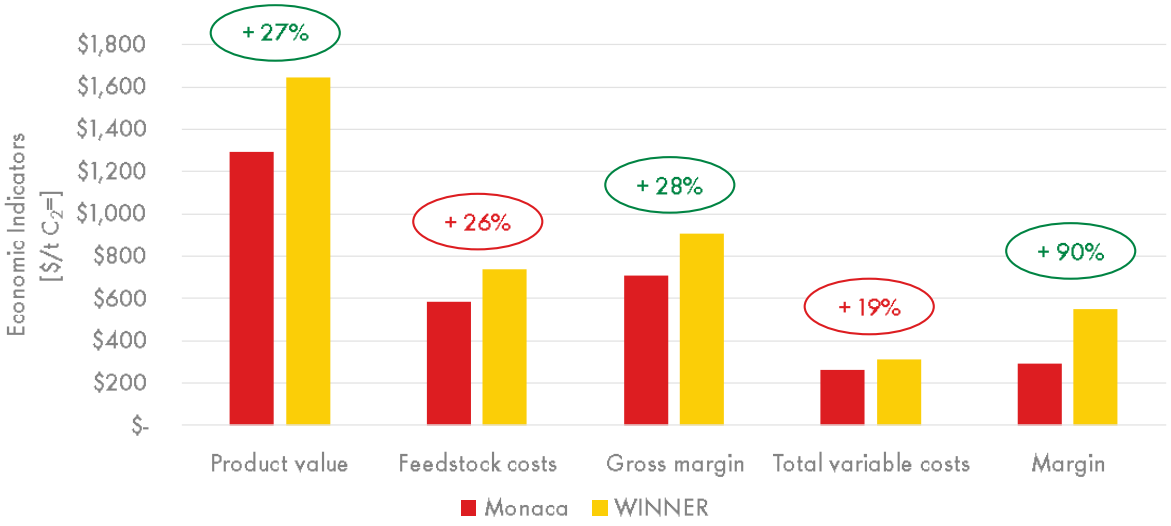

Figure 5-6: Comparison of economic outputs [$/tC$_2$=] for different performance indicators.

When assessing a low TRL technology like the WINNER process economically, the margin is a critical indicator. The margin, defined as the difference between the product value and the total cost of production, serves as an indicator of the profitability of the plant [101]. A positive margin indicates that the selling price of the products is higher than the total cost of production, indicating profitability. Figure 5-6 indicates a significant economic advantage for the WINNER process, as it approximately doubles the net margin compared to the Monaca benchmark. This conclusion, however, is heavily dependent on

the ability to overcome the technical challenges associated with scaling up the WINNER process to a production level of 1500 KTA.

A primary factor contributing to the favourable economics of the WINNER process is the high net export of fuel gas compared to the Monaca benchmark. In addition, the generation of 141 KTA of pressurized hydrogen as a valuable byproduct contributes to the total product value. As a result, the overall product value is roughly 30% higher at the specified plant capacity of 1500 KTA ethylene. Figure 5-7 visualizes the contributions of the different output products in $/tC$_2$= for the Monaca benchmark and the WINNER process. As such, Figure 5-7 is a detailed representation of the product value bars on the left-hand side of Figure 5-6.

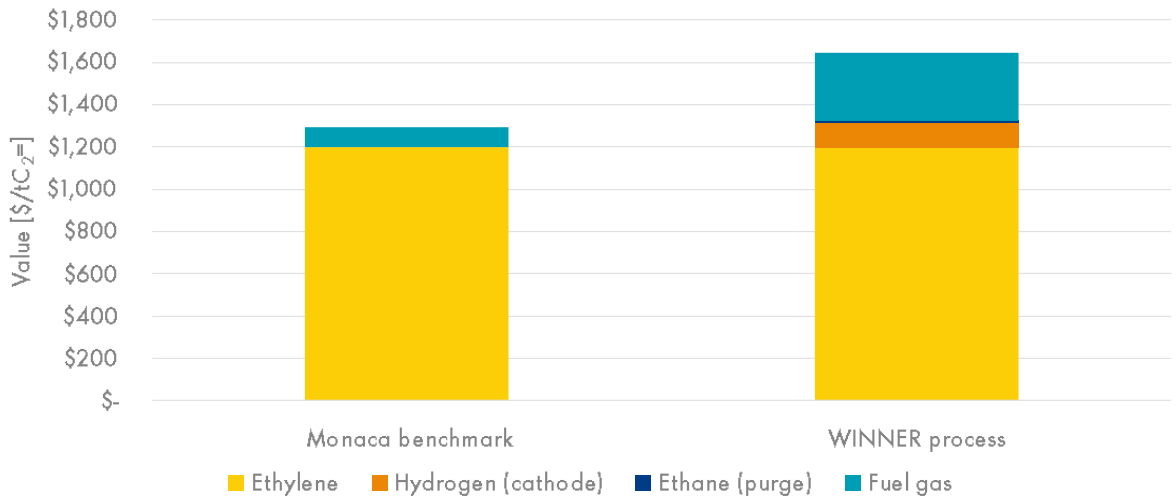

Figure 5-7: Stacked product value for the Monaca benchmark and the WINNER process in $/tC$_2$=.

Lastly, ~25% higher feedstock costs are observed in the WINNER process. This is a result of a higher total product output compared to the Monaca process (2415 KTA vs. 1926 KTA). This can be primarily attributed to the lower ethylene selectivity within the WINNER process, for a similar rated capacity of 1500 KTA.

5.4.2. NPV and IRR

Net Present Value (NPV) and Internal Rate of Return (IRR) are commonly used metrics in investment and planning to analyse the profitability of future projects. The NPV calculates the current value of a projected future stream of payments, representing the difference between the present values of cash inflows and outflows over a given period [103]. Equation (5-3) shows the formula for calculating a project's NPV [103].

$$NPV = \sum_{t=0}^{T} \frac{C_t}{(1+i)^t} - C_0 \tag{5-3}$$

Where:

T	is the plant lifetime [years],
C_t	is the net cash flow for year t [$],
i	is the discount rate [%],
C_0	is the initial investment [$].

The IRR is the yearly return that results in an NPV of zero. As shown in Equation (5-4), the calculation of IRR relies on the same formula as that of NPV [104].

$$0 = NPV = \sum_{t=0}^{T} \frac{C_t}{(1+IRR)^t} - C_0 \qquad (5\text{-}4)$$

The IRR can be calculated by restructuring Equation (5-4) and setting the NPV to zero. For the evaluation of this project, a discount rate of 10% is assumed, which is a commonly used value [103]. The discount rate denotes a return that could be earned in alternative investments. A positive NPV suggests that the projected earnings of a project or investment, discounted to their present value, exceed the anticipated costs, also measured in today's dollars. Generally, an investment with a positive NPV is considered profitable. When it comes to IRR, typically, a higher IRR makes an investment more desirable [104].

As a final economic KPI (Key Performance Indicator), the Minimum Selling Price (MSP) of ethylene is included. The MSP represents the minimum market price, under the principle of "ceteris paribus", at which ethylene must be sold to ensure a profitable investment case (NPV > 0). The Latin phrase "ceteris paribus" translates to "all other things being equal". It implies that while the price of ethylene is varied, all other input factors are held constant. A comparison of the economic KPIs for both the WINNER process and the Monaca benchmark is presented in Table 5-11.

Table 5-11: Comparison of economic KPIs (margin, NPV, and IRR) for the WINNER process and the Monaca benchmark.

Parameter	WINNER process	Monaca benchmark
Discount rate (i)	10%	10%
C_t (annual margin)	$816 million	$434 million
NPV	$6.6 billion	$2.5 billion
IRR	234%	35%
Ethylene MSP	$684/t$C_2$=	$1009/t$C_2$=

Upon economic comparison, the WINNER process outperforms the Monaca benchmark. The margin in the WINNER process approximately doubles, NPV nearly triples, and the IRR is roughly seven times higher compared to the Monaca benchmark. The MSP in the WINNER process is roughly 30% lower compared to the benchmark, suggesting that the

WINNER process can present a favourable investment case – with an NPV greater than zero – at a much lower ethylene selling price.

These outcomes highlight an extremely positive investment case for the WINNER process. However, it is critical to note that these results are largely dependent on the assumptions made regarding input parameters, such as the commodity prices of the feedstock and products. To account for these uncertainties and assess their impact on NPV and IRR, a sensitivity analysis on economic inputs is presented in Section 5.6.2.

5.5. Environmental Analysis

5.5.1. Product Carbon Footprint

Evaluating the environmental impact of the WINNER process compared to the Monaca benchmark involves calculating the associated carbon emissions from ethylene production. To quantify the environmental impacts of a product or technology, methods like Life Cycle Assessment (LCA) or PCF (Product Carbon Footprint) are used. An LCA is a recognized scientific tool to assess the environmental performance of a product system by considering all relevant aspects of its impacts from raw materials for manufacturing to disposal at end-of-life [105]. Both methods for emission calculations relate to scope 1, 2, and 3 emissions, which are terms that are widely used in the literature. They refer to classifications of GHG emissions based on origin and responsibility [106, 107]:

- Scope 1 emissions encompass GHG emissions from sources directly owned or controlled by an organization (e.g., stationary combustion and process emissions).

- Scope 2 emissions are GHG emissions caused indirectly by an organization due to the energy it purchases and uses (e.g., electricity, steam, and heat).

- Scope 3 emissions encompass GHG emissions from sources not owned or controlled by an organization, but which are a result of its activities. This includes emissions along the organization's value chain, such as those from the use and disposal of products from suppliers and encompasses all sources not within scope 1 and 2 boundaries (e.g., emissions from end products and extraction and production of purchased feedstocks).

As discussed earlier, scope 1, 2, and 3 emissions relate to boundaries of LCAs and PCFs. When the environmental performance of chemical products is assessed, the PCF (Product Carbon Footprint) is of specific interest. The PCF encompasses all the upstream life cycle emissions to produce an intermediate product, as illustrated in Figure 5-8. Feedstock, fuel, and utility flows are shown and categorized as scope 1, 2, or 3 emissions. It covers the life cycle stages of raw material extraction and intermediate product manufacturing. PCF can

therefore be regarded as the result of a Cradle-to-Gate LCA analysis of an intermediary product.

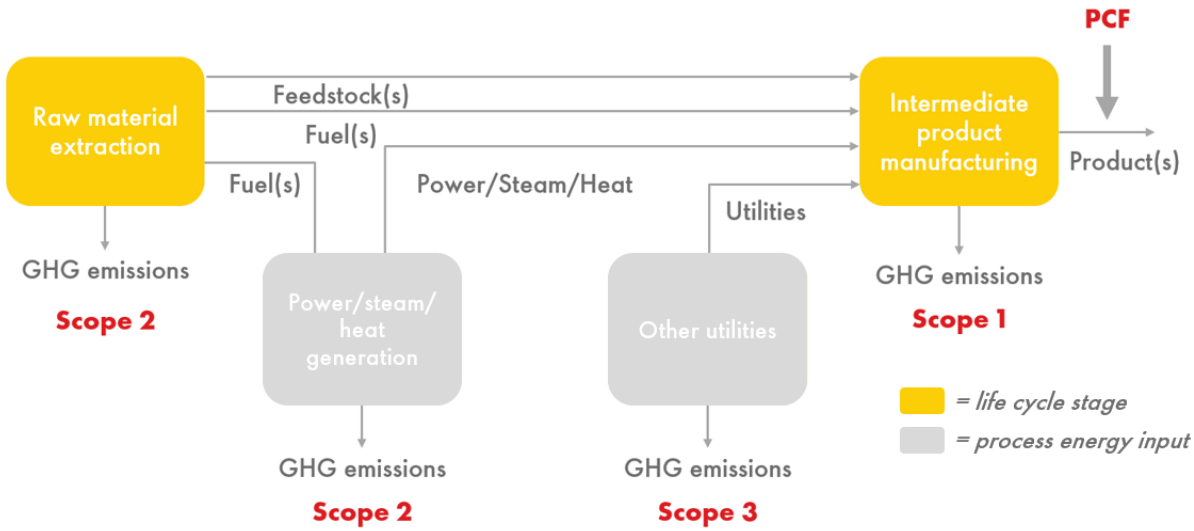

Figure 5-8: PCF upstream life cycle emissions for chemical intermediate product manufacturing (the figure was drawn based on [107]).

In this research, the focus is on calculating the PCF associated with carbon emissions from utility consumption, consequently excluding carbon emissions linked to raw material extraction. This approach was chosen because the PCF associated with feedstock inputs is similar in both the WINNER process and the Monaca benchmark. As such, this aspect was not included in the PCF comparison. Figure 5-9 shows the results of the PCF comparison between the WINNER process and the Monaca benchmark.

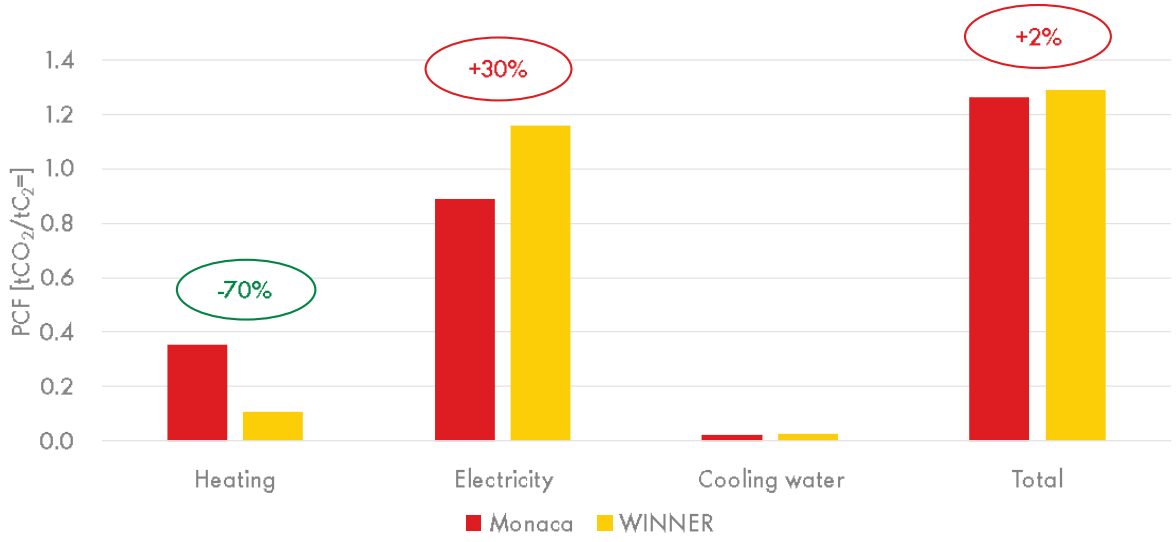

Figure 5-9: Product Carbon Footprint of produced ethylene based on utility consumption in $tCO_2/tC_2=$.

Upon analysis, the PCF indicates that both the WINNER process and the Monaca benchmark, when accounting for emissions resulting from utility consumption, have similar total PCFs. This is attributed to the substantial contribution to the PCF from the heating

requirements in the Monaca benchmark. Conversely, the PCF of the WINNER process is significantly influenced by the high electricity consumption. Notably, the carbon intensity of the U.S. grid in 2023 was significantly higher at 0.37 tCO_2/MWh [88] compared to 0.14 tCO_2/MWh for Monaca fuel gas. The increased carbon intensity for grid electricity is related to inefficiencies in electricity generation: the efficiency of electricity generation typically lies around 40%. In addition, the current U.S. grid has a significant reliance on fossil fuels in electricity generation, making up approximately 60% of the electricity generation mix [108]. This higher carbon intensity of electricity, in combination with the high share of electricity consumption in the WINNER process, leads to electricity consumption being the dominant contributor to the total PCF.

Conversely, the carbon footprint associated with cooling water processes is relatively small, due to the small contribution of cooling water to the total SEC and its low carbon intensity, estimated at 0.026 tCO_2/MWh [93].

To assess the decarbonization potential of the WINNER process, it is crucial to factor in scenarios involving renewable electricity. Accordingly, three distinct scenarios have been delineated, as outlined in Table 5-12. Notably, the proportion of non-renewable energy (non-RE) in the US 2023 scenario is higher than the approximately 60% referenced earlier. This discrepancy is attributed to the classification of nuclear electricity as a non-RE source.

Table 5-12: Different grid electricity scenarios for the U.S.

Scenario	Carbon Intensity [tCO_2/MWh]	RE share [%]	Non-RE share [%]
U.S. 2023 – Base Case	0.37	17	83
50% RE	0.23	50	50
100% RE	0.026	100	0

The carbon intensity for these scenarios is extrapolated using the carbon intensity of electricity generated from fossil fuels and renewable electricity generated by wind turbines. An LCA approximates the carbon footprint of wind turbine-generated renewable electricity at 0.026 tCO_2/MWh [109]. Figure 5-10 compares the PCF caused by utility consumption for the WINNER process and the Monaca benchmark for the different grid electricity scenarios. The two bars on the left represent the PCF in the U.S. 2023 grid scenario, with a renewable energy share of 17%. The two bars in the middle represent a 50% RE scenario. Lastly, the two bars on the right adhere to the 100% RE electricity scenario. Red, yellow, and light blue colours display carbon emissions caused by heating, electricity, and cooling water, respectively.

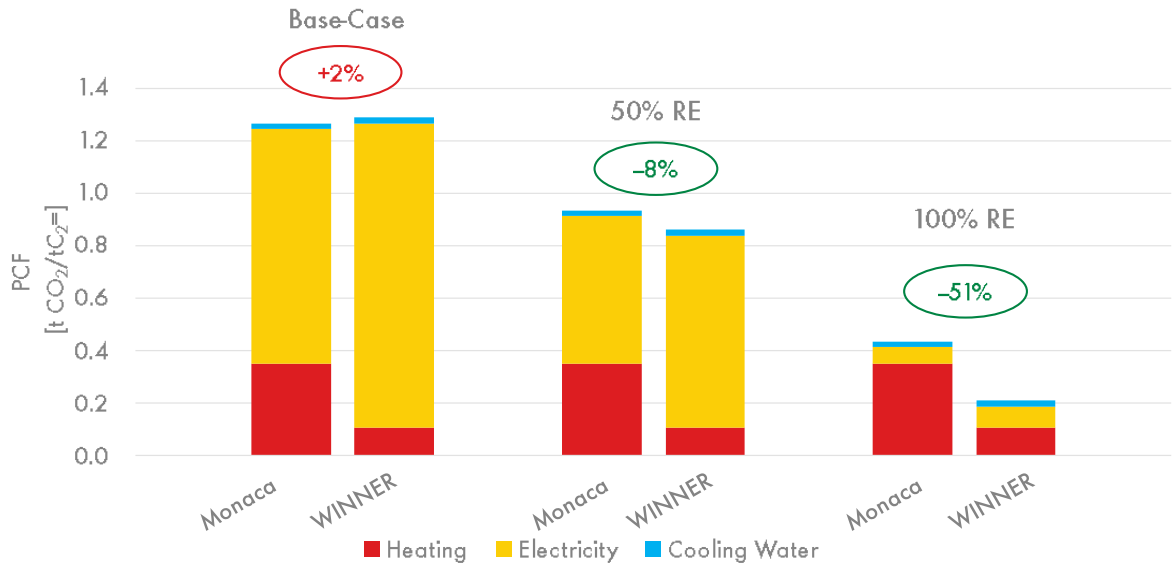

Figure 5-10: Comparison of the PCF caused by utility consumption for the WINNER process and the Monaca benchmark for different grid electricity scenarios.

As the proportion of renewable electricity increases, the carbon intensity of the grid decreases, leading to a corresponding reduction in the total PCF from utilities. Given the higher dependence of the WINNER process on electricity, its PCF decreases more with an increasing share of RE in the grid. In other words, the WINNER process benefits more from a decarbonizing grid than the Monaca benchmark. While the base case shows a slightly larger (2%) PCF for the WINNER process, the 50% RE scenario already results in an 8% PCF reduction. In the 100% RE scenario, the PCF of the WINNER process is roughly halved compared to the Monaca benchmark. The total PCF resulting from utility consumption in the 100% RE scenario is 0.21 $tCO_2/tC_2=$, representing a decrease of approximately 85% compared to the base case grid electricity of 1.29 $tCO_2/tC_2=$.

In the e-cracking scenario from Section 4.5.2, the heating duties in Figure 5-10 would be replaced by electrical power needs. As the carbon intensity of electricity decreases with a growing proportion of renewable energy, the carbon intensity of the fuel gas used for heating furnaces remains constant. If this share of energy, currently being fulfilled by burning fuel gas, is replaced by electricity to operate the electrical furnaces, the Monaca benchmark could approximately benefit as much from the reduction in carbon intensity as the WINNER process. Hence, electrifying furnaces is a significant development that could likely be implemented sooner than the WINNER process to electrify process duties.

Furthermore, a recommendation for future research is to investigate the implications of fuel gas sales on the project's Scope 3 emissions. These fuel gases will most likely be combusted at a later stage, resulting in associated carbon emissions. In the event of an evaluation of the WINNER process's Scope 3 emissions, these additional emissions should be considered.

5.5.2. Inflation Reduction Act

Recent developments in U.S. energy regulation may impact the profitability of hydrogen production within the WINNER process. Specifically, the Inflation Reduction Act (IRA) is a key policy instrument directing federal investments towards reducing carbon emissions, among other things. This legislation allocates nearly $400 billion in federal funds to green energy to significantly reduce the country's carbon emissions by the end of the decade [110].

One critical aspect of the IRA is the "45V Hydrogen Production Tax Credit", aimed at incentivizing the production of low-carbon hydrogen [111]. Given the substantial amount of hydrogen (141 KTA) produced as a byproduct in the WINNER process, this policy could significantly enhance the process's profitability. The "45V Hydrogen Production Tax Credit" offers payments over a 10-year period, based on the amount of hydrogen produced [112]. Table 5-13 presents the ranges of permitted carbon emissions per ton of hydrogen produced, alongside their corresponding tax credit. It is crucial to note, however, that these permitted carbon emissions are assessed on a "cradle-to-gate" lifecycle basis (Section 5.5.1). This implies that all emissions from raw material extraction up until the produced hydrogen exits the WINNER process plant should be included [113].

Table 5-13: Lifecycle ("cradle to gate") permitted carbon emissions and resulting tax credits according to the Hydrogen Production Tax Credit in the IRA [112].

Permitted carbon emissions [tCO_2/tH_2]	**Fraction of maximum tax credit [%]**	**Tax credit [$/tH_2$]**
2.5 – 4	20	600
1.2 – 2.5	25	750
0.45 – 1.2	33	1000
0 – 0.45	100	3000

Assigning carbon emissions to product outputs in the WINNER process is complex due to the byproduct nature of hydrogen production. Most carbon emissions from the process are traditionally tied to the production of ethylene, making the associated emissions from hydrogen production "free". One proposed methodology to calculate the carbon emissions associated with the WINNER process's hydrogen production is to focus exclusively on the electricity consumption in the PCEC reactor (59 MW). This approach neglects the carbon emissions tied to raw material extraction, but it provides a sense of how the hydrogen produced in the WINNER process would be classified under the IRA. Table 5-14 shows the "hydrogen footprint" for the WINNER process across the various grid scenarios, as introduced in Section 5.5.1. This table shows how the carbon emissions

associated with hydrogen production vary under different renewable energy adoption rates.

Table 5-14: Comparison of the carbon footprint associated with hydrogen production in the WINNER process across the various grid electricity scenarios.

Scenario	Carbon intensity [tCO_2/MWh]	Hydrogen footprint [tCO_2/tH_2]	Tax credit [$/$tH_2$]
U.S. 2023	0.37	1.30	750
50% RE	0.23	0.82	1000
100% RE	0.026	0.09	3000
IRA max credit limit	0.128	0.45	3000

The application of different tax credits varies across the U.S. 2023, 50% RE, and 100% RE grid scenarios. Notably, only the 100% RE grid scenario results in the maximum tax credit of \$3000/tH_2. Figure 5-11 demonstrates the impact of the increasing hydrogen price due to the IRA on the WINNER process's product value. The tax credits, as specified in Table 5-14, are added as an additional value over the base case hydrogen price of \$1200/tC_2=. The progressively increasing height of the orange bar represents the growing contribution of hydrogen sales to the product value under different electricity scenarios. The contribution from hydrogen revenue grows from 7% in the Base Case to 11% in the U.S. 2023 scenario, 12% in the 50% RE scenario, and finally to 21% in the 100% RE scenario. This trend emphasizes the economic benefits of decarbonizing utilities to leverage the 45V Hydrogen Production Tax Credit policy.

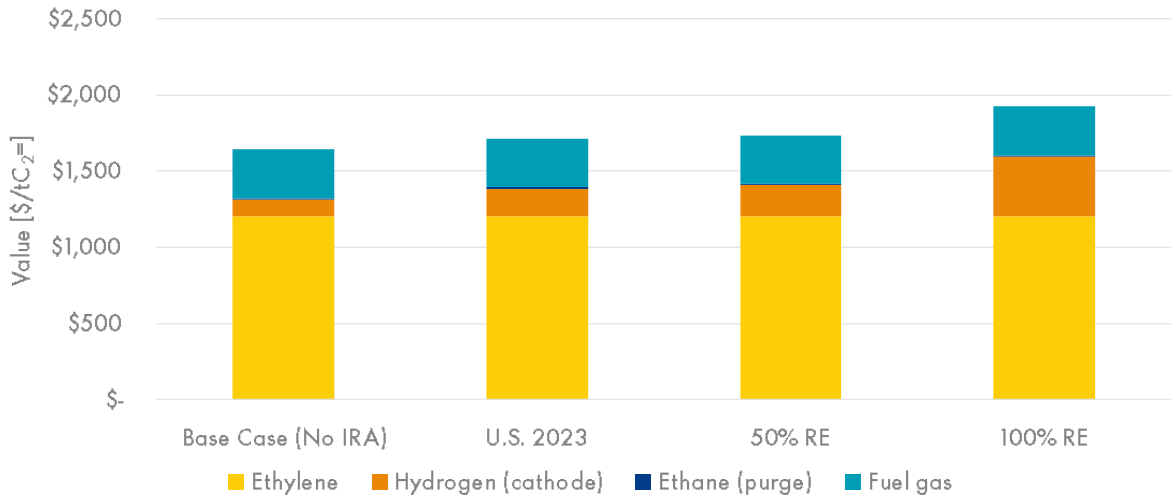

Figure 5-11: Product value for the WINNER project for the various electricity grid scenarios, taking into account the increase in hydrogen price in line with the IRA indicated in Table 5-14.

However, considering the goal of this policy is to promote the production of low-carbon hydrogen, it is unlikely these tax credits would still be applicable once the U.S. grid is entirely powered by renewable energy. Nevertheless, the current U.S. 2023 scenario provides a significant bonus compared to the currently assumed hydrogen price of $1200/t$H_2$ (refer to APPENDIX R). To be eligible for the maximum tax credit, the carbon intensity of electricity consumed in the PCEC reactor needs to be less than 0.128 tCO_2/MWh. This corresponds to a renewable energy share of approximately 75%. Thus, significant reductions in carbon intensity in the electricity consumed are necessary to fully leverage the benefits of the Hydrogen Production Tax Credit of the IRA.

5.5.3. Critical Raw Materials

When evaluating the environmental aspects of a novel technology, the use of critical raw materials within the process is a key consideration. For the WINNER process, these primarily originate from the complex components used in the PCEC reactor and the PtGa/ZSM-5 catalyst. The PCEC components, as introduced in Table 2-3 (Section 2.3.3), include the PBFM hydrocarbon electrode, BZCYYb electrolyte, and porous Ni-BZCYYb hydrogen electrode. Figure 5-12 illustrates the abundance of elements within the Earth's upper continental crust and is used to determine the availability of the PCEC materials:

- PBFM, or $(PrBa)_{0.95}(Fe_{0.9}Mo_{0.1})_2O_{5+\delta}$ consists of praseodymium (Pr), barium (Ba), iron (Fe), and molybdenum (Mo) [114]. Praseodymium, the least abundant among these, has an abundance of approximately 9 ppm [115].

- BZCYYB, or $BaZr_{0.1}Ce_{0.7}Y_{0.1}Yb_{0.1}O_{3-\delta}$ consists of barium (Ba), zirconium (Zr), cerium (Ce), yttrium (Y), and ytterbium (Yb). The least abundant of these elements, ytterbium, has an approximate abundance of 3 ppm. Yttrium, despite being a rare-earth element, has an abundance of 30 ppm [115].

- Ni-BZCYYb, which comprises similar materials as BZCYYb along with nickel, does not pose any availability issues due to nickel's status as a major industrial metal. However, the limited abundance of ytterbium and yttrium (as mentioned above) may pose challenges when scaling up the process [115].

- Finally, the PtGa/ZSM-5 catalyst consists of platinum (Pt), gallium (Ga), and Zeolite Socony Mobil-5 (ZSM-5). ZSM-5 is an aluminosilicate mineral that contains sodium (Na), aluminium (Al), silicon (Si), and oxygen (O) [116]. Among these, platinum is the rarest, with an abundance of approximately 0.004 ppm, placing it among the "rarest metals". Gallium, while not as rare, also has a relatively low abundance at 19 ppm [115].

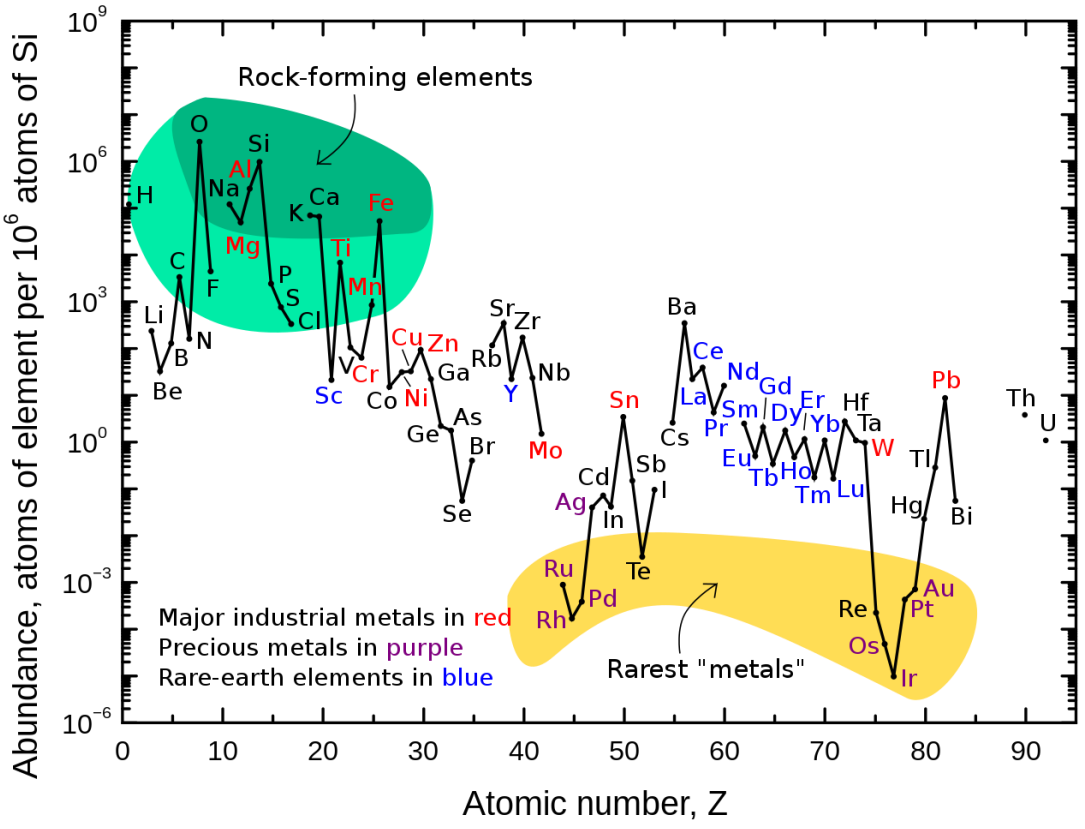

Figure 5-12: Elemental abundance (atom fraction) in Earth's upper continental crust, represented as a function of atomic number and compared to the abundance of silicon [115].

The use of platinum in the catalyst presents a significant bottleneck in terms of material abundance in the WINNER process, given its scarcity and the relatively low annual global extraction of platinum (only 172 tons in 2016) [115]. The PCEC electrode materials are likely to be quite expensive and not widely available due to the complexity and cost of the processes used to synthesize them, rather than the scarcity of the raw elements themselves [114].

Given the technology's low TRL, there is a lack of clarity on the exact quantities of the materials required for an industrial-scale plant. This uncertainty stems from immature process parameters, such as ethane conversion. As a result, the consumption of the PtGa/ZSM-5 catalyst has not yet been quantified and the degradation rates of electrode materials are unknown. Therefore, a critical next step involves determining the total material and catalyst requirement. By comparing this to the materials' availability, the feasibility of scaling up the process to industrial levels can be better evaluated.

5.6. Sensitivity Analysis

As part of the comprehensive assessment of both the technical and economic performance of the WINNER process, sensitivity analyses have been conducted. A sensitivity analysis determines how different values of input variables affect the model's output. It is instrumental in understanding how different input uncertainties affect the overall uncertainty of the model [117]. Section 5.6.1 covers the technical sensitivity analysis by considering the impact of variations in fractional conversion in the PCEC reactor on process KPIs. It does so by using the scenarios explained in Section 4.5. Section 5.6.2 shows the results of a sensitivity analysis of economic inputs on the NPV and IRR of the process.

5.6.1. Fractional Conversions

This sensitivity analysis varies the values of the fractional conversions in the PCEC reactor. The different scenarios are explained in detail in Section 4.5.1. Table 5-15 shows the three WINNER process scenarios: Conservative (Conser.), Base case (BC), and Future.

Table 5-15: Fractional conversions in the PCEC reactor for the different scenarios (repeated) [22, 66].

#	Stoichiometry	Fractional conversion			Limiting reactant
		Conser.	BC	Future	
1	$C_2H_6 \leftrightarrow C_2H_4(anode) + H_2(cathode)$	0.10	0.363	0.56	Ethane
2	$2C_2H_6 \leftrightarrow C_3H_8 + CH_4$	0.02	0.02	0.02	Ethane
3	$C_3H_8 \leftrightarrow C_3H_6 + H_2$	0.8	0.8	0.8	Propane
4	$2C_2H_4 \leftrightarrow C_4H_8$	0.23	0.23	0.05	Ethylene
5	$C_2H_6 + C_2H_4 \leftrightarrow C_3H_6 + CH_4$	0.032	0.032	0.07	Ethylene

Table 5-16 shows the results of the simulations of the scenarios on different fractional conversions within the PCEC reactor. The capacity of 1500 KTA of ethylene is kept constant in all three scenarios. In the case of the WINNER Conservative Scenario, this leads to a higher feedstock input due to lower ethane conversion and ethylene yield. Conversely, in the WINNER Future Scenario, this leads to a lower ethane feedstock input. The results for the Monaca simulation are included as a benchmark. Positive impacts on KPIs for the WINNER conservative and future scenario with respect to the WINNER base case are shown in green, while negative impacts are shown in red.

Table 5-16: Simulation results for variations in fractional conversions within the PCEC reactor, with positive and negative deviations from the base case highlighted in green and red, respectively.

Parameter	Unit	WINNER (Conservative)	WINNER (Base case)	WINNER (Future)	Monaca
S_{C2H4}	%	57	65	84	86
Single-pass X_{C2H6}	%	10	34	60	60
Y_{C2H4}	%	53	64	81	81
Annual H_2 production	KTA	149	148	118	N/a
SEC	MWh/tC_2=	16.9	4.5	3.0	5.8
NPV	$billion	-3.6	6.6	7.3	2.5
IRR	%	N/a	234	258	35
Margin	$/$tC_2$=	-254	544	599	289
MSP	$/$tC_2$=	1481	684	628	1009

The future scenario of the WINNER process outperforms the base case in all key aspects, showing the highest NPV ($7.3 billion), IRR (258%), and margin per ton of ethylene ($599/$tC_2$=), and the lowest ethylene MSP ($628/$tC_2$=). The only disadvantage of the future WINNER scenario is the lower annual H_2 production due to an increase in ethylene selectivity. This curtails hydrogen production via Reaction 3 (Table 5-15), as less ethane feedstock is required for 1500 KTA of ethylene output.

In contrast, the conservative scenario is economically unviable, with negative NPV and margins and no feasible IRR. The IRR is indicated with "N/a" since there is no positive rate of return that leads to an NPV equal to zero.

In technical terms, the WINNER process future scenario exhibits significant improvements in ethylene selectivity, ethane conversion, SEC, and yield compared to the base case. These values approach those of the optimized Monaca steam cracking process. However, the conservative scenario displays a strong decrease in technical performance parameters.

In summary, if the WINNER process realizes its future scenario, it could be more economically advantageous and technically equivalent to steam cracking. But if conservative estimates prove accurate during scaling, both economic and technical feasibility will be negatively impacted, leading to an unattractive outlook. Therefore, technological progress in R&D is required to achieve the "Future" scenario.

5.6.2. Economic Inputs

The base case for the WINNER process presents a strong economic argument for investment. However, this outcome relies heavily on the economic inputs used, primarily commodity prices for feedstocks and products, as well as utility consumption inputs. Estimating these values about 15 years in the future inherently involves a significant degree of uncertainty. The sensitivity analysis conducted identifies the input parameters that have the most significant impact on the projects' NPV and IRR. Table 5-17 shows the economic inputs that will be adjusted by -20%, -10%, +10%, and +20% compared to the base case.

Table 5-17: Economic inputs altered for sensitivity analysis.

Category	Input Change
Feed	Methane price
	Ethane price
	Propane price
Products	Ethylene price
	Hydrogen price
	Fuel gas price
Utilities	Electricity price
	Grid carbon intensity
	Carbon price

It is important to note that individual economic inputs have varying degrees of volatility. For instance, the price of hydrogen, especially low carbon hydrogen, could easily double or triple, as demonstrated in Section 5.5.2 about the IRA (Inflation Reduction Act). In contrast, inputs such as grid carbon intensity, ethylene price, and fuel gas price are not expected to exhibit such substantial deviations from their base values. Despite this, the adjustments of -20%, -10%, +10%, and +20% were chosen to demonstrate the sensitivity of these inputs on the economic KPIs.

Figure 5-13 visualizes the effects of modifying the input parameters listed in Table 5-17 on the NPV for the WINNER base case. The parameters are arranged in descending order of their impact on NPV. A wider bar implies a more substantial effect on the input parameter's modification on the NPV.

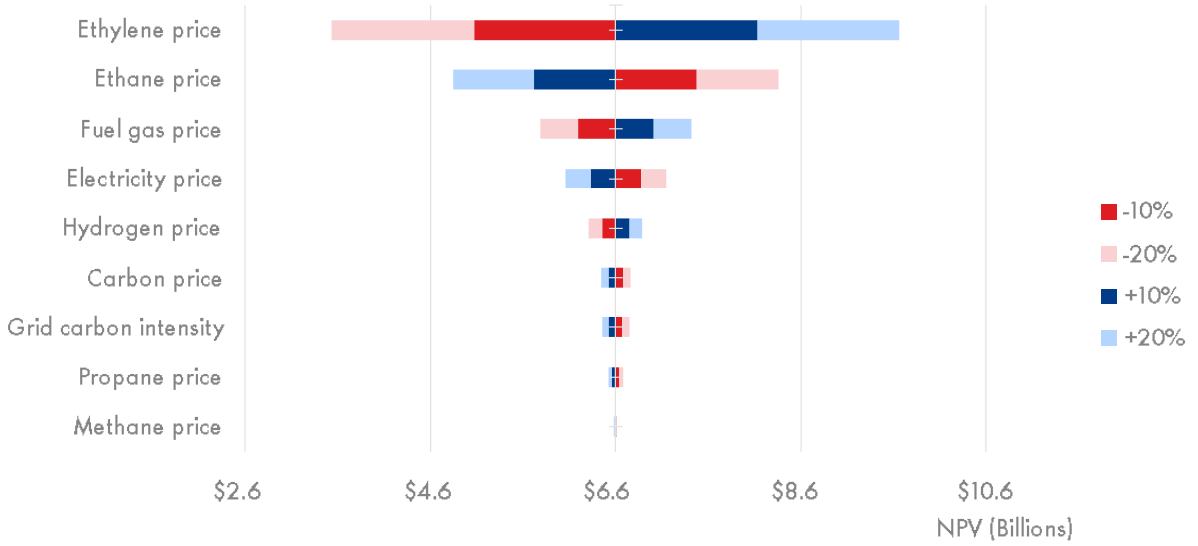

Figure 5-13: Sensitivity analysis showing the influence of percentual changes of economic inputs on the NPV (in billions of dollars) of the WINNER project.

Of all inputs, the ethylene price has the largest influence on the project's NPV. Given the substantial annual production of ethylene in the model (1500 KTA) and its relatively high base case price ($1200/t), even a small price fluctuation can significantly affect the NPV. For example, a 20% decrease in ethylene price results in an NPV of approximately $3.5 billion, whereas a 10% decrease leads to an NPV of roughly $5 billion. This demonstrates how to interpret the graph. An additional representation of this data, presenting the sensitivity of inputs in percentage change relative to the base NPV, can be found in APPENDIX U.

The ethane price, due to its high consumption (2328 KTA), is another sensitive input, although its impact is not as high as the ethylene price due to its lower base price ($450/t). Fuel gas price holds the third position in terms of its impact on the project's NPV. Economic inputs with minimal influence on the NPV include methane price, propane price, and grid carbon intensity. The latter, while significantly impacting the PCF (product carbon footprint) as discussed in Section 5.5.1., does not drastically affect the NPV.

A second sensitivity analysis is conducted on the impact on the IRR for this project. This analysis indicates the same sensitivity of the input parameters on the output IRR. As a result, the descending order of input parameters is similar in Figure 5-14. The same holds for a sensitivity analysis on the operational margin (APPENDIX U, Figure 0-13). Therefore, it can be concluded that the NPV, IRR, and operational margin have similar relationships and sensitivities with respect to their input parameters.

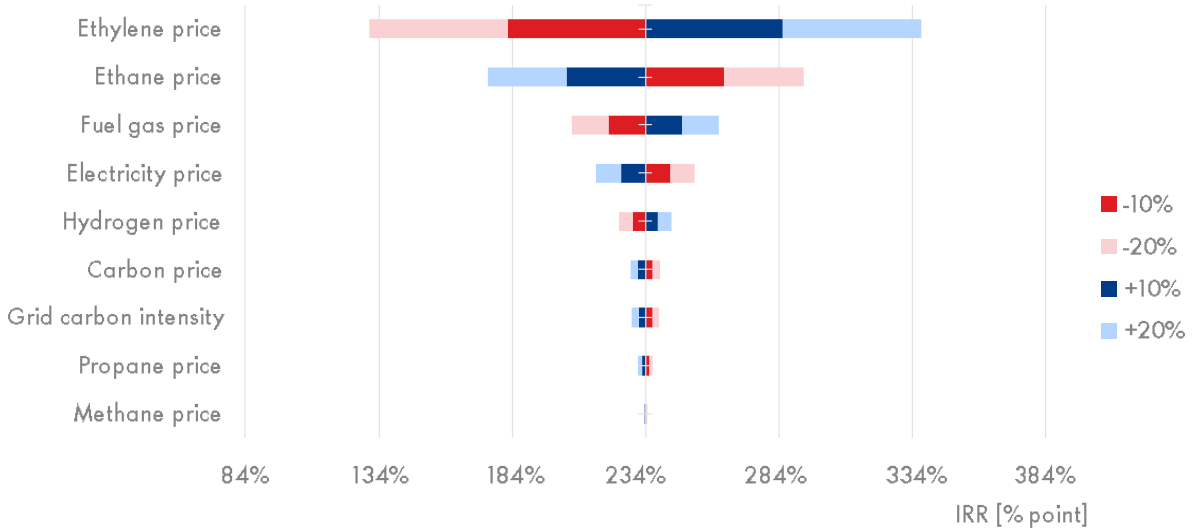

Figure 5-14: Sensitivity analysis showing the influence of percentual changes of economic inputs on the IRR (in percentage point) of the WINNER project.

6. Conclusions and Recommendations

This chapter sums up the conclusions, limitations, and recommendations from this study. Section 6.1 addresses the main research question, providing eight sub-conclusions substantiated by the results. These conclusions relate to energy consumption, technical parameters, process economics, environmental impacts, and sensitivity analysis outcomes. The conclusions stem from certain research choices, leading to the study's limitations in terms of technical and modelling constraints, which Section 6.2 covers. Finally, Section 6.3 offers recommendations for this research and future work in the field of PCECs for ethylene production.

6.1. Conclusions

The primary objective of this research was to address the following research question:

"What is the techno-economic performance and environmental impact of electrochemically enhanced ethylene production in proton-conducting electrochemical cells (PCECs), and how does this process compare to commercial ethane steam cracking in these aspects?"

The techno-economic and environmental performance of the WINNER process offer significant improvements compared to traditional ethane steam cracking. This conclusion is supported by eight sub-conclusions, which include four concerning energy consumption and technical parameters (1-4), two related to process economics (5 and 6), one addressing the environmental impacts (7), and one regarding the sensitivity analyses conducted (8).

1. The WINNER process has the potential to decrease the Specific Energy Consumption (SEC) by approximately 20% compared to commercial ethane steam cracking (where the latter is referred to as the Monaca benchmark).

2. The WINNER process curtails thermal energy demand by electrochemically enhancing ethylene production in PCECs, leading to a lower required operating temperature (550°C vs. 850°C).

3. Thermal energy consumption decreases by roughly 80%. There is a corresponding 30% increase in electricity consumption.

4. Process parameters, such as ethylene selectivity (65% vs. 84%), single-pass ethane conversion (34% vs. 60%), and ethylene yield (64% vs. 81%) show a disadvantage for the WINNER process compared to the Monaca benchmark. However, the SEC (expressed in MWh/t ethylene) decreases, indicating a potential to reduce carbon emissions associated with utility consumption. An overview of the key technical results is shown in Table 6-1.

Table 6-1: Comparative analysis on key process parameters and energy consumption-related results for the WINNER process base case versus the Monaca benchmark.

Parameter	Unit	WINNER process (Base case)	Monaca Benchmark
Annual C_2= production	KTA	1500	1500
Annual H_2 production	KTA	148	N/A
S_{C2H4}	%	65	84
Single-pass X_{C2H6}	%	34	60
Y_{C2H4}	%	64	81
$T_{Operating}$	°C	550	850
SEC	MWh/tC_2=	4.5	5.8
Heating duty	MWh/tC_2=	0.5	2.6
Electrical duty	MWh/tC_2=	3.1	2.4
Cooling duty	MWh/tC_2=	1.0	0.8

5. From an economic viewpoint, the WINNER process outperforms the Monaca benchmark based on the current input parameters and system configuration. The primary economic Key Performance Indicators (KPIs) evaluated include the annual margin (C_t), Net Present Value (NPV), Internal Rate of Return (IRR), and the Minimum Selling Price (MSP) of ethylene. The results for these KPIs for both process simulations are shown in Table 6-2. The WINNER process margin approximately doubles, the NPV nearly triples, and the IRR is roughly seven times higher compared to the Monaca benchmark. Moreover, the MSP of ethylene in the WINNER process is roughly 30% lower than the benchmark.

6. Thus, the WINNER process can deliver a profitable investment case, where NPV is greater than zero, even at a considerably lower ethylene selling price. A key advantage of the WINNER process over the Monaca benchmark is the production of pure (99.97%) and pressurized (50 bar) hydrogen. This high-value byproduct can be sold without the need for further product separation, thus adding to the economic benefits of the process.

Table 6-2: Economic KPIs (margin, NPV, IRR, and ethylene MSP) comparison between the WINNER process base case and the Monaca benchmark.

Parameter	WINNER process	Monaca benchmark
C_t (annual margin)	$816 million	$434 million
NPV	$6.6 billion	$2.5 billion
IRR	234%	35%
Ethylene MSP	$684/t	$1009/t

7. In terms of environmental impacts, current Product Carbon Footprints (PCFs) attributed to emissions from utility consumption are roughly the same in both processes. The WINNER process aims to electrify utilities, but with the current U.S. grid carbon intensity (0.37 tCO_2/MWh), this leads to an increase in carbon emissions compared to the carbon intensity of fuel gas for thermal furnaces (0.14 tCO_2/MWh for Monaca and 0.24 tCO_2/MWh for WINNER). Figure 6-1 visualizes this issue, suggesting that to reduce the utility-based PCF in the WINNER process, the U.S. grid electricity's carbon intensity needs to decrease through a more significant contribution from renewable energy sources. Achieving this would pave the way for the WINNER process to potentially decarbonize the utility-based PCF of ethylene production.

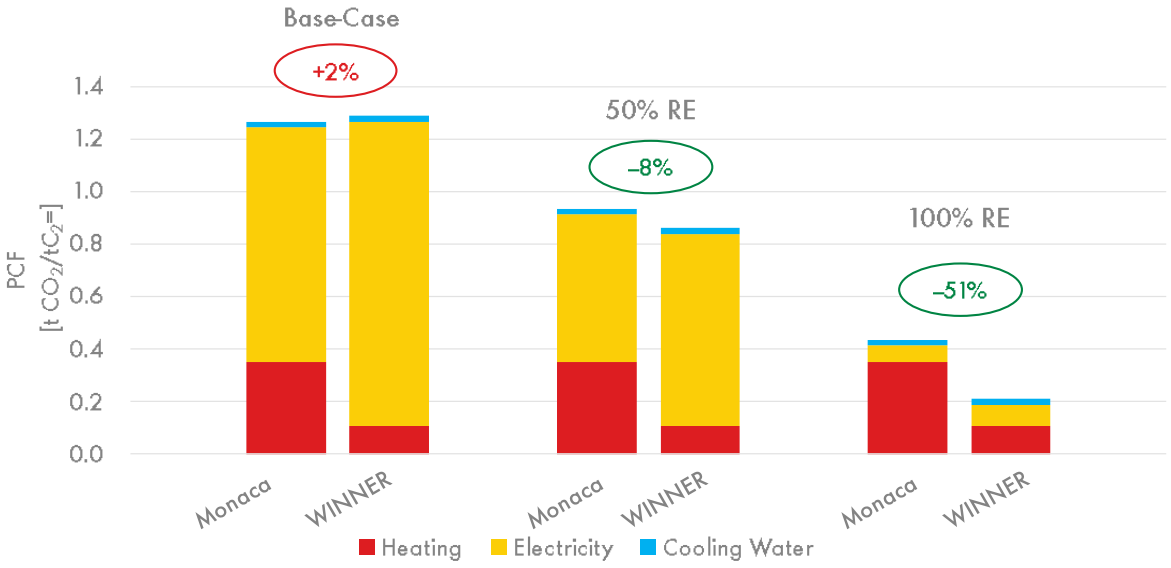

Figure 6-1: Comparative analysis of the PCF associated with utility consumption in the WINNER process and the Monaca benchmark under various grid electricity scenarios.

8. Sensitivity analysis reveals that the most influential input parameters are the prices of ethylene, ethane, and fuel gas. These commodity prices are characterized by high uncertainty due to limited availability of open-source data on chemical pricing.

Therefore, for any future investment considerations, it is crucial to accurately estimate the prices of these commodities as much as possible.

In summary, this research provides strong evidence of the WINNER process's superior techno-economic performance and its potential environmental benefits over the Monaca benchmark.

6.2. Limitations

This research comes with a set of limitations, which can be observed when critically evaluating the assumptions taken, the methodology used, and the results obtained. Section 6.2.1 highlights the technical limitations of the current study, while Section 6.2.2 emphasizes the limitations concerning modelling.

6.2.1. Technical

There are technical limitations to the conclusions presented in this thesis. Firstly, the study relies on lab-scale experimental data on technical parameters such as ethane conversion, ethylene selectivity, and ethylene yield. These parameters have been used to model an industrial-scale ethylene production plant with a capacity of 1500 KTA. However, this approach relies on the assumption that lab-scale parameters can be scaled to industrial operation without notable discrepancies in PCEC reactor process parameters. In practice, this does not necessarily have to be the case, due to challenges in scaling up electrochemical cells such as:

- Complications with mass and charge transport
- Heat management issues
- Material availability and associated cost
- Manufacturing challenges
- System integration barriers

Secondly, the data availability limitation is reflected in the use of a mixed feedstock in the reference experiments [6], which consists of 10% ethane and 90% argon. The reason for the use of argon in electrochemical experiments is to control the reaction, act as a carrier gas, regulate pressure, reduce ethane partial pressure to enhance electricity, and improve mass transport and electrode stability. However, the use of argon increases the required reactor volume due to the inert gas volume flowing through the reactor. So, in a commercial plant, it would never be used – the feedstock must be pure ethane. This discrepancy between experimental and industrial feedstock could negatively affect the plant's performance when scaled up. Addressing this limitation led to the introduction of the WINNER process conservative scenario, where the dependence of feed concentration

on fractional conversions was examined. The conservative scenario revealed a diminished economic advantage, suggesting that the investment case may not hold up.

Thirdly, the final technical limitation is the current density of 40 mA/cm^2 used in the experimental setup. A low current density leads to low production rates. To counteract this effect, the PCEC area should be scaled up to reach the same capacity. This leads to an increase in reactor volume, given that the membrane area of the PCEC is inversely proportional to the current density of the cell (APPENDIX P, Equation (0-6)). This, in turn, leads to increased CAPEX and inefficient use of space. When looking at the analogy of solid oxide electrolyzer cells (SOECs), it was found that for SOECs to become economically competitive, current densities are required to increase from typically 0.7 A/cm^2 to 1.5 A/cm^2 in 2030 [80]. One of the goals of the WINNER process is to reach a Faradaic Efficiency (FE) of 95% at a current density of 1 A/cm^2 [8]. This suggests that the target current densities are closer to 1 A/cm^2 rather than the 40 mA/cm^2 used in the experiments [6]. The associated recommendation for further research can be found in Section 6.3.

6.2.2. Modelling

Besides the technical constraints, limitations are also present in the modelling of the WINNER process. These primarily relate to the modelling of the separation train in AspenPlus. Currently, the distillation columns in the WINNER process model are not identical to the columns in the Monaca benchmark. This introduces a difference in heat integration for the WINNER process compared to the benchmark, leading to the choice of introducing a heat adaption methodology to account for these differences.

Secondly, the AspenPlus model uses fixed fractional conversions from literature to simulate the reactions occurring inside the PCEC reactor. Ideally, this static model would be converted into a dynamic model by creating a kinetic reactor model.

6.3. Recommendations

It is essential to outline some key recommendations for both continuing this thesis work and paving the way for future research. Section 6.3.1 proposes focus areas to improve this current thesis work. Section 6.3.2 offers suggestions on new areas of research that could contribute to the overall progress of the PCEC technology for ethylene production.

6.3.1. This Study

Validate lab-scale data for industrial process conditions.

In line with the limitations outlined in Section 6.2.1, a key recommendation for further research is to validate the lab-scale data under industrial-scale process conditions. This implies the use of a feedstock that does not contain any inert gas (argon) and consists of nearly 100% ethane feed. This requires R&D (research and development) to make

technological progress. Single-pass ethane conversion needs to be conserved at 36% when moving from a 10%/90% ethane/argon mixture to a pure ethane feed. Similarly, the performance needs to be preserved when scaling the current density by a factor of 25 from 40 mA/cm^2 to 1 A/cm^2.

Implement modelling improvements for more precise comparison.

The heat integration level of the WINNER process in the model developed in this thesis does not align precisely with the Monaca benchmark. As such, future research should aim to model the process to achieve an optimized level of heat integration that is comparable to the benchmark. This will give a more accurate comparison of the separation duties and bypass the need for the heat integration adoption procedure (Section 4.4.1). Additionally, it is advised to create a kinetic reactor model for the PCEC reactor, based on the reliable experimental data obtained at relevant process conditions. This would contribute to a more robust and accurate understanding of the reactor performance under real-world operational scenarios.

Optimize process design for enhanced performance and efficiency.

Further research should explore using high-pressure ethane feed, such as 30 bar, which aligns better with industry standards and prevents significant compression across the reactor membrane. Additionally, investigating the effect of reordering separation units in the process design could lower separation duties. For example, by positioning the de-ethanizer before the PCEC reactor (front-end de-ethanizer). These changes in process design could ultimately enhance the overall process performance, reduce costs, and further increase the attractiveness of the WINNER process. Moreover, the possibility to include additional separation units to be able to individually recover byproducts such as butene and propylene should be considered. This evaluation can substantiate the choice of investing in an additional separation unit based on expected revenues of byproduct sales.

Incorporate degradation mechanisms.

Currently, the influence of degradation mechanisms, such as coking, are not fully accounted for. For example, when increasing the ethane concentration from 10% to 100%, other coking pathways can be expected to occur. Moreover, additional factors impacting the lifetime and operation times of the PCECs have not been sufficiently investigated. Therefore, it is recommended to include these degradational elements in future research to provide a more comprehensive understanding of the PCEC's operational viability over time.

6.3.2. Future Research

Address material constraints and identify alternatives for scalable operation.

It is suggested to explore cheaper and more abundant dehydrogenation catalysts, as this directly impacts the economic feasibility of the process. Moreover, determining the total requirements of (scarce) materials in the PCEC reactor will help to evaluate the viability of scaling up to industrial levels. It is critical to align the process requirements with material availability and identify potential bottlenecks. The scarcity of platinum, currently used in the PtGa/ZSM-5 catalyst, appears to be a crucial constraint that needs attention in future research.

Invest in development of cell components.

Advancements in cell components offer a significant opportunity to improve the techno-economic feasibility of the WINNER process. Such advancements primarily relate to developments in material engineering, particularly in the design and composition of electrodes and electrolytes. One technological development could be the enhancement of proton-transference capacity of the electrolyte, which could increase FE and pave the way for operating at higher current densities. Similar technological improvements in electrode manufacturing can be thought of.

Investigate alternative operation modes.

To enhance the flexibility and productivity of the WINNER process, it is recommended to investigate the reversible operation through fuel cell mode for the co-production of ethylene and electricity, as detailed in (APPENDIX D). This has the potential to add significant value to the overall process, improving its economic feasibility. Moreover, studying the possibility to complement the WINNER process with the electrification of furnaces (e-crackers) could be instrumental. This innovative approach indicates an opportunity for complete process electrification in the future, steering the chemical industry towards sustainability.

Create modular PCEC reactor design for optimal future implementation.

For effective future implementation and operational resilience, a modular setup of PCEC reactors is recommended, ensuring continuous operation during downtime and maintenance. In Shell's portfolio, for example, a 1500 KTA separation train can be paired with 17 PCEC reactors, each of 100 KTA capacity. This configuration allows for the uninterrupted operation of the 1500 KTA separation train, even accounting for downtime and maintenance of up to 2 PCEC reactors at any given time.

Literature References

1. Alshammari, A., et al., *Production of Ethylene and its Commercial Importance in the Global Market*. 2016. p. 82-115.
2. Statista Research Department. *Ethylene demand and production capacity worldwide from 2015 to 2022*. 2023 [cited 2023 13/07]; Available from: https://www.statista.com/statistics/1246694/ethylene-demand-capacity-forecast-worldwide/.
3. BP, *bp Statistical Review of World Energy*. 2022, British Petroleum. p. 60.
4. Ren, T., M. Patel, and K. Blok, *Olefins from conventional and heavy feedstocks: Energy use in steam cracking and alternative processes*. Energy, 2006. **31**(4): p. 425-451.
5. Amghizar, I., et al., *New Trends in Olefin Production*. Engineering, 2017. **3**(2): p. 171-178.
6. Wu, W., et al., *Electrochemically Engineered, Highly Energy-Efficient Conversion of Ethane to Ethylene and Hydrogen below 550 °C in a Protonic Ceramic Electrochemical Cell*. ACS Catalysis, 2021. **11**(19): p. 12194-12202.
7. Ding, D., et al., *A Novel Low-Thermal-Budget Approach for Co-Production of Ethylene and Hydrogen via Electrochemical Non-Oxidative Deprotonation of Ethane*. Energy & Environmental Science, 2018. **11**.
8. Fontaine, M.-L. *WINNER - World class Innovative Novel Nanoscale optimized electrodes and electrolytes for Electrochemical Reactions*. 2021 [cited 2022 15/12/2022]; Available from: https://www.sintef.no/projectweb/winner/.
9. Van Geem, K., M. Reyniers, and G. Marin, *Challenges of Modeling Steam Cracking of Heavy Feedstocks*. Oil & Gas Science and Technology-Revue D Ifp Energies Nouvelles, 2008. **63**: p. 79-94.
10. Haribal, V., et al., *Intensification of Ethylene Production from Naphtha via a Redox Oxy-Cracking Scheme: Process Simulations and Analysis*. Engineering, 2018. **4**.
11. Chemanalyst. *Ethylene Price Trend and Forecast*. 2023 [cited 2023 08/06]; Available from: https://www.chemanalyst.com/Pricing-data/ethylene-40#:~:text=The%20Middle%20East%20however%20witnessed,compared%20to%20Q3%20of%20FY21.
12. Procurement Resource. *Ethylene Price Trand and Forecast*. 2023 [cited 2023 08/06]; Available from: https://www.procurementresource.com/resource-center/ethylene-price-trends.
13. Chemanalyst. *Propylene Price Trend and Forecast*. 2023 [cited 2023 22/06]; Available from: https://www.chemanalyst.com/Pricing-data/propylene-51.
14. Fernández, L. *Price of propylene worldwide from 2017 to 2022*. 2022 [cited 2023 07/02]; Available from: https://www.statista.com/statistics/1170576/price-propylene-forecast-globally/.

15. Procurement Resource. *Butene Price Trend and Forecast.* 2022 [cited 2023 22/06]; Available from: https://www.procurementresource.com/resource-center/butene-price-trends.
16. Intratec. *Butene Price.* 2023 [cited 2023 22/06]; Available from: https://www.intratec.us/chemical-markets/butene-price.
17. Everett, R., et al. *Energy Systems and Sustainability: Power for a Sustainable Future (2nd ed.).* 2012.
18. Gao, Y., et al., *Recent Advances in Intensified Ethylene Production—A Review.* ACS Catalysis, 2019. **9**(9): p. 8592-8621.
19. Anthonykutty, J., et al., *Renewable feedstock for steam crackers: Catalytic upgrading of crude tall oil (CTO) into bio-naphtha.* AIChE Ethylene Producers Conference Proceedings, 2013: p. 103-104.
20. Magovern, R.L., *Process Economics Program.* 1971, Report.
21. Wang, Z., et al., *Low Temperature Pyrolysis Characteristics of Oil Sludge under Various Heating Conditions.* Energy & Fuels, 2007. **21**(2): p. 957-962.
22. Thiruvenkataswamy, P., et al., *Safety and techno-economic analysis of ethylene technologies.* Journal of Loss Prevention in the Process Industries, 2016. **39**: p. 74-84.
23. Sundaram, K.M. and G.F. Froment, *Modeling of thermal cracking kinetics—I: Thermal cracking of ethane, propane and their mixtures.* Chemical Engineering Science, 1977. **32**(6): p. 601-608.
24. Weissermel, K., *Olefins*, in *Industrial Organic Chemistry*. 2003. p. 59-89.
25. Bin Rosli, M.N. and N. Aziz, *Simulation of ethane steam cracking with severity evaluation.* IOP Conference Series: Materials Science and Engineering, 2016. **162**: p. 012017.
26. Gärtner, C.A., A.C. van Veen, and J.A. Lercher, *Oxidative Dehydrogenation of Ethane: Common Principles and Mechanistic Aspects.* ChemCatChem, 2013. **5**(11): p. 3196-3217.
27. Theofanidis, S.A., et al., *CO2-oxidative ethane dehydrogenation over highly efficient carbon-resistant Fe-catalysts.* Journal of Catalysis, 2020. **388**: p. 52-65.
28. Maffia, G., A. Gaffney, and O. Mason, *Techno-Economic Analysis of Oxidative Dehydrogenation Options.* Topics in Catalysis, 2016. **59**.
29. Wang, L.-C., et al., *Non-oxidative dehydrogenation of ethane to ethylene over ZSM-5 zeolite supported iron catalysts.* Applied Catalysis B: Environmental, 2019. **256**: p. 117816.
30. Saito, H. and Y. Sekine, *Catalytic conversion of ethane to valuable products through non-oxidative dehydrogenation and dehydroaromatization.* RSC Advances, 2020. **10**(36): p. 21427-21453.
31. Sattler, A., et al., *Catalytic limitations on alkane dehydrogenation under H2 deficient conditions relevant to membrane reactors.* Energy & Environmental Science, 2022. **15**(5): p. 2120-2129.

32. Ahn, S.-J., et al., *Effects of pressure, contact time, permeance, and selectivity in membrane reactors: The case of the dehydrogenation of ethane.* Separation and Purification Technology, 2018. **194**: p. 197-206.
33. Sun, S. and K. Huang, *Efficient and selective ethane-to-ethylene conversion assisted by a mixed proton and electron conducting membrane.* Journal of Membrane Science, 2020. **599**: p. 117840.
34. Liu, S., et al., *Cogeneration of ethylene and energy in protonic fuel cell with an efficient and stable anode anchored with in-situ exsolved functional metal nanoparticles.* Applied Catalysis B: Environmental, 2018. **220**: p. 283-289.
35. Kasyanova, A.V., et al., *Electrolyte materials for protonic ceramic electrochemical cells: Main limitations and potential solutions.* Materials Reports: Energy, 2022. **2**(4): p. 100158.
36. Xu, X. and L. Bi, *Chapter 4 - Proton-conducting electrolyte materials*, in *Intermediate Temperature Solid Oxide Fuel Cells*, G. Kaur, Editor. 2020, Elsevier. p. 81-111.
37. Zhu, L., et al., *Ammonia-fed reversible protonic ceramic fuel cells with Ru-based catalyst.* Communications Chemistry, 2021. **4**(1): p. 121.
38. Lei, L., et al., *Mathematical modeling of proton-conducting electrochemical cells for ethylene production from ethane.* Journal of Power Sources, 2022. **531**: p. 231272.
39. Fegley, B., *Chapter 6 - The Second Law of Thermodynamics and Entropy*, in *Practical Chemical Thermodynamics for Geoscientists*, B. Fegley, Editor. 2013, Academic Press: Boston. p. 173-224.
40. Lide, D., *CRC handbook of chemistry and physics.* 1977.
41. Gallucci, F., *3 - Packed bed membrane reactors*, in *Current Trends and Future Developments on (Bio)Membranes*, A. Basile and F. Gallucci, Editors. 2023, Elsevier. p. 59-75.
42. Amiri, T.Y., K. Ghasemzageh, and A. Iulianelli, *Membrane reactors for sustainable hydrogen production through steam reforming of hydrocarbons: A review.* Chemical Engineering and Processing - Process Intensification, 2020. **157**: p. 108148.
43. Ding, H., et al., *High-performing and stable electricity generation by ceramic fuel cells operating in dry methane over 1000 hours.* Journal of Power Sources, 2018. **401**: p. 322-328.
44. Hwang, S.-T., *Inorganic membranes and membrane reactors.* Korean Journal of Chemical Engineering, 2001. **18**(6): p. 775-787.
45. Gallucci, F., A. Basile, and F.I. Hai, *Introduction – A Review of Membrane Reactors*, in *Membranes for Membrane Reactors*. 2011. p. 1-61.
46. Duan, C., et al., *Readily processed protonic ceramic fuel cells with high performance at low temperatures.* Science, 2015. **349**(6254): p. 1321-6.
47. Reis Bernardes, F., et al., *Synthesis and Application of H-ZSM-5 Zeolites with Different Levels of Acidity as Synergistic Agents in Flame Retardant Polymeric Materials.* Polymers (Basel), 2019. **11**(12).

48. Bard, A.J., L.R. Faulkner, and H.S. White, *Electrochemical Methods: Fundamentals and Applications*. 2022: Wiley.
49. Saidi, M. and M. Safaripour, *Pure Hydrogen and Propylene Coproduction in Catalytic Membrane Reactor-Assisted Propane Dehydrogenation.* Chemical Engineering & Technology, 2020. **43**(7): p. 1402-1415.
50. Borry III, R.W.I., E;, *Non-oxidative conversion of methane with continuous hydorgen removal*, in *Conference: Natural gas conference, Houston, TX (United States), 24-27 Mar 1997*. 1997, Univ. of California, Berkeley, CA (United States): Houston.
51. Dou, B., et al., *Hydrogen production from catalytic steam reforming of biodiesel byproduct glycerol: Issues and challenges.* Renewable and Sustainable Energy Reviews, 2014. **30**: p. 950-960.
52. Zhu, H., S. Ricote, and R.J. Kee, *Faradaic efficiency in protonic-ceramic electrolysis cells.* Journal of Physics: Energy, 2022. **4**(1): p. 014002.
53. Kee, B.L., et al., *Thermodynamic Insights for Electrochemical Hydrogen Compression with Proton-Conducting Membranes.* Membranes (Basel), 2019. **9**(7).
54. Long, N.V.D., et al., *Novel retrofit designs using a modified coordinate descent methodology for improving energy efficiency of natural gas liquid fractionation process.* Journal of Natural Gas Science and Engineering, 2016. **33**: p. 458-468.
55. Uwitonze, H., I. Lee, and K.S. Hwang, *Alternatives of integrated processes for coproduction of LNG and NGLs recovery.* Chemical Engineering and Processing - Process Intensification, 2016. **107**: p. 157-167.
56. Mehrpooya, M., et al., *Energy and advanced exergy analysis of an existing hydrocarbon recovery process.* Energy Conversion and Management, 2016. **123**: p. 523-534.
57. Qyyum, M.A., et al., *State-of-the-art assessment of natural gas liquids recovery processes: Techno-economic evaluation, policy implications, open issues, and the way forward.* Energy, 2022. **238**: p. 121684.
58. Thabet, K., et al., *Chapter 4 - Protonic-based ceramics for fuel cells and electrolyzers*, in *Solid Oxide-Based Electrochemical Devices*, M. Lo Faro, Editor. 2020, Academic Press. p. 91-122.
59. Meng, Y., et al., *Review: recent progress in low-temperature proton-conducting ceramics.* Journal of Materials Science, 2019. **54**(13): p. 9291-9312.
60. Wasylenko, D.J., et al., *Direct Comparison of Electrochemical and Spectrochemical Kinetics for Catalytic Oxygen Reduction.* Journal of the American Chemical Society, 2014. **136**(36): p. 12544-12547.
61. Jones, M., *The 'quarter-power equation' for resistive heating faults.* Science & Justice, 2022. **62**(2): p. 239-245.
62. Cooper, R., *Personal Communications on Ethylene Specifications*, T. Steneker, Editor. 2023.

63. Engineering ToolBox. *Hydrocarbons - Physical Data*. 2017 [cited 2023 04/05]; Available from: https://www.engineeringtoolbox.com/hydrocarbon-boiling-melting-flash-autoignition-point-density-gravity-molweight-d_1966.html.
64. Diggles, M. *Methane Gas Volume Expansion Ratios and Ideal Gas Deviation Factors for the Deep-Water Bering Sea Basins*. Peng-Robinson Equation of State 2006 [cited 2023 05/06]; Available from: https://pubs.usgs.gov/of/2005/1451/equation.html#:~:text=The%20Peng%2DRobinson%20equation%20of,factor%20of%20each%20species%20involved.
65. Zhao, Y.G., Daniel; You, Fengqu;. *Property package*. 2016 [cited 2023 02/05]; Available from: https://processdesign.mccormick.northwestern.edu/index.php/Property_package.
66. Hu, H., et al., *Techno-Economic Analysis on an Electrochemical Non-oxidative Deprotonation Process for Ethylene Production from Ethane*. 2019: United States. p. Medium: ED; Size: 127 p.
67. Hussain, Y.A., *Thermodynamic Models & Physical Properties*. 2011. p. 24.
68. Speight, J.G., *The chemistry and physics of coking*. Korean Journal of Chemical Engineering, 1998. **15**(1): p. 1-8.
69. Shell Global. *Shell Polymers Monaca*. 2023 [cited 2023 15/06]; Available from: https://www.shell.com/about-us/major-projects/pennsylvania-petrochemicals-complex.html.
70. Müller, H., *FUELS | Gaseous*, in *Encyclopedia of Analytical Science (Second Edition)*, P. Worsfold, A. Townshend, and C. Poole, Editors. 2005, Elsevier: Oxford. p. 505-511.
71. Dincer, I. and M.A. Rosen, *Chapter 2 - Exergy and Energy Analyses*, in *Exergy (Second Edition)*, I. Dincer and M.A. Rosen, Editors. 2013, Elsevier. p. 21-30.
72. Aspentech. *Energy Management - Optimize energy use*. 2023 [cited 2023 17/06]; Available from: https://www.aspentech.com/en/applications/engineering/energy-management.
73. Winterbone, D.E. and A. Turan, *Chapter 19 - Pinch Technology*, in *Advanced Thermodynamics for Engineers (Second Edition)*, D.E. Winterbone and A. Turan, Editors. 2015, Butterworth-Heinemann: Boston. p. 447-465.
74. Lieberman, M.B., *Market Growth, Economies of Scale, and Plant Size in the Chemical Processing Industries*. The Journal of Industrial Economics, 1987. **36**(2): p. 175-191.
75. Sulaymon, A. and A. Abbar, *Scale-Up of Electrochemical Reactors*. 2012.
76. Global, S. *Shell and Dow start up e-cracking furnace experimental unit*. 2022 [cited 2023 11/07]; Available from: https://www.shell.com/business-customers/chemicals/media-releases/2022-media-releases/shell-and-dow-start-up-e-cracking-furnace-experimental-unit.html.

77. Zarabi Golkhatmi, S., M.I. Asghar, and P.D. Lund, *A review on solid oxide fuel cell durability: Latest progress, mechanisms, and study tools.* Renewable and Sustainable Energy Reviews, 2022. **161**: p. 112339.
78. Towler, G. and R. Sinnott, *Chapter 7 - Capital Cost Estimating*, in *Chemical Engineering Design (Second Edition)*, G. Towler and R. Sinnott, Editors. 2013, Butterworth-Heinemann: Boston. p. 307-354.
79. Sunfire. *WORLD'S LARGEST HIGH-TEMPERATURE ELECTROLYSIS MODULE DELIVERIES STARTED*. 2022 [cited 2023 14/07]; Available from: https://www.sunfire.de/en/news/detail/worlds-largest-high-temperature-electrolysis-module-deliveries-started.
80. van 't Noordende, H., F. van Berkel, and M. Stodolny, *Next Level Solid Oxide Electrolysis*. 2023.
81. Perrin, O. and A. Kuzmanovic, *Fueling the future of mobility: hydrogen electrolyzers*, M. Deloitte, Editor. 2021.
82. Anghilante, R., et al., *Bottom-up cost evaluation of SOEC systems in the range of 10–100 MW*. International Journal of Hydrogen Energy, 2018. **43**(45): p. 20309-20322.
83. Zhang, C. and M.M. El-Halwagi, *Estimate the Capital Cost of Shale-Gas Monetization Projects*, A.I.o.C.E. (AIChE), Editor. 2017.
84. U.S. Energy Information Administration. *Natural Gas Weekly Update*. Natural Gas 2023 [cited 2023 08/06]; Available from: https://www.eia.gov/naturalgas/weekly/archivenew_ngwu/2023/03_02/.
85. International Energy Agency. *Simplified levelised cost of petrochemicals for selected feedstocks and regions, 2017*. 2022 [cited 2023 26/05]; Available from: https://www.iea.org/data-and-statistics/charts/simplified-levelised-cost-of-petrochemicals-for-selected-feedstocks-and-regions-2017.
86. Index Mundi. *Propane Daily Price*. 2023 [cited 2023 22/06]; Available from: https://www.indexmundi.com/commodities/?commodity=propane&months=120.
87. Evans, P. *Chiller Cooling Capacity – How to calculate*. 2017 [cited 2023 17/07]; Available from: https://theengineeringmindset.com/chiller-cooling-capacity-calculate/#:~:text=Using%20the%20energy%20equation%20of,can%20calculate%20the%20cooling%20capacity.&text=We%20add%20273.15K%20to,Q%20%3D%202%2C500kW%20of%20cooling.
88. Our World in Data. *Carbon intensity of electricity, 2000 to 2022*. 2023 [cited 2023 23/06]; Available from: https://ourworldindata.org/grapher/carbon-intensity-electricity?tab=chart&country=~USA.
89. Engineering ToolBox. *Fuels - Higher and Lower Calorific Values*. 2003 [cited 2023 13/6]; Available from: https://www.engineeringtoolbox.com/fuels-higher-calorific-values-d_169.html.

90. Engineering ToolBox. *Combustion of Fuels - Carbon Dioxide Emission*. 2003 [cited 2023 14/06]; Available from: https://www.engineeringtoolbox.com/co2-emission-fuels-d_1085.html.
91. Energy Information Administration. *ELECTRICITY DATA BROWSER*. 2023 [cited 2023 22/06]; Available from: https://www.eia.gov/electricity/data/browser/#/topic/7?agg=0,1&geo=g&endsec=vg&linechart=ELEC.PRICE.US-ALL.A~ELEC.PRICE.US-RES.A~ELEC.PRICE.US-COM.A~ELEC.PRICE.US-IND.A&columnchart=ELEC.PRICE.US-ALL.A~ELEC.PRICE.US-RES.A~ELEC.PRICE.US-COM.A~ELEC.PRICE.US-IND.A&map=ELEC.PRICE.US-ALL.A&freq=A&ctype=linechart&ltype=pin&rtype=s&pin=&rse=0&maptype=0.
92. Ulrich, G.D. and T.V. Palligarnai, *How to Estimate Utility Costs*. Chemical Engineering, 2006. **April 2006**.
93. Schulze, C., S. Thiede, and C. Herrmann, *Life Cycle Assessment of Industrial Cooling Towers*, in *Progress in Life Cycle Assessment*, L. Schebek, C. Herrmann, and F. Cerdas, Editors. 2019, Springer International Publishing: Cham. p. 135-146.
94. Costley, D.B., Matthew;, *Carbon should cost 3.6 times more than US price, study says*, in *AP News*. 2022.
95. Sanchez, B. *More than 60% of energy used for electricity generation is lost in conversion*. 2020.
96. US Environmental Protection Agency. *U.S. Electricity Grid & Markets*. 2023 [cited 2023 23/06]; Available from: https://www.epa.gov/green-power-markets/us-electricity-grid-markets.
97. Ritchie, H.R., Pablo. *Which countries have put a price on carbon?* 2022 [cited 2023 23/06]; Available from: https://ourworldindata.org/carbon-pricing.
98. Dolphin, G. *World Carbon Pricing Database*. 2022 [cited 2023 23/06]; Available from: https://www.rff.org/publications/data-tools/world-carbon-pricing-database/.
99. Rennert, K., et al., *Comprehensive evidence implies a higher social cost of CO2*. Nature, 2022. **610**(7933): p. 687-692.
100. Ember. *Carbon Price Tracker*. 2023 [cited 2023 31/07]; The latest data on EU and UK ETS carbon prices]. Available from: https://ember-climate.org/data/data-tools/carbon-price-viewer/.
101. Towler, G. and R. Sinnott, *Chapter 8 - Estimating Revenues and Production Costs*, in *Chemical Engineering Design (Second Edition)*, G. Towler and R. Sinnott, Editors. 2013, Butterworth-Heinemann: Boston. p. 355-387.
102. Castro, L.F., *Personal Communications on Process Evaluations*, T. Steneker, Editor. 2023.
103. Fernando, J. *Net Present Value (NPV): What It Means and Steps to Calculate It*. 2023 [cited 2023 21/07]; Available from: https://www.investopedia.com/terms/n/npv.asp.

104. Fernando, J. *Internal Rate of Return (IRR) Rule: Definition and Example*. 2023 [cited 2023 21/07]; Available from: https://www.investopedia.com/terms/i/irr.asp.
105. Hauschild, M.Z., R.K. Rosenbaum, and S. Irving Olsen, *Life Cycle Assessment, theory and applications*. 2018. 1215.
106. Nationalgrid. *What are scope 1, 2 and 3 carbon emissions?* 2023 [cited 2023 30/01/23]; Available from: https://www.nationalgrid.com/stories/energy-explained/what-are-scope-1-2-3-carbon-emissions.
107. wbcscChemicals, *Life Cycle Metrics for chemical products*. 2014: p. 120.
108. U.S. Energy Information Administration. *What is U.S. electricity generation by energy source?* 2023 [cited 2023 20/07]; Available from: https://www.eia.gov/tools/faqs/faq.php?id=427&t=3.
109. Berg, J.M.B., *Comparison of Lifecycle Greenhouse Gas Emissions of Various Electricity Generation Sources*, World Nuclear Association, Editor. 2011. p. 6.
110. Badlam, J., et al., *The Inflation Reduction Act: Here's what's in it*. 2022.
111. Vargas, M., K. MCNutt, and C. Seiple, *Green hydrogen: what the Inflation Reduction Act means for production economics and carbon intensity*. 2023.
112. Monahan, K. and M. Beck *Hydrogen tax credits in the U.S. Inflation Reduction Act*. Canadian Climate Institute, 2023.
113. Zacarias, M.M., Cy, *How the 45V Tax Credit Definition Could Make or Break the Clean Hydrogen Economy*. CSIS, 2023.
114. Zhou, J., et al., *Layered perovskite (PrBa)0.95(Fe0.9Mo0.1)2O5+δ as electrode materials for high-performing symmetrical solid oxide electrolysis cells*. Materials Letters, 2019. **257**: p. 126758.
115. Wikipedia contributors. *Abundance of elements in Earth's crust*. 2023 16/07/2023 [cited 2023 24/07]; Available from: https://en.wikipedia.org/w/index.php?title=Abundance_of_elements_in_Earth%27s_crust&oldid=1165624404.
116. ACS Material LLC. *ZSM-5 - Zeolite Socony Mobil–5*. 2019 [cited 2023 24/07]; Available from: https://www.acsmaterial.com/blog-detail/zsm-5-molecular-seive.html#:~:text=The%20ZSM%2D5%20molecular%20sieve%20is%20a%20highly%20siliceous%20aluminosilicate,range%20from%200%20to%2027.
117. Kenton, W. *Sensitivity Analysis Definition*. 2023 [cited 2023 21/07]; Available from: https://www.investopedia.com/terms/s/sensitivityanalysis.asp#:~:text=Sensitivity%20analysis%20determines%20how%20different,to%20the%20model's%20overall%20uncertainty.
118. Moreira, J. *Steam Cracking : Kinetics and Feed Characterisation*. 2015.
119. Hasany, M., et al., *Effect of hydrogen combustion reaction on the dehydrogenation of ethane in a fixed-bed catalytic membrane reactor*. Chinese Journal of Chemical Engineering, 2015. **23**(8): p. 1316-1325.

120. Basile, A., S. Liguori, and A. Iulianelli, *2 - Membrane reactors for methane steam reforming (MSR)*, in *Membrane Reactors for Energy Applications and Basic Chemical Production*, A. Basile, et al., Editors. 2015, Woodhead Publishing. p. 31-59.
121. Doherty, M.F., et al., *INTRODUCTION TO DISTILLATION OPERATIONS*, in *Perry's Chemical Engineers' Handbook*, D.W. Green and M.Z. Southard, Editors. 2019, McGraw-Hill Education: New York.
122. Al-Dunainawi, Y. and M. Abbod, *Hybrid Intelligent Approach for Predicting Product Compositions of a Distillation Column.* International Journal of Advanced Research in Artificial Intelligence, 2016. *5*: p. 28-34.
123. Corripio, A.B., *Multicomponent distillation.* 2013. p. 32.
124. Chemanalyst. *Hydrogen Price Trend and Forecast.* 2023 [cited 2023 22/06]; Available from: https://www.chemanalyst.com/Pricing-data/hydrogen-1165#:~:text=Conclusively%2C%20Hydrogen%20prices%20in%20the,the%20end%20of%20the%20quarter.&text=The%20Hydrogen%20price%20trend%20showcased,the%201st%20quarter%20of%202023.
125. Chemanalyst. *Raffinate Price Trend and Forecast.* 2023; Available from: https://www.chemanalyst.com/Pricing-data/raffinate-1175.

APPENDIX A. Naphtha Steam Cracking

Figure 0-1 shows the process scheme of naphtha steam cracker. A steam cracker can be separated into two separate sections, a hot and a cold one. In the hot section, the naphtha feedstock is cracked at a temperature between 750 – 900 °C [4]. In the cold section, the reactor effluent is separated into different products, usually increasing the purity since this is required for polymer production [5].

First, liquid naphtha is pre-heated and thermally cracked in the presence of steam (A). Steam is added to the reactor tubes to lower the partial pressure of hydrocarbons (B). A low partial pressure improves the olefin yield and the addition of steam decreases carbon deposition. During cracking, naphtha flows through the tubes of the cracking furnace, which is operated at temperatures of ~850°C. In this way, the heat required for the highly endothermic cracking reaction is provided by the combustion of fuel outside of the reactor tubes. Coming out of the cracking furnace, the product stream is at a temperature of ~800°C, after which it is quenched to 300°C - 400°C using transfer line heat exchangers (C). The quenching is done to prevent further cracking of the products. Next, a primary fractionator removes heavy hydrocarbons, tar, and oily material from the cracked gasses (D). The product stream is further quenched until it reaches near-ambient temperatures to remove residual heavy components. This marks the end of the thermal cracking process itself. However, to separate and purify the products into useful components, a relatively complex and energy-consuming downstream section is needed [10, 118].

The product steam coming out of the primary fractionator at the end of the "hot" section in Figure 0-1 is led through the "cold" section of separation units to recover products with the desired purity. The "cold" section of the naphtha steam cracker starts with a multistage compression system that increases the pressure to around 40 bar (E), after which the steam is led through drying and acid gas removal (AGR) units (F & G). Using a separation train of distillation columns, the light components from the compressed stream are sequentially separated from the heavy fractions to produce high-purity ethylene and propylene. This separation train consists of a demethanizer (DM), de-ethanizer (DE), deacetylenizer (DA), C_2-splitter, depropanizer (DP), C3 splitter, and debutanizer (DB), separating chemicals based on their differences in boiling point. By doing so, the lightest component present in the stream will be recovered at the top of a distillation unit, while the residual of heavier components moves onto the next separation unit to repeat this process. Eventually, hydrogen, methane, ethylene, ethane, propylene, propane, C4 hydrocarbons and C5+ hydrocarbons are the products that are recovered [10, 118].

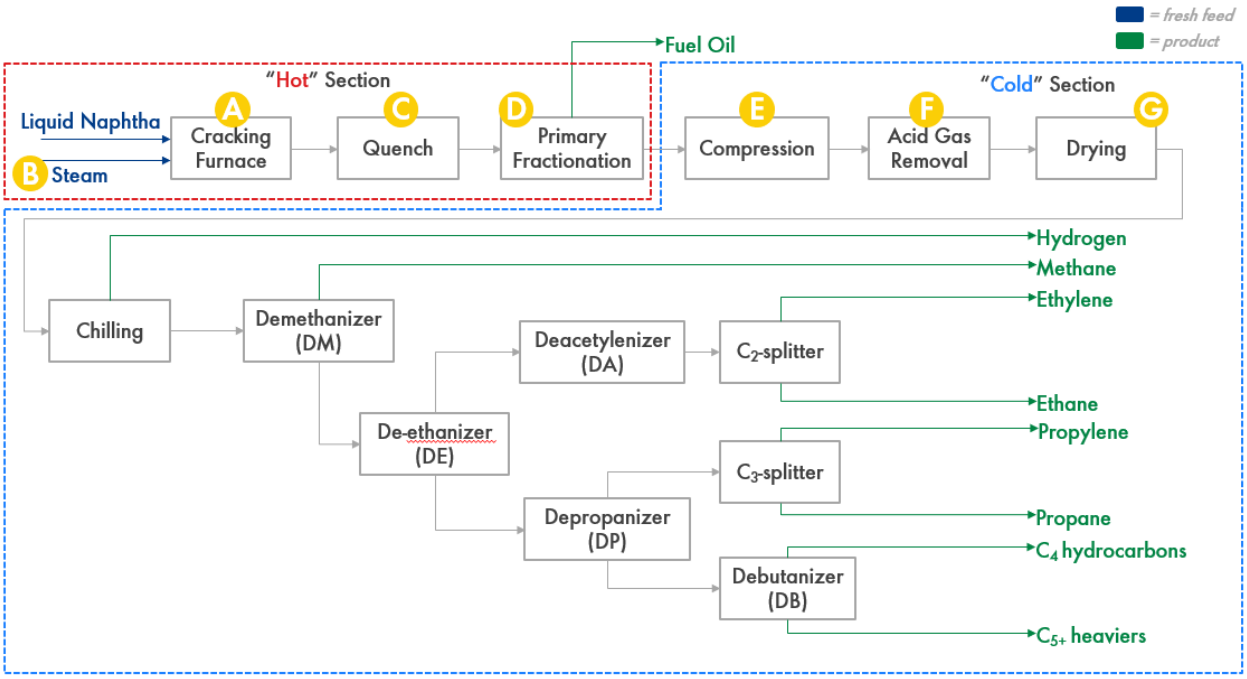

Figure 0-1: Naphtha steam cracking process scheme (the figure was drawn based on [10]).

APPENDIX B. Specifications of steam cracking processes

Table 0-1: Overview of specifications of commercial ethylene production through steam cracking (table was made based on [4, 22, 25]).

	Naphtha	Ethane
Products	Ethylene, hydrogen, methane, acetylene, ethane, propylene, propane, butadiene, C_4 compounds, C_5+ compounds	Ethylene, hydrogen, methane, acetylene, ethane, propylene, propane, butadiene
Cracking temperature [°C]	750 - 900	880 - 900
Cracking pressure [bar]	1.7 – 2.5	1.3 – 3.5
SEC (GJ/t ethylene)	26 – 31	17 – 21
SEC (GJ/t HVCs)	14 – 17	16 – 19
CO_2 emissions (tCO_2/t ethylene)	1.8 – 2.0	1.0 – 1.2
CO_2 emissions (tCO_2/t HVCs)	1.6 – 1.8	1.0 – 1.2
Ethylene yield (wt%)	29 – 34	80 – 84
Propylene yield (wt%)	13 – 16	1 – 1.6
Butadiene yield (wt%)	4 – 5	1 – 1.4
Aromatics and C4+ yield (wt%)	10 – 16	2 – 3
HVCs yield (wt%)	55	82
Methane yield (not counted as HVCs) (wt%)	13 – 14	4.2
Hydrogen yield (not counted as HVCs) (wt%)	1	4.3

APPENDIX C. Examples of Passive Membranes

Sun et al. investigated the conversion of ethane to ethylene using an active Mixed Proton and Electron Conducting (MPEC) membrane without the use of an external circuit. The membrane itself provided the necessary electrons for the hydrogen electrode. This MPEC membrane can provide the necessary electrons for the hydrogen electrode, simplifying the system and reducing energy consumption. However, this method might offer less control over selectivity and reaction kinetics compared to systems with external circuits [33].

Ahn et al. employed a hydrogen-selective silica membrane in the dehydrogenation of ethane. This membrane selectively extracts hydrogen from the product stream, shifting the reaction equilibrium towards ethylene production and enhancing conversion rates. The main advantage of this approach is the increased ethylene selectivity. However, it may not offer the same level of control over reaction kinetics as methods that use external electrical circuits [32].

Hasany et al. developed a mathematical model to study the effect of hydrogen removal in a fixed-bed catalytic membrane reactor during ethane dehydrogenation. This study offers insights into the benefits of using membrane reactors for improved reaction performance, such as enhanced selectivity, conversion rates, and catalyst lifetime. However, this model-based study does not directly compare different types of membranes or their specific advantages and disadvantages [119].

APPENDIX D. PCECs in fuel cell mode

Two main operating modes for PCECs in ethylene production have been identified, namely the fuel cell mode and the hydrogen pump mode [38]. The fuel cell mode involves the simultaneous production of ethylene and power. For now, this application is not further explored in this project as the focus is on co-generating ethylene and hydrogen. However, this might be an interesting operation mode to explore at a later stage. The overall reaction of the fuel cell mode is identical to the ODH reaction as shown in Equation (0-1).

$$C_2H_6 + \frac{1}{2}O_2 \rightarrow C_2H_4 + H_2O \quad (0\text{-}1)$$

The reaction mechanism for the co-generation of ethylene and power can be observed in Figure 0-2. At the anode, ethane is dehydrogenated into ethylene and hydrogen. Subsequently, hydrogen is oxidized into H^+-ions and electrons. These half-reactions are displayed in Equations (0-2) and (0-3).

$$C_2H_6 \rightarrow C_2H_4 + H_2 \quad (0\text{-}2)$$

$$H_2 \rightarrow 2H^+ + 2e^- \quad (0\text{-}3)$$

Next, the H^+-ions permeate through the electrolyte, and react with oxygen and electrons at the cathode side of the PCEC to form water according to Equation (0-4):

$$\frac{1}{2}O_2 + 2H^+ + 2e^- \rightarrow H_2O \quad (0\text{-}4)$$

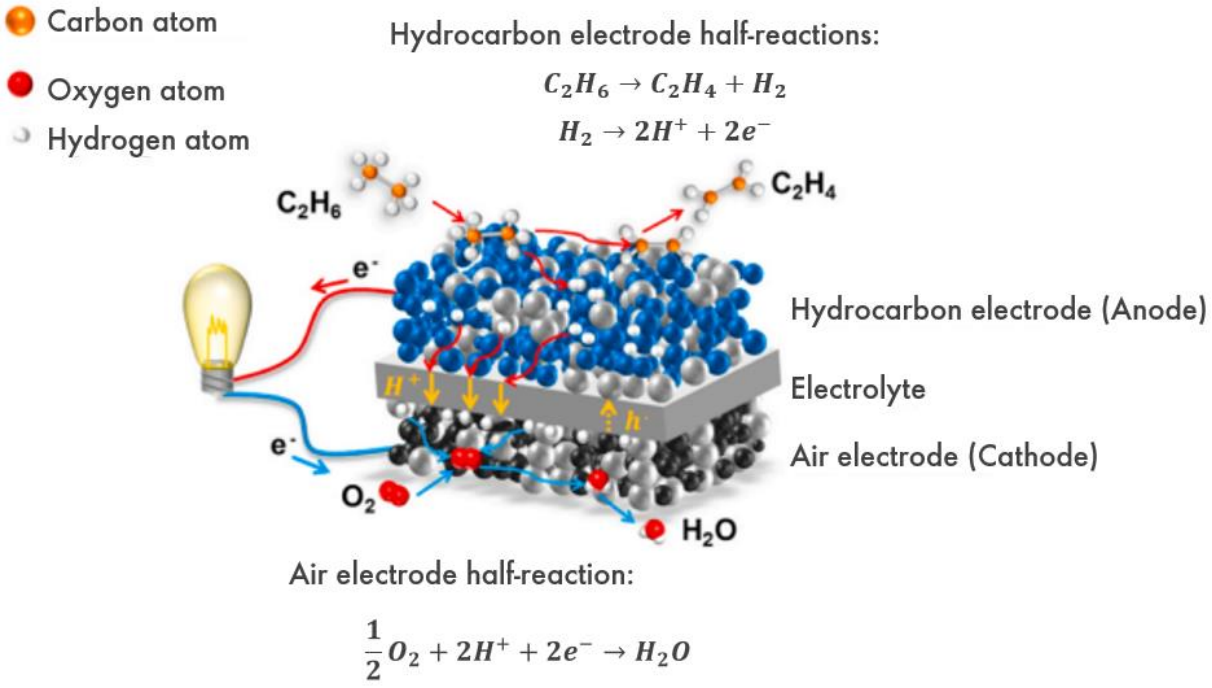

Figure 0-2: Reaction mechanism of PCECs for the co-production of ethylene and electricity in fuel cell mode [38].

APPENDIX E. Electrical Energy Calculations for Electrochemical Hydrogen Compression

In a proton-conducting membrane, the crossing of protons must be offset by an equal external electrical current to uphold charge balance. Thus, the hydrogen flow through the membrane should match the total proton transport. Equation (0-5) uses this correlation to calculate the required electrical current [53].

$$I = \frac{z\dot{m}F}{M_{H_2}} \tag{0-5}$$

Where z = 2 is the number of electrons per mole of hydrogen, $\dot{m}$ is the rate of hydrogen that diffuses through the membrane, F is Faraday's constant, and M_{H2} = 2.016 kg/kmol is the molecular weight of hydrogen. Equation (0-5) can be rewritten to Equation (0-6) to calculate the required membrane area in the reactor:

$$A_{mem} = \frac{z\dot{m}F}{j * M_{H_2}} \tag{0-6}$$

Where j is the current density over PCEC and is equal to 40 mA/cm^2 in the base case scenario. The cell voltage is related to the current, resistance, and open-circuit-voltage (OCV) following Equation (0-7):

$$E_{cell} = E_{OCV} + IR \tag{0-7}$$

Equation (0-8) calculates the OCV, assuming a purely proton-conducting membrane. The OCV depends on the compression ratio and the operating temperature:

$$E_{OCV} = \frac{R_{gas}T}{nF} ln(\frac{p_{out}}{p_{in}}) \tag{0-8}$$

R represents the resistance the protons experience when diffusion through the membrane. It is related to the ASR (Area Specific Resistance) and $A_{membrane}$ following (Equation (0-9):

$$R = \frac{ASR}{A_{mem}} \tag{0-9}$$

Equation (0-10) shows the formula for the electrical energy requirement for hydrogen compression and diffusion:

$$P_{cell} = E_{cell}I \tag{0-10}$$

When substituting Equations (0-5), (0-7), and (0-9) into Equation (0-10), the gravimetric power density can be calculated:

$$\frac{P_{cell}}{\dot{m}} = ASR \left(\frac{zF}{M_{H_2}}\right)^2 \frac{\dot{m}}{A_{mem}} + \frac{zF}{M_{H_2}} E_{OCV} \tag{0-11}$$

The specific energy of compression [kWh/kg H_2] is directly proportional to the ASR, the hydrogen mass flow rate, and inversely proportional to the membrane area.

APPENDIX F. General definitions of performance parameters in PCECs

- Faradaic Efficiency ($\eta_{Faradaic}$) for hydrogen pumping mode is defined as:

$$\eta_{Faradaic} = \frac{V_{H2\ cell}}{V_{H2\ theoretical}} * 100\% \quad (0\text{-}12)$$

Where:

$V_{H2\ cell}$ is the total measured flow of hydrogen evolved from the cell [L/min]

$V_{H2\ theoretical}$ is the theoretical flow of hydrogen at 100% efficiency [L/min]

- Theoretical flow of hydrogen is expressed as:

$$V_{H2\ theoretical} = \frac{A}{2F} * V_m \quad (0\text{-}13)$$

Where:

A is the applied current [A]

F is the Faradaic constant = $9.6485332123310\times10^4$ [C/mol]

V_m is the molar volume at Standard Temperature and Pressure (STP) [L/mol]

- Hydrogen extraction (R_{H2}) is expressed as:

$$R_{H2} = \frac{V_{H2\ H2side}}{V_{H2\ total}} \quad (0\text{-}14)$$

Where:

$V_{H2\ H2\ side}$ is the measured volume of hydrogen recovered at the high-pressure side of the reactor (H_2-side) [L/min]

$V_{H2\ cell}$ is the total measured volume of hydrogen evolved from the cell [L/min]

APPENDIX G. Wu et al. Aspen Flowsheet

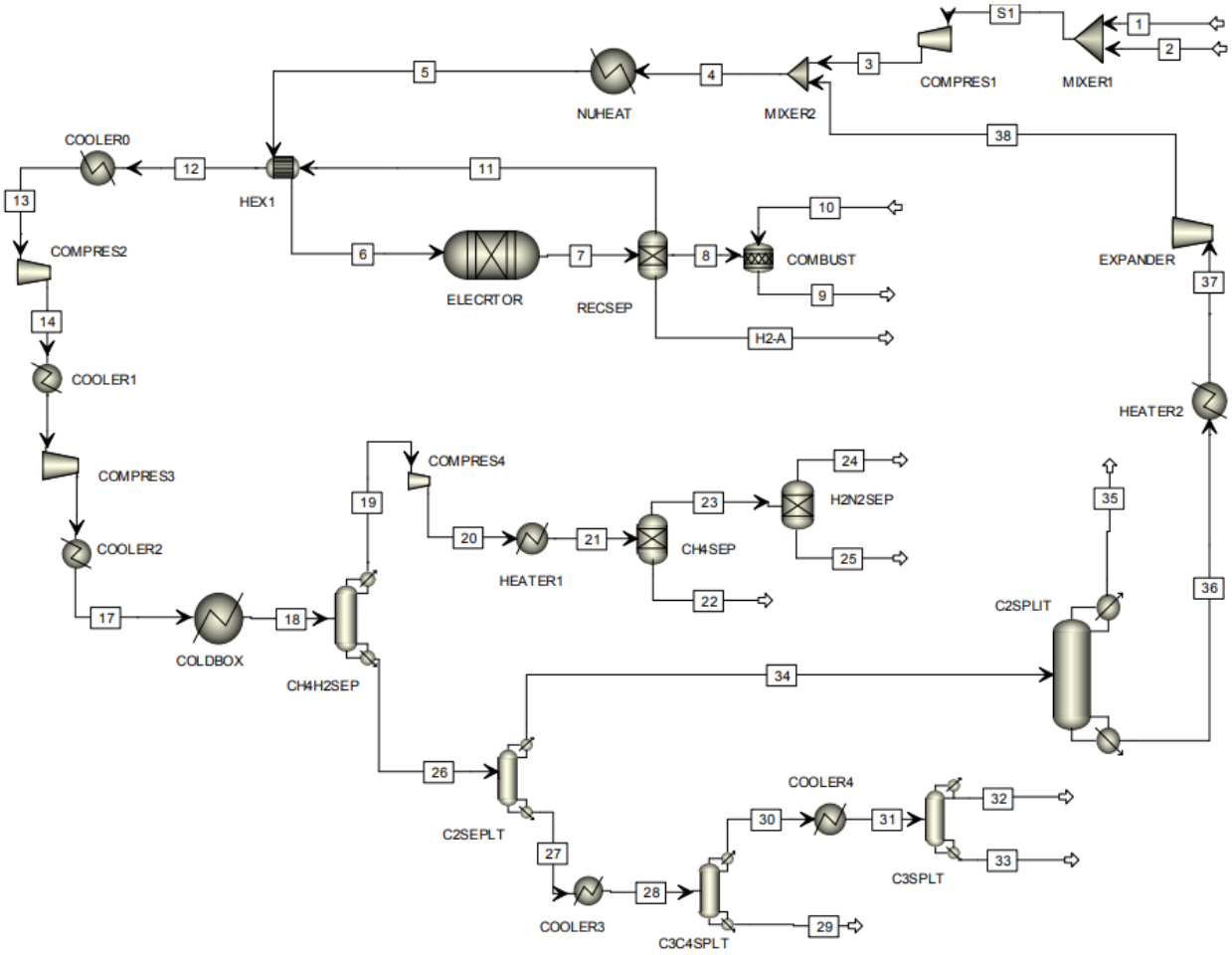

Figure 0-3: Detailed Aspen Plus flowsheet as presented by Wu et al. [6].

APPENDIX H. Aspen Plus property package selection and PENG-ROB EOS

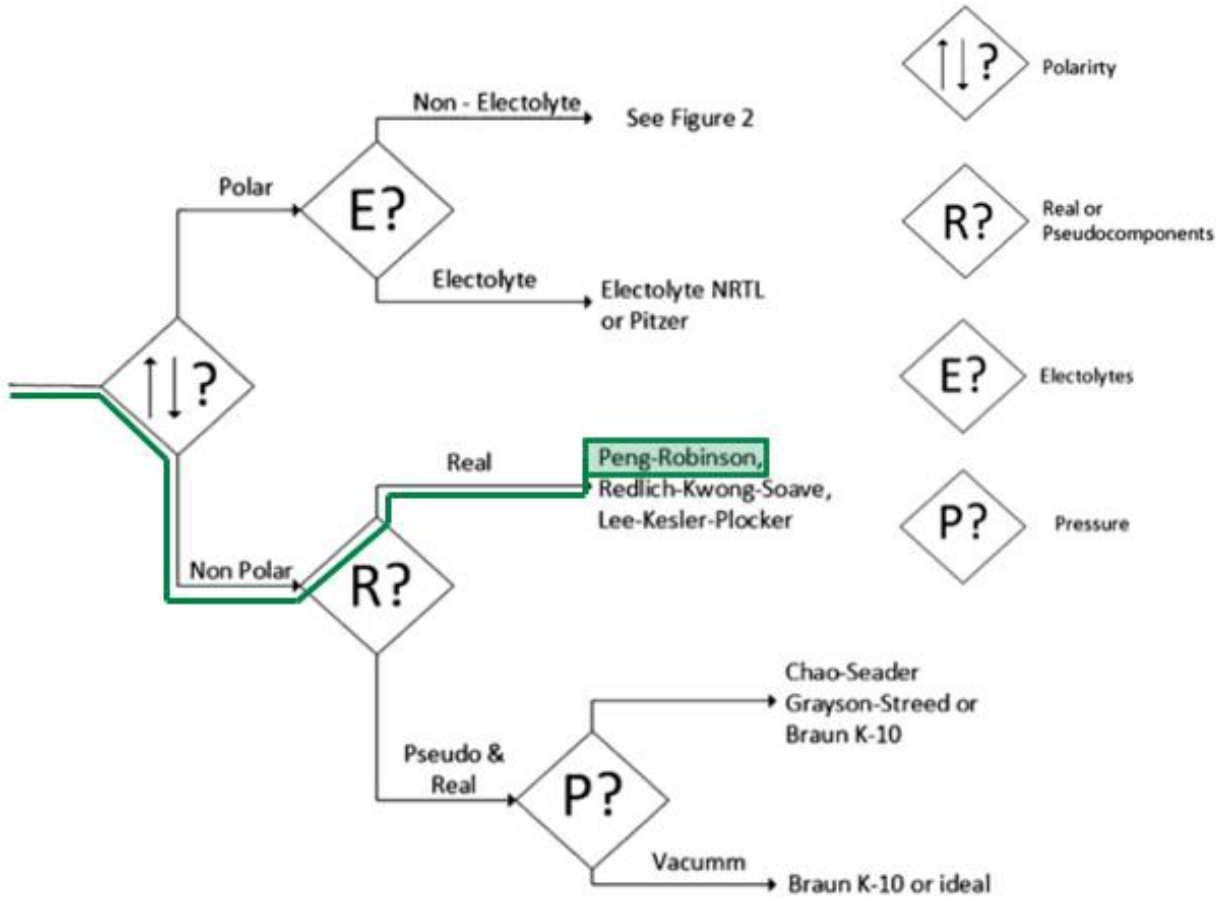

Figure 0-4: Property model selection decision tree [65]

Peng Robinson EOS (equations of state) [64]:

$$P = \frac{RT}{V_m - b} - \frac{a\alpha}{V_m^2 + 2bV_m - b^2} \tag{0-15}$$

$$a = \frac{0.45724 R^2 T_c^2}{P_c}$$

$$b = \frac{0.07780 R T_c}{P_c}$$

$$\alpha = \left(1 + \left(0.37464 + 1.54226\omega - 0.26992\,\omega^2\right)\left(1 - T_r^{0.5}\right)\right)^2$$

$$T_r = \frac{T}{T_c}$$

Where ω is the acentric factor for the species, P_c is the critical pressure, and T_c is the critical temperature.

APPENDIX I. Aspen Plus flowsheet

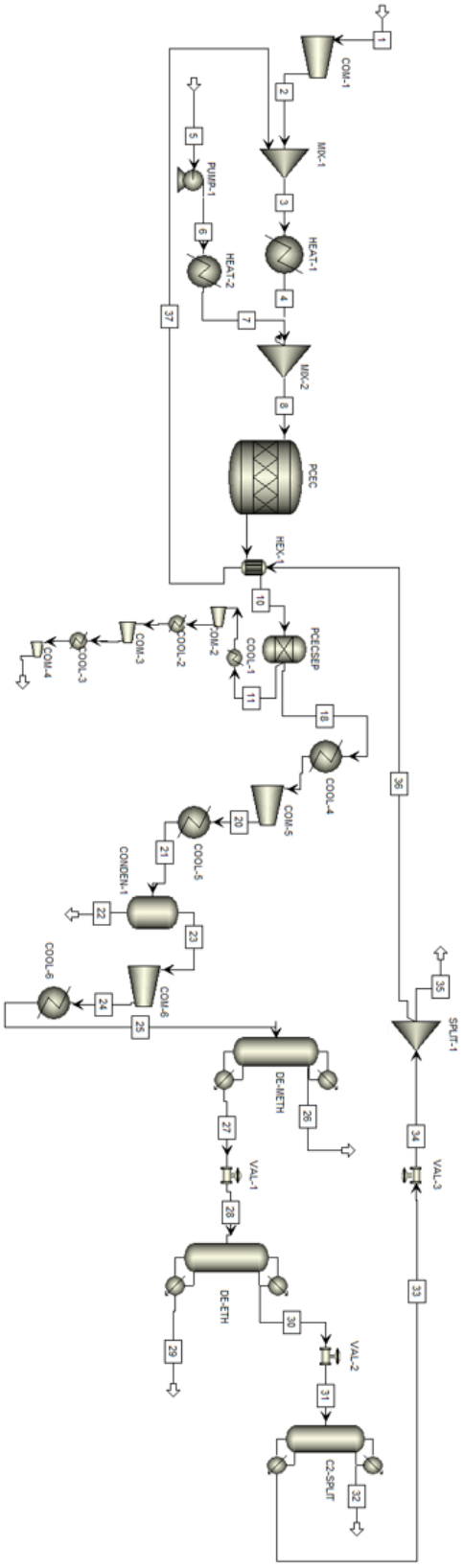

Figure 0-5: Aspen Plus flowsheet.

APPENDIX J.Overview of Design Choices

Membrane reactor configuration

- Planar membrane reactor
- Hydrocarbon electrode: Catalyst-integrated 3D ultra-porous perovskite $(PrBa)_{0.95}(Fe_{0.9}Mo_{0.1})_2O_{5+\delta}$ (PBFM) – thickness: 80 µm
- Electrolyte: Acceptor-doped barium zirconate cerate $BaZr_{0.1}Ce_{0.7}Y_{0.1}Yb_{0.1}O_{3-\delta}$ (BZCYYb) – thickness: 15 µm
- Hydrogen electrode: Porous Ni-BZCYYb support $Ni\text{-}BaZr_{0.1}Ce_{0.7}Y_{0.1}Yb_{0.1}O_{3-\delta}$ – thickness 450 µm
- Current collectors and wires: silver mesh and wires
- Catalyst: PtGa/ZSM-5

Feedstock specifications

- Hydrocarbon feedstock
  - Methane concentration: 1.8 wt%
  - Ethane concentration: 96.2 wt%
  - Propane concentration: 2.0 wt%
  - Temperature: 25°C
  - Pressure: 1 bar
  - No further contaminants
- Steam
  - Volume: 2 wt% of hydrocarbon feed
  - Temperature: 25°C
  - Pressure: 1 bar

Product specifications

- Ethylene (refer to Table 3-6)
  - Purity: 99.95%
- Hydrogen
  - Purity: 99.97%
  - Pressure: 50 bar

PCEC process parameters

- FE = 99.5% at j = 0.040 A/cm^2
- FE = 95% at j = 1 A/cm^2
- Hydrogen removal rate (R_{H2}) = 95%
- Temperature = 550°C
- Pressure = 1 bar

Separation train

- Only ethylene is recovered as an individually separated component (i.e., no depropanizer, C_3-splitter, and separation of CH_4 and H_2.
- Cooling and compression system reaches T = -50 °C and p = 35
- Condenser operates at T=25 °C and p = 20 bar
- Demethanizer operates at T = -50 °C and p = 35 bar
- De-ethanizer operates at T = ~0 °C and p = 30 bar
- C_2-splitter operates at T = ~-8 °C and p = 25 bar
- Purge 1% of recycle stream to prevent accumulation of species in the system.

WINNER KPIs (to check)

- ASR (Area Specific Resistance) of cells/stacks: < 1 $\Omega.cm^2$ at 650 °C,
- Faradaic Efficiency (FE) > 95%
- H_2 removal rate > 98%
- Validation of the durability of cells for at least 3,000 hours and validation of short stacks/mini reactors for at least 1,000 hours of operation
- Processing of hydrogen with a production loss rate of less than 1.2% / 1,000 hours

APPENDIX K. Aspen Plus stream and process unit overview

Table 0-2: Overview of Aspen Plus streams with pressure and temperature

#	Name	Pressure [bar]	Temperature[°C]
1	C_2H_6 feedstock	1	25
2	(Compressed) C_2H_6 feedstock	1	25
3	Mix of C_2H_6 recycle and fresh feed	1	372
4	Heated C_2H_6 recycle and fresh feed	1	550
5	H_2O	1	25
6	(Compressed) H_2O	1	25
7	Superheated steam	1	550
8	Mixed superheated steam and heated C_2H_6 feed	1	550
9	PCEC reactor product stream feeding into HEX-1	1	550
10	Product stream leaving HEX-1	1	215
11	Separated H_2 (cathode)	1	215
12	Cooled H_2 (first stage)	1	25
13	Compressed H_2 (first stage)	5	260
14	Cooled H_2 (second stage)	5	25
15	Compressed H_2 (second stage)	20	226
16	Cooled H_2 (third stage)	20	25
17	Compressed H_2 (third stage)	50	150
18	PCEC reactor product stream (minus separated H_2 in PCECSEP)	1	215
19	Cooled product stream (fist stage)	1	70
20	Compressed product stream (fist stage)	15	276
21	Cooled product stream (second stage)	15	25
22	Condensed H_2O	15	25
23	Product stream (without H_2O)	15	25

24	Compressed product stream (second stage)	35	88
25	Cooled product stream (third stage)	35	-50
26	Demethanizer tops (CH_4, H_2)	35	-111.5
27	Demethanizer bottoms (C_{2+} mix)	35	12.6
28	C_{2+} mix valve (1) discharge	30	5.9
29	De-ethanizer bottoms (C_3H_6, C_3H_8, C_4H_8)	30	105.8
30	De-ethanizer tops (C_2H_4, C_2H_6)	30	1.1
31	C_2H_4 and C_2H_6 valve (2) discharge	25	-6.4
32	C_2-splitter tops (C_2H_4 product)	25	-20.9
33	C_2-splitter bottoms (C_2H_6 recycle)	25	1.7
34	C_2H_6 recycle valve (3) discharge	1	-88.4
35	C_2H_6 recycle purge (1%)	1	-88.4
36	C_2H_6 recycle cold-in heat exchanger	1	-88.4
37	C_2H_6 recycle hot-out heat exchanger	1	542

Table 0-3: Overview of temperature changing process units (i.e., coolers and heaters).

Name	**p [bar]**	**T_{in} [°C]**	**T_{out} [°C]**
COOL-1	1	215	25
COOL-2	5	260	25
COOL-3	20	226	25
COOL-4	1	215	70
COOL-5	15	276	25
COOL-6	35	88	-50
HEAT-1	1	372	550
HEAT-2	1	25	550

Table 0-4: Overview of pressure changing process units (i.e., compressors, pumps, and valves).

Name	P_{in} [bar]	P_{out} [bar]	T_{in} [°C]	T_{out} [°C]
COM-1	1	1	25	25
COM-2	1	5	25	260
COM-3	5	20	25	226
COM-4	20	50	25	150
COM-5	1	15	70	276
COM-6	15	35	25	88
PUMP-1	1	1	25	25
VAL-1	35	30	12.6	6
VAL-2	30	25	1.1	-6
VAL-3	25	1	1.7	-88

APPENDIX L. Analysis of CO_2/CO Absence and SMR Improbability

Wu et al. reported no CO_2 or CO presence in the product stream at operating temperatures of 550°C or below. They explained this in line with the BZCYYb electrolyte material exhibiting nearly pure proton-conducting behaviour below 600°C [6]. Above this temperature, BZY-based proton conductors begin to show oxide ion (O^{2-}) conductivity, suggesting that the formation of CO_2/CO is highly improbable during operation at 550°C. The absence of CO_2/CO in the product stream is advantageous, as it mitigates the concern of CO_2 poisoning of BZCYYb electrolyte material, a common issue in electrochemical hydrocarbon processing. Moreover, the probability of SMR (Steam Methane Reforming) under these operational conditions is minimal, for the following three reasons [120]:

- The absence of an SMR-specific catalyst (often containing nickel) significantly diminishes the chance of SMR happening under the specified conditions of T=550°C and p=1 bar.
- The relatively low methane concentration in the feed (1.8 wt%) reduces the likelihood and impact of any methane reacting.
- The operating conditions are not facilitative for SMR, which typically occurs in the temperature range of 800 - 1000°C at a pressure between 14 – 20 bar. Thus, conversion at a temperature of 550°C and pressure of 1 bar is assumed to be negligible.

This simplifies the separation train, because of the absence of CO_2/CO in the product stream.

APPENDIX M. Cryogenic Distillation

Cryogenic distillation, the state-of-the-art separation method in ethane steam crackers, is chosen in this process design as well. This technique separates gases according to their boiling points, using the fact that different gases condense at different temperatures [121]. The process of cryogenic distillation is explained in line with the different component letters in Figure 0-6 [122].

Following the cooling and condensing stages, the liquefied gases (A) enter the distillation column (B). As the temperature increases, the liquefied gases evaporate at their own unique boiling points, moving upwards in the distillation column. The rising vapor at the top of the column is then cooled and condensed (C). A reflux drum (D) recovers part of the condensed liquid as the “distillate” (E). Simultaneously, a part of the condensed liquid, known as the “reflux” (E) Simultaneously, a part of the condensed liquid, known as the "reflux" (F), is returned to the distillation column. At the base of the column, a reboiler (G) vaporizes the residual liquids, enabling them to re-enter the column. Heavier components with relatively higher boiling points are collected as the bottom product (H). This process ensures a thorough and efficient separation of the various gas components.

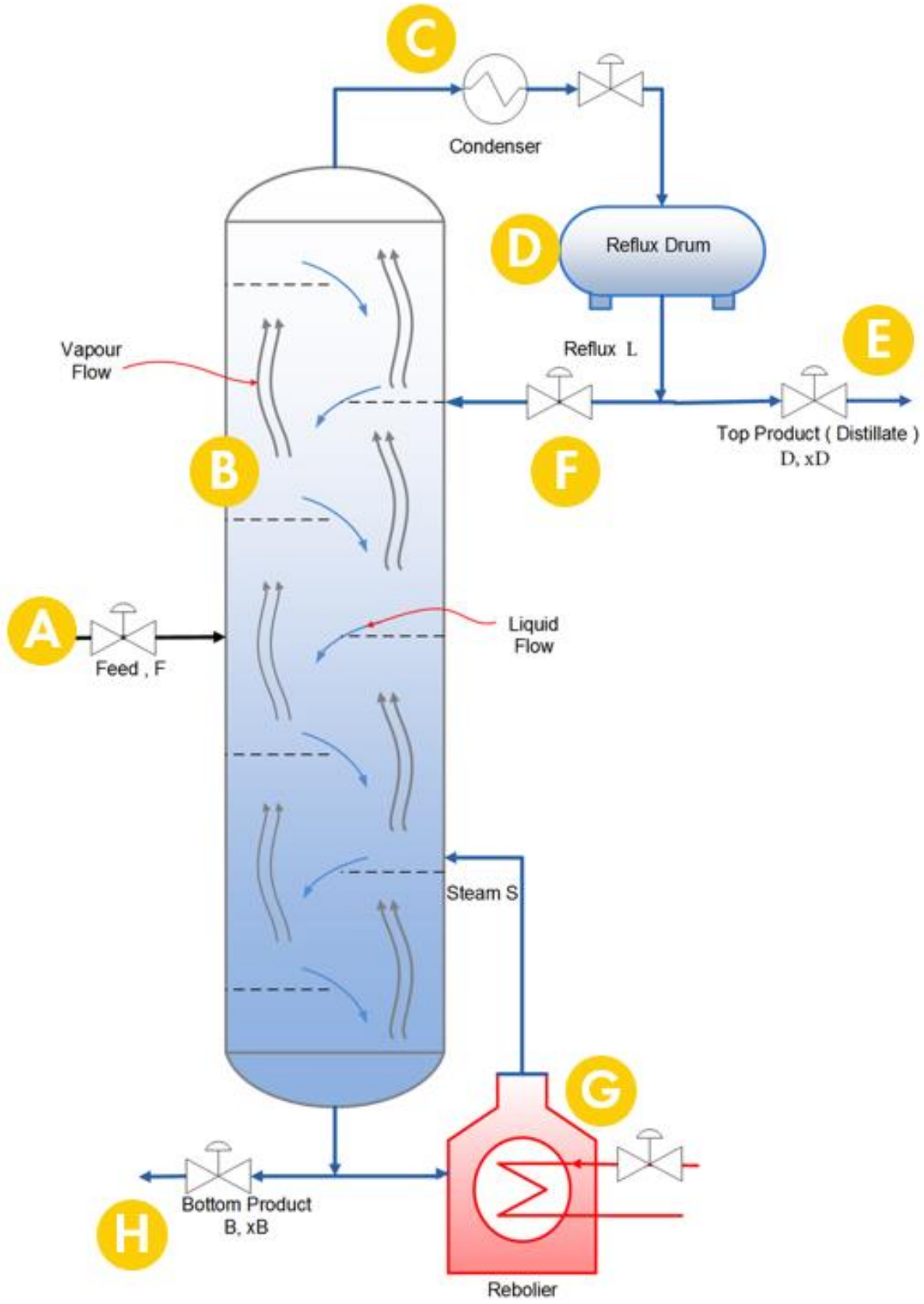

Figure 0-6: Schematic diagram of a cryogenic distillation column [122].

APPENDIX N. Distillation Columns Specifications

In Aspen Plus, the Light Key (LK) and Heavy Key (HK) components determine the separation requirements for a distillation process. The LK represents the lightest product intended for separation, primarily accumulating in the distillate. It is the heaviest component in the distillate with a non-negligible concentration. The goal is to reduce the LK content in the bottom product. Conversely, the HK represents the heaviest product targeted for separation, predominantly found in the bottom stream. It is the lightest component in the bottom product with a significant concentration. The aim is to minimize the HK content in the distillate [123]. Table 0-5, Table 0-6, and Table 0-7 present the distillation column specifications.

Table 0-5: Demethanizer (DE-METH) unit specifications.

Demethanizer	Component / Value
Incoming stream	H_2, CH_4, C_2H_4, C_2H_6, C_3H_6, C_3H_8, C_4H_8
Pressure (condenser and reboiler)	35 bar
Reflux ratio	14.6
Number of actual stages	23
Light Key (LK)	CH_4 – recovery = 0.98
Boiling point LK at atm	-162 °C
Heavy key (HK)	C_2H_4 – recovery = 0.0001
Boiling point HK at atm	-104 °C
Distillate	H_2, CH_4
Bottom product	C_2H_4, C_2H_6, C_3H_6, C_3H_8, C_4H_8

Table 0-6: De-ethanizer (DE-ETH) unit specifications.

De-ethanizer	Component / Value
Incoming stream	C_2H_4, C_2H_6, C_3H_6, C_3H_8, C_4H_8
Pressure (condenser and reboiler)	30 bar
Reflux ratio	1.37
Number of actual stages	40
Light Key (LK)	C_2H_6 – recovery = 0.999
Boiling point LK at atm	–89 °C

Heavy key (HK)	C_3H_6 – recovery = 0.001
Boiling point HK at atm	-48 °C
Distillate	C_2H_4, C_2H_6
Bottom product	C_3H_6, C_3H_8, C_4H_8

Table 0-7: C_2-splitter (C2-SPLIT) unit specifications.

C_2-splitter	**Component / Value**
Incoming stream	C_2H_4, C_2H_6
Pressure (condenser and reboiler)	25 bar
Reflux ratio	12.3
Number of actual stages	82
Light Key (LK)	C_2H_4 – recovery = 0.999
Boiling point LK at atm	–104 °C
Heavy key (HK)	C_2H_6 – recovery = 0.0001
Boiling point HK at atm	-89 °C
Distillate	C_2H_4 – purity = 99.95%
Bottom product	C_2H_6

APPENDIX O. Heat Integration Adaptation Methodology

The AEA (Aspen Energy Analyzer) is used in combination with an AspenPlus model of the Rhineland SC to adapt for differences in heat integration between the WINNER process and the Monaca benchmark. Assuming the Rhineland SC demonstrates similar heat integration to the Monaca benchmark, this model offers an appropriate reference point. The AEA estimates the potential energy savings based on pinch technology (Section 4.4.1) and utility planning tools. Figure 0-7 shows the available energy savings for the base case scenario according to the AEA.

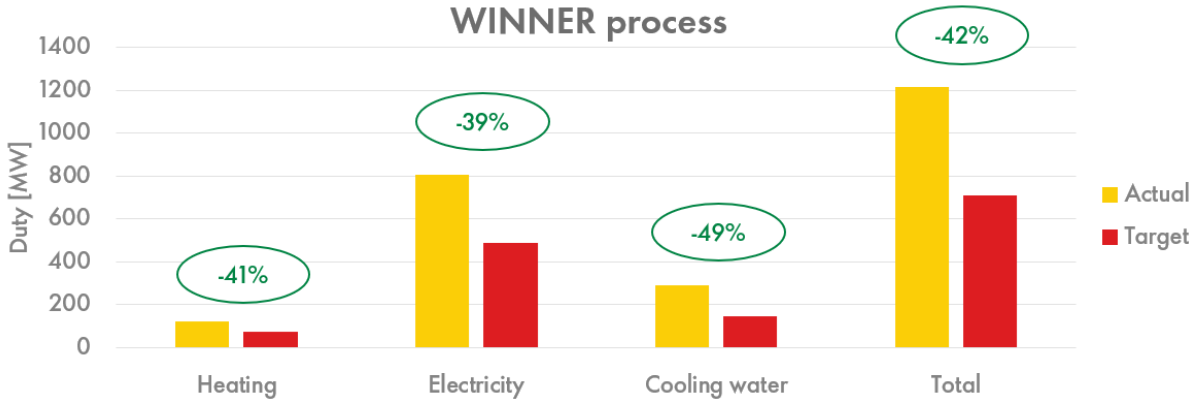

Figure 0-7: Available energy savings for the WINNER process (1500 KTA) according to the AEA.

Figure 0-8 shows the available energy savings according to the AEA for simulation of the 1500 KTA ethylene Rhineland SC in AspenPlus. These are significantly lower compared to the available savings in the WINNER process. However, there is still room for improvements that will lead to a decrease in duties.

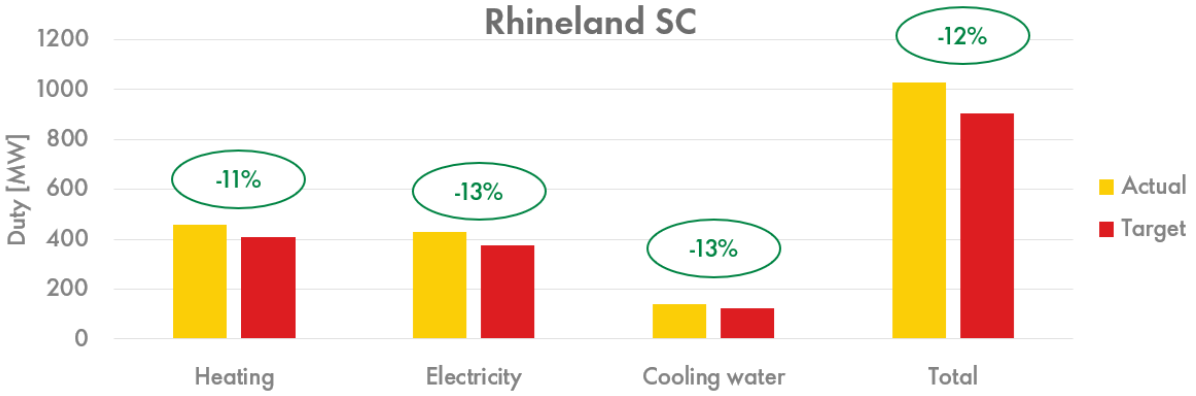

Figure 0-8: Available energy savings for the Rhineland SC (1500 KTA) according to the AEA.

The available savings in the Rhineland SC, actual, and target are combined to calculate the adapted duties for the process in Equation (0-16).

$$Adapted\ duty = \frac{Target\ duty}{(1 - available\ savings)} \tag{0-16}$$

This ensures that the WINNER process and the Rhineland SC (and therefore the Monaca benchmark) have the same degree of heat integration. Figure 0-9 shows the outcome of the adaptation for heat integration. The indicated percentages represent the adapted savings transitioning from the current process to the adjusted scenario, assuming the same level of heat integration as the benchmark.

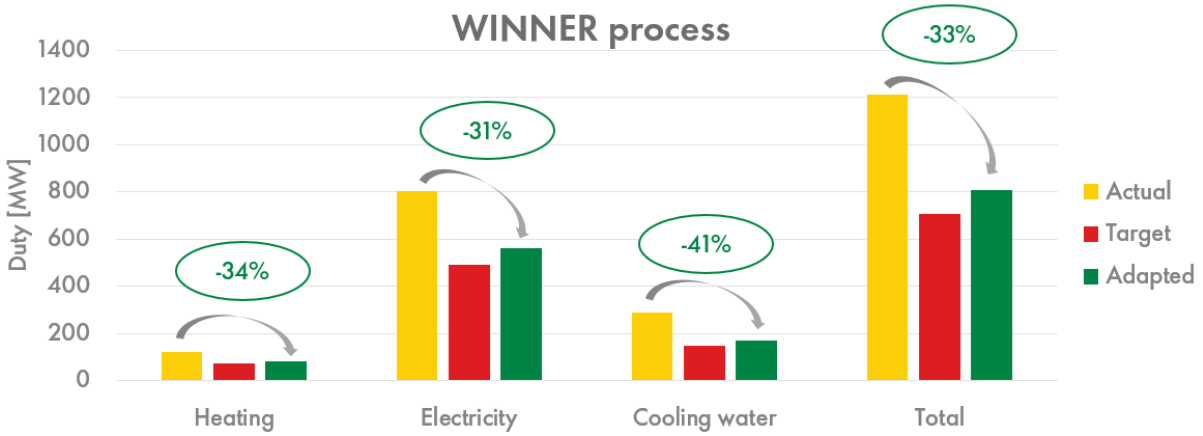

Figure 0-9: WINNER process duties (1500 KTA) after adaptation for heat integration (repeated).

APPENDIX P. PCEC Reactor CAPEX Estimation

This Appendix outlines the procedure undertaken to estimate the ISBL (inside battery limits) CAPEX costs of the PCEC reactor. Based on three different references with data on SOEC cost estimates, four different scenarios are made [80-82]. SOECs are in their scale-up phase, with the first multi-megawatt (2.6 MW) high-temperature SOEC *MultiPLHY* project currently being installed [79]. There are still a lot of uncertainties and differences in cost estimations for current SOEC projects, let alone future CAPEX estimations for these systems.

Therefore, it is decided to combine data available in the literature on bottom-up CAPEX estimations of electrolyzer systems [80-82], into four different scenarios with corresponding total direct costs as presented in Table 0-14. This resulted in a cost estimation for the ISBL PCEC reactor costs based on a nominal capacity of 59 MW for hydrogen splitting and compression over the electrolytic membrane.

Table 0-8: SOEC cost scenarios and corresponding ISBL costs [80-82].

Scenario	SOEC direct costs [$/kW]	PCEC reactor ISBL costs [$MM]
1: Current (2020) – Conservative	~3600	212
2: Current (2020) – Progressive	~1200	72
3: Upscaling (2030) – Conservative	~1200	69
4: Upscaling (2030) – Progressive	~450	27

The underlying data analysis using the SOEC cost data is shown in Table 0-14. Three different cost estimates are combined to come to the scenarios as presented above.

APPENDIX Q. Utility Specifications

Table 0-9: Caloric values and specific CO_2 emissions of fuels [89] [90] [109]

Fuel type	LHV [MWh/t]	Spec. CO_2 emissions [tCO_2e/t]	Spec. CO_2 emissions [tCO_2e/MWh]
Hydrogen	33.3	0	0
Methane	13.9	2.75	0.18
Ethane	13.3	2.93	0.22
Propane	12.9	2.99	0.22
Power	N/A	N/A	0.369 [88]
Renewable Power	N/A	N/A	0.026 [109]

Table 0-10: Refinery fuel specifics [89, 90].

Component	Composition	LHV [MWh/t]	Carbon Intensity [CO_2/t]	Price [$/MWh]
Hydrogen	30%	33.3	0	36
Methane	70%	13.9	2.75	10.8
Total	100%	19.7	1.93	18.4

Table 0-11: Fuel gas production specifications in the WINNER process.

Component	Production [t/h]	Fraction [wt%]	LHV [MWh/t]	Calorific Flow [MW]	Carbon Intensity [tCO_2/MWh]
Methane	10.8	12	13.90 [89]	150.5	0.20 [90]
Hydrogen (Anode)	0.9	1	33.30 [89]	29.4	0 [90]
Propane	2.5	3	12.88 [89]	31.9	0.23 [90]
Propylene	18.3	21	12.68 [89]	232.2	0.25 [90]
Butene	55.1	63	12.55 [89]	691.3	0.25 [90]

Table 0-12: Fuel gas production specifications in the Monaca benchmark process.

Component	Production [t/h]	Fraction [wt%]	LHV [MWh/t]	Calorific Flow [MW]	Carbon Intensity [tCO_2/MWh]
Fuel gas (plain)	33.0	65	19.72 [89]	650.3	0.10 [90]
Propylene	4.6	9	12.68 [89]	58.7	0.25 [90]
Butene	8.0	16	12.55 [89]	100.9	0.25 [90]
Pygas	4.3	9	11.89 [89]	51.5	0.26 [90]
CGO	0.6	1	11.89 [89]	6.7	0.26 [90]
ECR	0.2	0	11.89 [89]	1.9	0.26 [90]

APPENDIX R. Feedstock and Product Prices

Table 0-13: Commodity bulk prices [USD/t] for steam cracking products.

Product	Europe [$/t]	North America [$/t]	Middle East [$/t]	Asia-Pacific [$/t]	Reference
Hydrogen	1700	1200	1300	1450	[124]
Methane	450	150	150	200	[84]
Ethane	600	450	300	700	[85]
Ethylene	1300	1200	1100	1100	[11] [12]
Propane	700	1000	700	950	[86]
Propylene	1000	1200	1000	1000	[13, 14]
Butene	950	1050	1200	1250	[15, 16]
Raw C4	750	850	1000	1050	[125]
Fuel Gas	700	700	700	700	[89]

APPENDIX S. PCEC Reactor CAPEX Estimation

Table 0-14: ISBL PCEC reactor cost estimation based on SOEC data [80-82].

	SOEC CAPEX estimate				
		Base-case (2020)		Upscaling (2030)	
		[USD/kW]			
ISPT	Direct costs [$/kW]	$	2,392	$	584
	Site installation, etc.	$	719	$	180
	Total direct costs	$	3,110	$	764
	Total direct costs - Conservative	$	4,666	$	1,145
	Total direct costs - Progressive	$	1,555	$	382
Deloitte	Full System Costs - Conservative	$	2,583	$	1,572
	Full System Costs - Progressive	$	898	$	561
EIFER	Installed Capital Cost - Conservative	N/a		$	816
	Installed Capital Cost - Progressive	N/a		$	427
Combined	Total Direct Costs - Conservative	$	3,624	$	1,178
	Total Direct Costs - Progressive	$	1,227	$	457

Costs	Current (2020) - Conservative		Current (2020) - Progressive
Total ISBL costs [$/kW]	$	3,624	$ 1,227
PCEC Reactor costs [$]	$	212,221,558	$ 71,836,422
PCEC Reactor costs [$MM]	$	212	$ 72

Costs	Upscaling (2030) - Conservative		Upscaling (2030) - Progressive
Total ISBL costs [$/kW]	$	1,178	$ 457
PCEC Reactor costs [$]	$	68,976,116	$ 26,740,026
PCEC Reactor costs [$MM]	**$**	**69**	**$ 27**

APPENDIX T.Cost of Ethylene Manufacturing

Table 0-15: Overview of OPEX for the WINNER process and benchmark.

Expenditure	UOM	WINNER [1500 KTA]	Monaca [1500 KTA]
Feedstock costs	$/tC$_2$=	735	585
Product Value	$/tC$_2$=	1643	1294
Gross margin	$/tC$_2$=	908	709
NHFC	$/tC$_2$=	292	491
Fuel costs	$/tC$_2$=	0	0
Electricity costs	$/tC$_2$=	214	165
Cooling costs	$/tC$_2$=	14	12
Carbon costs	$/tC$_2$=	63	65
Catalysts costs	$/tC$_2$=	22	22
Total VC	$/tC$_2$=	**313**	**263**
VC margin	$/tC$_2$=	595	446
Fixed costs	$/tC$_2$=	44	157
CEM	$/tC$_2$=	649	911
Margin	**$/tC$_2$=**	**551**	**289**
Margin	**MM$/yr**	**826**	**434**

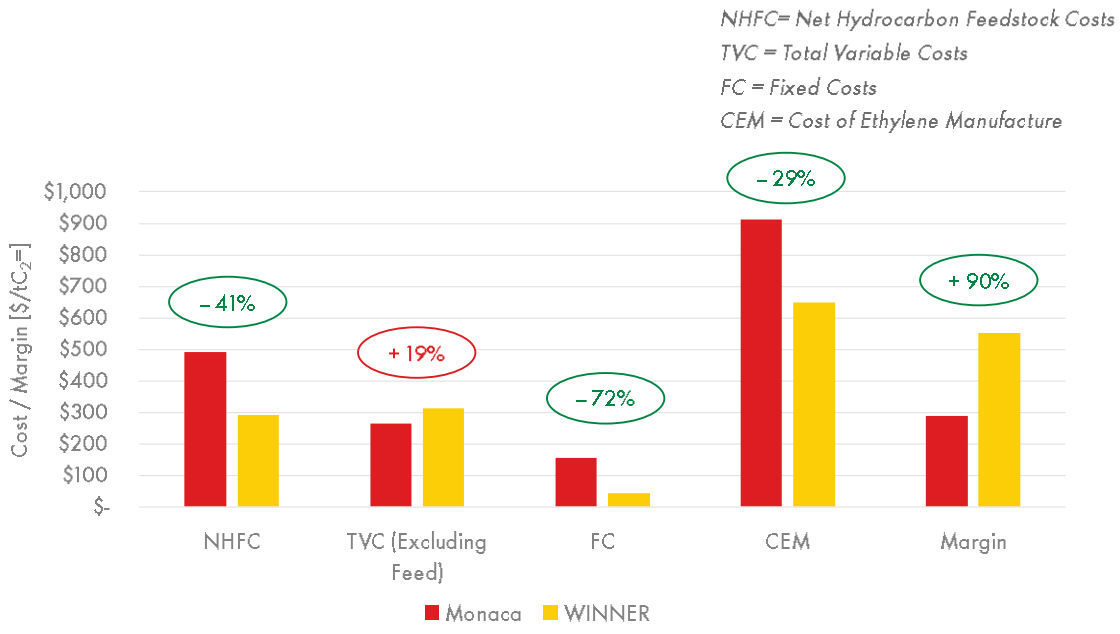

Figure 0-10: Visualization of OPEX-related parameters for the WINNER process and Monaca benchmark.

APPENDIX U. Additional Graphs for Economic Inputs Sensitivity Analysis

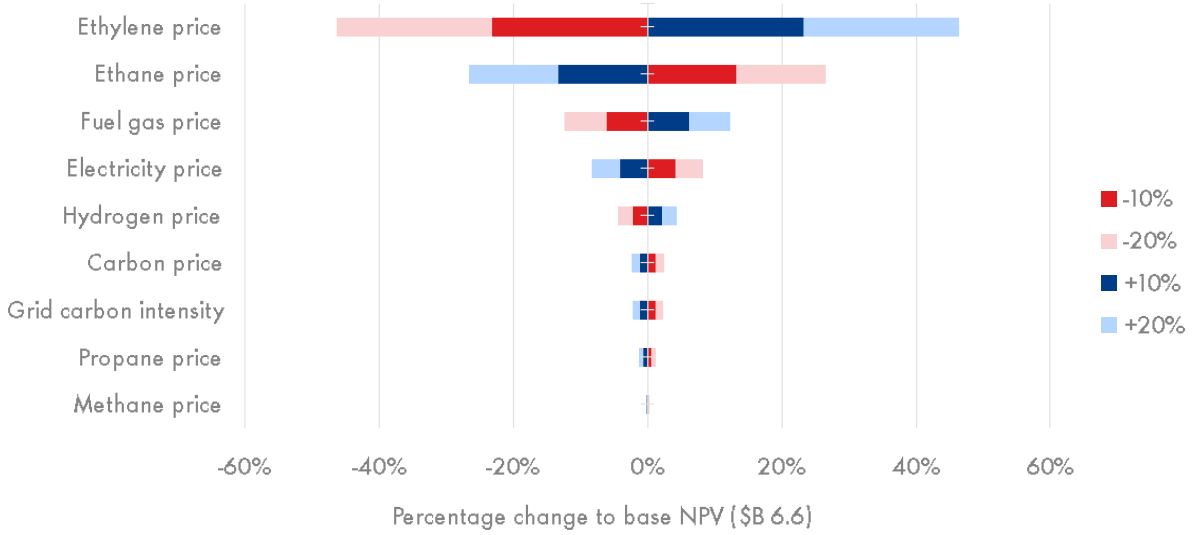

Figure 0-11: Sensitivity analysis showing the influence of percentual changes of economic inputs on the NPV (in percentual change with respect to the base NPV) of the WINNER project.

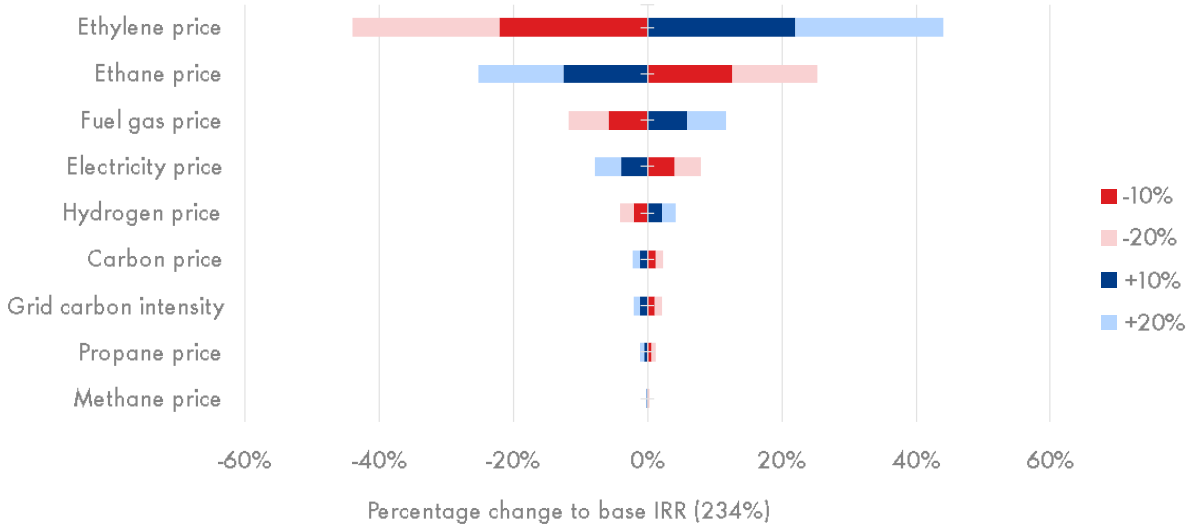

Figure 0-12: Sensitivity analysis showing the influence of percentual changes of economic inputs on the IRR (in percentual change with respect to the base IRR) of the WINNER project.

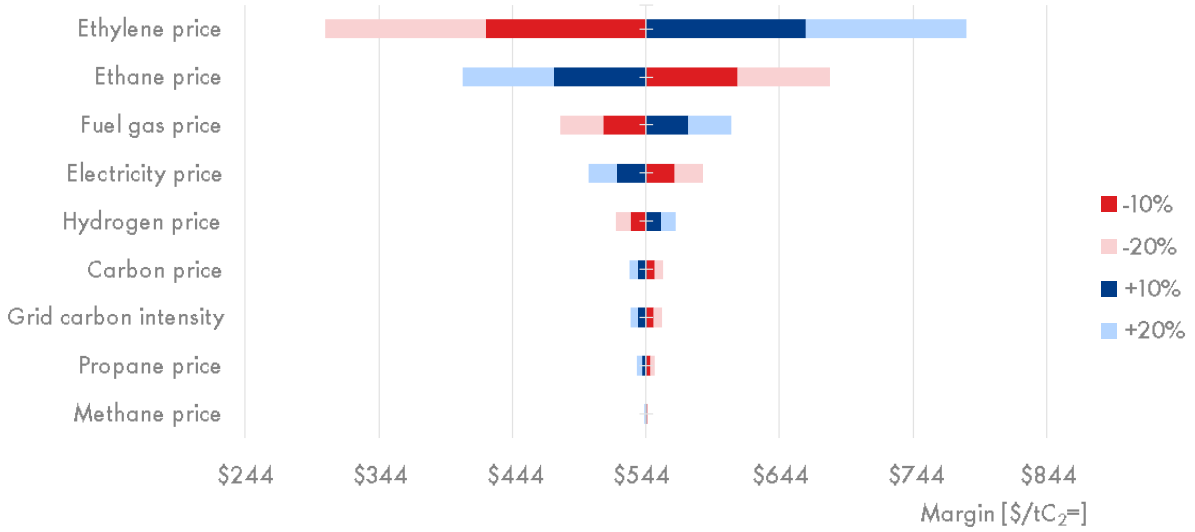

Figure 0-13: Sensitivity analysis showing the influence of percentual changes of economic inputs on the margin (in dollars per ton of ethylene produced) of the WINNER project.